NASA Technical Memorandum 84624

Predictions of Entry Heating for Lower Surface of Shuttle Orbiter

C. L. W. Edwards and Stanley R. Cole

JULY 1983

25th Anniversary
1958-1983

NASA

NASA Technical Memorandum 84624

Predictions of Entry Heating for Lower Surface of Shuttle Orbiter

C. L. W. Edwards and Stanley R. Cole
Langley Research Center
Hampton, Virginia

National Aeronautics
and Space Administration

**Scientific and Technical
Information Branch**

1983

SUMMARY

A broad base of thermocouple and phase-change-paint data was assembled and correlated to the nominal-design 14414.1 and proposed STS-1 (first flight of the space transportation system) entry trajectories. Averaged data from phase-change-paint tests compared favorably with thermocouple data for predicting heating rates. Laminar and turbulent radiation-equilibrium heating rates were computed on the lower surface of the Shuttle orbiter for both trajectories, and the lower-surface centerline results were compared both with aerodynamic-heating design data and with flight values from the STS-1 and STS-2 trajectories. The peak laminar-heating values from the aerodynamic-heating design-data book were generally 40 to 60 percent higher than the laminar estimates of this study, except at the 55-percent location of maximum span where the design-data-book values were less than 10 percent higher.

Estimates of both laminar and turbulent heating rates compared favorably with flight data. Peak turbulent heating rates were estimated to occur 200 to 400 sec later in the trajectory than the laminar peaks and could be more than twice the magnitude of the design-data values. Therefore, a precise determination of flight boundary-layer transition becomes a critical exercise in thermal-protection-system evaluation. The cause of the increased heating in the vicinity of 55 percent of the span could not be resolved with the simplified approach employed in this study. However, the phase-change-paint data were found to be a very effective means of mapping the region of influence.

INTRODUCTION

An aerothermal analysis of the heating on the lower surface of the Shuttle orbiter during entry was initiated at the Langley Research Center as direct support to a study sponsored by the Johnson Space Center of the strength and integrity of the thermal protection system (TPS) of the Space Shuttle orbiter. The analysis reported herein was intended to be an independent assessment of the radiation-equilibrium heating rates and surface temperatures expected on the lower surface of the orbiter for the nominal-design trajectory. In order to design the primary TPS, these results would then be compared with the data contained in "Space Shuttle Orbiter Entry Aerodynamic Heating Data Book" by J. W. Haney and C. T. Petrilla (SD73-SH-0184, C Revision, Book I, October 1978) which were established by the Rockwell International Corporation. The existing base of experimental tunnel heat-transfer data was extensively surveyed to collect the most appropriate data to form a sound empirical approach to heating predictions. The resulting correlations for laminar heating rates are a vital part of the approach and were formulated on the basis of combined thermocouple and phase-change-paint data.

The estimates of local inviscid conditions and flight stagnation-point heating rate required to apply the correlations were generated by straightforward and well-known techniques. The method of Fay and Riddell (ref. 1) was used to determine stagnation-point heating rates. Local inviscid-flow conditions were based on a modification of a tangent-cone approximation technique presented in reference 2.

The turbulent heating rates presented in this paper were generated by laminar-to-turbulent heat-transfer ratios based on well-known approximations to classical boundary-layer equations. The same approach was also subsequently applied in the Shuttle Flight Certification Program. During flight certification, the analysis was extended to include portions of the orbiter other than the lower surface; however, the results presented herein contain only lower-surface data. Neither the empirical approach developed and employed for these studies nor the predicted results have appeared in a referenceable document.

SYMBOLS

In addition to a technique description and a discussion of calculated results, data from the lower-surface center line are compared with flight data from the first and second flights of the space transportation systems (STS-1 and STS-2) to assess both the analytical approach and predicted results.

b	wing span
C_p	pressure coefficient; specific heat
c	local axial chord length
g	gravitational constant, 32.152 ft/sec^2
h	altitude
l	body length
M	Mach number
M_{ns}	effective Mach number normal to shock
N_{Pr}	Prandtl number
N_{St}	Stanton number
p	static pressure
$\dot{q}$	heating rate per unit area
$\dot{q}_{conv}$	convective heating rate per unit area
$\dot{q}_{ref}$	Fay-Riddell radiation-equilibrium heating rate per unit area at stagnation point of 1-ft-radius sphere in flight
$R_{c,x}$	local Reynolds number in conical flow
R_x^*	reference-temperature Reynolds number
$R_{\infty,l}$	free-stream Reynolds number based on orbiter body length
T	temperature
t	time

U	film heat-transfer coefficient
U_{ref}	film heat-transfer coefficient at stagnation point of 1-ft-radius sphere in flight (or its scale equivalent)
V	velocity
x	axial distance aft of leading edge (or nose)
y	lateral distance spanwise from fuselage center line
α	angle of attack
γ	ratio of specific heats for air
ε	surface emissivity
η_r	recovery factor
θ_s	shock angle
μ	viscosity coefficient
ρ	density
σ	Stefan-Boltzmann constant for radiant-heating calculations

Subscripts:

aw	adiabatic wall
c	conical-flow conditions
lam	laminar
o	stagnation or total conditions
pc	phase-change paint
ref	radiation-equilibrium conditions at stagnation point of 1-ft-radius sphere in flight (or its scale equivalent)
s	conditions behind oblique shock
turb	turbulent
w	wall
∞	free stream

Superscript:

*	reference-temperature conditions

Abbreviations:

AEDC	Arnold Engineering Development Center
STS	space transportation system
TPS	thermal protection system

ANALYTICAL APPROACH

The most desirable and comprehensive approach to the aerothermal-analysis task would be a coupled inviscid and viscous theoretical solution of either the complete vehicle or the windward-side flow field at the entry flight conditions representing peak heating coupled with appropriate validating experimental results. This is particularly true if the basic solutions could be systematically perturbed and validated by experimental data in order to identify and evaluate parameters which most significantly influence the orbiter's aerothermal environment.

Areas of concern for the lower surface include real-gas effects (equilibrium and finite-rate chemistries), geometric influences such as abrupt changes in leading-edge sweep and control surfaces, shock interactions, shear layers downstream of shock interactions, boundary-layer transition, and excursions in flight profile. The sides and upper surfaces may have additional complexities resulting from separation, interacting or interfering flows, and possible vortex scrubbing. After surveying the available numerical techniques, however, it was quickly determined that a comprehensive theoretical approach was not practical for this effort. This decision was reached because a good coupled inviscid and viscous solution for complex configurations like the orbiter at its intended flight conditions was not state of the art; also, the probability of successfully applying such codes within the prohibitively short time frame of either the TPS strength-and-integrity study or the first flight certification would have been very tenuous and could have jeopardized the possibility of any real assessment of the heating.

Therefore, an alternative approach based on the existing Shuttle aerothermodynamic data base was adopted as the best approach for quickly meeting both the TPS strength-and-integrity study objectives and subsequent first-flight-certification objectives. A survey of available data was conducted to collect the most pertinent heat-transfer data. Contacts were also made with several past experimental analysts who were active during the development phases of the Shuttle to secure additional insight and data. The most consistent and comprehensive heating data generated in any one facility seemed to be the data obtained at a Mach number of 8 in the AEDC von Kármán Gas Dynamics Facility Tunnel B (referred to herein as AEDC Tunnel B). Three series of heating tests (refs. 3, 4, and 5) were conducted on 0.0175-scale models at angles of attack and Reynolds numbers based on length which could be used to approximate key portions of the nominal-design 14414.1 entry trajectory illustrated in figure 1(a) as well as the proposed STS-1 trajectory illustrated in figure 1(b). These data do not contain real-gas effects. Therefore, the predicted heating rates could be significantly higher than those measured in flight in the early portions of the trajectories where considerable nonequilibrium flows are known to exist; however, as the flows tend to reach equilibrium later in the trajectories, the real-gas effects should tend to become negligible. (See ref. 6.)

The initial 1450-sec interval of each trajectory covered all the major heating conditions and was the basic flight interval used throughout this study. The peak

heating condition usually occurs between 400 and 1000 sec as illustrated by the $\dot{q}_{ref}$ curves which represent the stagnation-point radiation-equilibrium heating rate on a 1-ft-radius sphere. (See fig. 1.) The two trajectories of interest are defined in figures 2 and 3. Four sets of experimental test conditions were used to approximate the flight Reynolds numbers and angles of attack of the nominal-design trajectory as shown in figures 2(a) and 3(a), respectively. Five corresponding stepwise approximations for the proposed STS-1 entry trajectory are presented in figures 2(b) and 3(b). No interpolations of the experimental data were performed during this analysis, and the step functions illustrated in figures 2 and 3 cause slight discontinuities that are sometimes evident in subsequent heating histories.

Four spanwise locations were selected to represent the key features of the lower surface based on a visual analysis of all experimental data. The locations include the lower center line and the 40-, 55-, and 70-percent locations of maximum span. No thermocouples were located at the 55-percent span location; however, the phase-change-paint data consistently indicated a narrow region of increased heating there. The thermocouple data obtained along the 50- and 60-percent spans do not indicate increased heating.

Thermocouple Data

The thermocouple pattern and test conditions for the thermocouple data employed are illustrated in figure 4. There were an additional 23 thermocouples on the forward portion of the lower center line which are not shown. The basic form of the data employed is the film heat-transfer coefficient U nondimensionalized by the coefficient for stagnation-point radiation-equilibrium heating to a scale equivalent to a 1-ft-radius sphere in flight. The equivalent wind-tunnel sphere radius was 0.0175 ft in references 3, 4, and 5.

Phase-Change-Paint Data

A fairly comprehensive description of the phase-change-paint test technique and the assumptions required to obtain aerodynamic-heating estimates are contained in reference 7. Basically, a model constructed of a dark-colored insulating material having well-defined thermal properties which are well-known is coated with a temperature-sensitive paint prior to injection into an airstream. The paint employed is a light-colored opaque solid which becomes a colorless liquid at a specific temperature. Paints which change phase at almost any given temperature are available. When the model is injected into the test airstream, the paint in the areas of high heating melts first and exposes the darker model surface with the peripheries of these areas being denoted as melt lines. These areas, which enlarge with time, are photographed with a motion-picture camera operating at a known preset rate. These photographs give a precise time history of the distinct melt lines which, coupled with a knowledge of the model thermal properties, presents sufficient information to conduct a one-dimensional transient heat-conduction analysis and to extract surface heat-transfer coefficients.

Tracings of the phase-change-paint melt lines and of the heat-transfer-coefficient ratios U/U_{ref} that they represent, approximating the earliest portions of both the design (14414.1) and STS-1 trajectories, are illustrated in figure 5 for an angle of attack of 40° and a Reynolds number of 1×10^6. Figure 5(a) was generated from the data presented in reference 4. A key objective of that study was to investigate the heating of a series of deflected elevons; however, only those data

representing undeflected elevons were employed here. Figures 5(b) to 5(j) were generated from data contained in reference 5. A major objective of that study was to investigate blockage and the possible influence of local cross flows that might be established by cutting away portions (notches) of one side of the model as evident in figures 5(h) to 5(j). The data from that study compared favorably with the complete orbiter data to the extent that no apparent effects due to the notches were observed. Figure 6 (taken from ref. 4) contains the only set of phase-change-paint data applicable to the plateau denoted by $\alpha = 35°$ and $R_{\infty,l} \approx 1.9 \times 10^6$, which was used to define the second time interval of the nominal trajectory where U/U_{ref} was assumed constant. The interval denoted by $\alpha \approx 30°$ and $R_{\infty,l} \approx 3.75 \times 10^6$ is represented by figure 7. The data shown in figures 7(a) to 7(d) were taken from reference 4, and the data shown in figures 7(e) to 7(q) were taken from reference 5. Phase-change-paint data applicable to the last step function of both trajectories ($\alpha \approx 30°$ and $R_{\infty,l} \approx 7 \times 10^6$) are represented in figures 8(a) and 8(b), which were derived from reference 4, and in figures 8(c) to 8(j), which were generated from data contained in reference 5.

Averaged Thermocouple and Phase-Change-Paint Data

Values of U/U_{ref} for the 0-, 40-, 55-, and 70-percent locations of maximum span were extracted from the data sets and plotted as functions of nondimensional axial location x/c. The data for constant angle of attack and Reynolds number that were used to represent both the first 600 sec of the nominal-design 14414.1 trajectory and the first 850 sec of the STS-1 trajectory are illustrated in figure 9. The circular symbols always represent the thermocouple data so that an easy comparison can be made with the phase-change-paint data. The symbol key shown in the upper right corner of figure 9 is consistent with those provided at the end of the test-condition legends in figure 5 so that individual phase-change-paint tracings can be easily keyed to the data plots. The curves represent the author's "simple fairing" of the individual data sets. Data from these curves, rather than the individual data points, were used in subsequent heating calculations along the entry trajectory for direct comparison with the aerodynamic-heating data book. A more rigorous and systematic fairing of the data could be based on laminar and/or turbulent decays in heating with distance.

The experimental data to approximate the trajectory parameters between 600 and 850 sec used an angle of attack of 35° and a Reynolds number based on length of approximately 2×10^6 as illustrated in figure 10. The scarcity of data available for $\alpha = 35°$ makes the curve fairing at this condition questionable. The experimental data sets used to approximate between 850 and 1050 sec of the nominal-design 14414.1 trajectory are illustrated in figure 11. The data of figure 12 were used over the interval between 1050 and 1450 sec of the nominal-design 14414.1 trajectory and also between 1250 and 1450 sec for the STS-1 entry trajectory. Both of these data sets were obtained at $\alpha = 30°$ but at separate Reynolds numbers. The data obtained at a Reynolds number of 4×10^6 and shown in figure 11(a) appear laminar along the lower center line. However, a comparison of these data with the low Reynolds number data of figure 9 indicates probable boundary-layer transition at the 55-percent span location and possibly at the 40- and 70-percent span locations as well. The highest Reynolds number data ($R_{\infty,l} \approx 8 \times 10^6$ shown in fig. 12) exhibit boundary-layer transition at all spanwise locations. Transition seems to occur about 55 percent of the axial distance down the lower center line, about 40 to 45 percent of the chord at $2y/b = 0.40$, about 15 percent of the chord at $2y/b = 0.55$, and about 20 to 25 percent of the chord at $2y/b = 0.70$.

Figures 13, 14, and 15 contain the additional averaged experimental data which were combined with the data in figures 9 and 12 to approximate the proposed STS-1 trajectory. The heat-transfer-coefficient ratios presented in figure 13 ($\alpha = 40°$ and $R_{\infty,l} \approx 2 \times 10^6$), representing the interval between 850 and 1000 sec of the proposed STS-1 entry, appear to be essentially laminar at all four spanwise locations. The data in figure 14 representing the next interval between 1000 and 1150 sec are also at $\alpha = 40°$ but at approximately twice the Reynolds number. There is an indication of possible transition at the 0-, 40-, and 55-percent spanwise locations, whereas the most outboard location has a more laminar characteristic longitudinal distribution. The data representing the STS-1 interval between 1150 and 1250 sec ($\alpha = 35°$ and $R_{\infty,l} \approx 8 \times 10^6$) clearly exhibit transition at all four spanwise locations. Transition seems to occur at about 60 percent of the local chord for the center line and at about 30 percent of the local chord at the other three spanwise locations.

METHODOLOGY FOR EXTRAPOLATING WIND-TUNNEL DATA TO FLIGHT

The heat-transfer-coefficient ratios measured at a Mach number of 8 in the AEDC Tunnel B at flight angles of attack and flight free-stream Reynolds numbers based on vehicle length were assumed to represent adequately the ratios expected in those portions of the flight trajectory not dominated by real-gas effects. No corrections for Mach number and wall-temperature effects were made. A simple procedure for calculating flight radiation-equilibrium heating rates and surface temperatures was derived in the following manner:

If the convective heating is defined by

$$\dot{q}_{conv} = U(T_{aw} - T_w) \tag{1}$$

then multiplying both sides of equation (1) by $U_{ref}/\dot{q}_{ref}$ and collecting terms gives

$$\frac{\dot{q}_{conv}}{\dot{q}_{ref}} = \frac{U}{U_{ref}} \frac{T_{aw} - T_w}{\dot{q}_{ref}} U_{ref} \tag{2}$$

The subscript ref refers to stagnation-point heating on a 1-ft-radius sphere or a scaled equivalent. The relationship for convective heating to the nose of the sphere can be defined as

$$\dot{q}_{ref} = U_{ref}(T_o - T_{ref}) \tag{3}$$

Similarly, the reference-condition relation for radiant heating is

$$\dot{q}_{ref} = \sigma\varepsilon T_{ref}^4 \tag{4}$$

Thus, $\dot{q}_{ref}$ is defined as a radiation-equilibrium heating rate. Therefore, solving equation (4) for T_{ref}, substituting T_{ref} into equation (3), and collecting terms yields

$$U_{ref} = \frac{\dot{q}_{ref}}{T_o - \left(\frac{\dot{q}_{ref}}{\sigma\varepsilon}\right)^{1/4}} \tag{5}$$

Substituting this relation for U_{ref} into equation (2) and simplifying gives

$$\dot{q}_{conv} = \dot{q}_{ref} \frac{U}{U_{ref}} \frac{T_{aw} - T_w}{T_o - \left(\frac{\dot{q}_{ref}}{\sigma\varepsilon}\right)^{1/4}} \tag{6}$$

Setting the right-hand side of equation (6) equal to the radiant-heating relation gives

$$\sigma\varepsilon T_w^4 = \dot{q}_{ref} \frac{U}{U_{ref}} \frac{T_{aw} - T_w}{T_o - \left(\frac{\dot{q}_{ref}}{\sigma\varepsilon}\right)^{1/4}} \tag{7}$$

which can be evaluated for radiation-equilibrium wall temperatures at flight conditions by a simple iterative procedure. The emissivity ε was held constant at 0.9 throughout.

Methodology for Calculating Turbulent Heating

The procedure used to calculate turbulent heating was based on conical-flow edge conditions. The conical-flow assumption was adopted on the basis of previous work at the Johnson Space Center as illustrated in figure 16 where experimental pressure data along the lower-surface center line are compared with wedge and conical-flow estimates. The conical-edge conditions were used in conjunction with empirical reference-temperature techniques to calculate a turbulent-to-laminar heat-transfer-coefficient ratio U_{turb}/U_{lam}. The turbulent flight heating was then determined by simply applying this ratio to the laminar flight values based on the wind-tunnel data.

The following approach was established to approximate conical-flow conditions at the edge of the boundary layer. A conical shock angle was estimated from the simple relation

$$\theta_s = \alpha^{1.035} \tag{8}$$

which is an empirical fit of data from reference 8 and gives reasonable results for Mach numbers above 10. The following relations were also taken from reference 8 to calculate conditions immediately behind the conical shock angle θ_s:

$$\frac{p_s}{p_\infty} = \xi = \frac{2\gamma M_\infty^2 \sin^2\theta_s - (\gamma - 1)}{\gamma + 1} \tag{9}$$

$$\left(\frac{V_s}{V_\infty}\right)^2 = 1 - \frac{2(\xi^2 - 1)}{M_\infty^2[(\gamma + 1)\xi + (\gamma - 1)]} \tag{10}$$

$$\frac{T_s}{T_\infty} = \xi\left[\frac{(\gamma - 1)\xi + (\gamma + 1)}{(\gamma + 1)\xi + (\gamma - 1)}\right] \tag{11}$$

$$\frac{\rho_s}{\rho_\infty} = \frac{p_s}{p_\infty}\left(\frac{T_s}{T_\infty}\right)^{-1} \tag{12}$$

$$M_s^2 = \frac{M_\infty^2[(\gamma + 1)\xi + (\gamma - 1)] - 2(\xi^2 - 1)}{\xi[(\gamma - 1)\xi + (\gamma + 1)]} \tag{13}$$

The conical pressure at the boundary-layer edge was approximated by

$$\frac{p_c}{p_\infty} = \frac{\gamma M_\infty^2 \sin^2\alpha}{1 - \frac{1}{4}\left(\frac{M_{ns}^2 + 5}{6M_{ns}^2}\right)} \tag{14}$$

where M_{ns} is an effective Mach number normal to the shock and is defined by

$$M_{ns} = (0.87M_\infty - 0.554)\sin\alpha - 0.53 \tag{15}$$

This expression coupled with equation (14) has been assessed and shown to be very accurate in an appendix to reference 9. The conical compression between shock and boundary-layer edge was calculated from equations (9) and (14):

$$\frac{p_c}{p_s} = \frac{p_c}{p_\infty}\left(\frac{p_s}{p_\infty}\right)^{-1} \tag{16}$$

The following isentropic relations were employed to define the edge conditions further:

$$\frac{T_c}{T_\infty} = \frac{T_s}{T_\infty}\left(\frac{p_c}{p_s}\right)^{\frac{\gamma-1}{\gamma}} \tag{17}$$

$$\left(\frac{V_c}{V_\infty}\right)^2 = \left(\frac{V_s}{V_\infty}\right)^2 \left\{\frac{2}{(\gamma - 1)M_s^2}\left[1 - \left(\frac{p_c}{p_s}\right)^{\frac{\gamma-1}{\gamma}}\right] + 1\right\} \tag{18}$$

$$\frac{\rho_c}{\rho_\infty} = \frac{p_c}{p_\infty}\left(\frac{T_c}{T_\infty}\right)^{-1} \tag{19}$$

Viscosity was determined from the Sutherland equation

$$\mu_c = \frac{2.329 \times 10^{-8} T_c^{3/2}}{T_c + 215.933} \tag{20}$$

and local Mach number was determined from

$$M_c^2 = \frac{\rho_c V_c^2}{\gamma_c} \tag{21}$$

A set of modified Eckert reference temperatures were calculated by

$$\frac{T^*}{T_c} = 1.0 + 0.0393\eta_r M_c^2 + 0.5\left(\frac{T_w}{T_c} - 1\right) \tag{22}$$

where T_w is the wall temperature and η_r is the recovery factor which was taken to be $\sqrt{N_{Pr}}$ for laminar flow and $\sqrt[3]{N_{Pr}}$ for turbulent flow. The Prandtl number N_{Pr} was held constant at 0.71 throughout this study. A reference Reynolds number was calculated from

$$R_x^* = R_{c,x}\left(\frac{T^*}{T_c}\right)^{-1.76} \tag{23}$$

where

$$R_{c,x} = \frac{\rho_c V_c x}{\mu_c} \tag{24}$$

A laminar Stanton number was approximated from

$$N_{St,lam} = \frac{0.332\sqrt{3}}{\sqrt{R_x^* N_{Pr}^{2/3}}} \tag{25}$$

and a turbulent Stanton number was approximated from

$$N_{St,turb} = \frac{0.222(1.15)}{\left(\log_{10} R_x^*\right)^{2.584}} \tag{26}$$

which is based on a Prandtl-Schlichting relation for average skin-friction coefficient. Since the heat-transfer coefficient can be defined in terms of Stanton number as

$$U = gV\rho c_p N_{St} \tag{27}$$

the turbulent heat-transfer coefficient becomes simply

$$U_{turb} = U_{lam}\frac{N_{St,turb}}{N_{St,lam}} \tag{28}$$

The turbulent convective heating can be defined as

$$\dot{q}_{turb} = U_{turb}(T_{aw} - T_w) \tag{29}$$

and set equal to the radiant heating to yield

$$\sigma\varepsilon T_w^4 = U_{turb}(T_{aw} - T_w) \tag{30}$$

Equations (22) to (30) can be iterated for the turbulent radiation-equilibrium wall temperature. One or two iterations are all that are required if the values of laminar radiation-equilibrium temperatures are used as a first guess.

RESULTS AND DISCUSSION

Comparisons for Nominal-Design 14414.1 Entry Trajectory

Laminar heating.- The experimental values of U/U_{ref} were assumed laminar and were utilized to calculate the laminar radiation-equilibrium heating rates and surface temperatures at four spanwise locations over the nominal-design 14414.1 entry trajectory. Figure 17 presents a summary comparison of the peak laminar heating rates from the aerodynamic-heating design-data book with those determined in this study which occur at $R_{\infty,l} \approx 1 \times 10^6$. The present estimates are considerably lower than those from the design-data book, approximately 60 percent at the center line and the outboard span location ($2y/b = 0.70$). In the region beginning at $2y/b = 0.40$ and ending at approximately $2y/b = 0.55$, the conservatism in peak heating exhibited by the design-data book is diminished. This diminished conservatism is most evident at the 55-percent span location where less than a 10-percent margin is exhibited beginning approximately halfway down the wing chord ($x/c = 0.5$). However, it should be noted that the design data are still conservative everywhere when compared with the experimental laminar-heating predictions presented here.

Turbulent heating.- An estimate of turbulent heating rates was also made for the nominal-design 14414.1 trajectory. This analysis did not depend on any estimate of onset of transition; instead, a turbulent-heating calculation was made by scaling the laminar-heating values of the wind-tunnel data for U/U_{ref} throughout the trajectory to define an upper boundary for the heating. In this way the effect of any subsequent estimate of transition on lower-surface heating could be evaluated immediately.

Comparison of design and current estimates.- Figure 18 presents the present-study estimates of laminar and turbulent heating-rate histories as well as those from the aerodynamic-heating design-data book at five axial locations ($x/c = 0.10$, 0.25, 0.50, 0.75, and 0.90) for the four locations of maximum span ($2y/b = 0.00$, 0.40, 0.55, and 0.70). The 10-percent axial-location ($x/c = 0.10$) data are illustrated in figure 18(a). The solid curves are direct traces of the design-data-book histories. The data-book four-digit identification numbers (body points), as well as scales and units of heating rates, were retained for easy reference. The design-data-book four-digit curve letters (ABCD) can also be used to identify quickly the general surface locations for the data presented herein. When $A = 1$ and $D = 0$ (i.e., 1BC0), the curve is identified with the lower-surface fuselage center line. For the center-line curves, BC defines the nondimensional axial location x/l. When $A = 2$, the curve corresponds to a location on the lower surface of the wing. For these lower-wing curves, B identifies the orbiter half-span location (i.e., $B = 2y/b \times 10$) and CD identifies the percentage of local wing chord (i.e., $CD = x/c \times 100$). The design-data book does not contain curves at the 55-percent spanwise location; therefore, the curves at the 50-percent (2510) and the 60-percent (2610) span locations were

included for comparison. The jagged appearance of the present calculations is primarily a result of the stepwise approximation of the design trajectory.

The heating estimates from the aerodynamic-heating design-data book are sufficient to accommodate turbulent heating for the forward locations (x/c = 0.10) on the 40- and 70-percent span locations. At the center line and the 55-percent span locations, however, the current estimate of peak turbulent heating is approximately 30 percent higher than the design data. Greater disparity (turbulent to laminar and turbulent to design-data book) occurs at increasing axial distances from the nose and leading edges as illustrated in figures 18(b) and 18(e). When the design-data book did not contain body points in close proximity to the calculated values, the curves on either side were reproduced and presented for comparison. For example, at 25-percent chord for the 55-percent span location, the comparison included axial points before (xx20) and after (xx30) as well as spans inboard (x5xx) and outboard (x6xx) of the point of interest.

The peak turbulent heating occurs at a later time in the trajectory than the laminar peaks which is in the correct direction to coincide with the changes in edge and reference Reynolds numbers. The reasonably good agreement in slopes and magnitudes between the turbulent heating-rate histories from this study and the turbulent-heating portions of the design-data-book curves illustrated in figure 18 is gratifying; however, the simplified approach employed here may not be rigorous enough to exclude fortuity. However, a partial validity check of the turblent-heating methodology was conducted by using the method of reference 10 at $t = 480$ sec to calculate the equivalent equilibrium airflow conditions corresponding to perfect-gas parameters defined by equations (8) to (22). Even though large variations occurred in some parameters, like static temperature and local Mach number, the ratio of turbulent to laminar Stanton numbers increased less than 10 percent. Therefore, the analysis appears adequate to infer that in the event of possible transition at 1000 sec (or earlier) into the entry, a more comprehensive and rigorous effort may be required to validate the TPS.

Heating Estimates for Proposed STS-1 Entry Trajectory

During the Shuttle Flight Certification Program the same methodology was employed to generate rapid independent estimates of the aerothermal environment associated with the proposed STS-1 entry trajectory depicted graphically in figure 1(b). Although only results for the lower surface are presented here, many other regions on the orbiter were examined during the certification prior to first flight. The upper wing, fuselage sides and top, canopy region, orbiter-maneuvering-system (OMS) pods, vertical tail, and local surface discontinuities such as the reaction-control-system (RCS) nozzles and payload bay joints and hinges were examined by this technique. The results presented here are limited to the same regions previously discussed for the TPS strength-and-integrity study: namely, the lower-surface center line along with the 40-, 55-, and 70-percent locations of maximum span. The five sets of averaged experimental heat-transfer-coefficient ratios employed to approximate the proposed STS-1 trajectory are presented in figures 9 and 12 to 15.

Since the proposed STS-1 trajectory was expected to produce a somewhat more benign aerothermal environment than the nominal-design 14414.1 trajectory, the laminar- and turbulent-heating estimates for both trajectories are presented together for easy comparison in figure 19. A general reduction in peak laminar heating during the STS-1 trajectory for longitudinal locations less than 75 percent of the local chord at all spanwise locations is readily apparent in figures 19(a) to 19(d). The

differences in heating rates and any associated aerothermal advantages during the STS-1 trajectory become less clear or pronounced toward the rear of the orbiter, probably because of the transitional and/or turbulent wind-tunnel data that had to be employed.

The estimated turbulent boundary peaks for the two trajectories tend to be more nearly equal than the laminar peaks. The major difference seems to be a later occurrence of the turbulent peaks during the STS-1 trajectory than during the nominal-entry 14414.1 trajectory. However, based on a comparison of some key parameters, for example, the Reynolds number curves presented in figure 2, it is likely that transition is also delayed approximately the same time interval. In any event, the values from the aerodynamic-heating design-data book for peak laminar heating are adequate to accommodate turbulent heating if it should occur later than 1000 sec into the nominal-design 14414.1 entry trajectory, and into the STS-1 entry as well, as long as transition (fully turbulent flow) does not occur prior to 1200 sec into the entry trajectory.

Data Comparisons of Flight Heating Rates

Flight heating rates along the lower-surface center line of the orbiter measured during the STS-1 and STS-2 entries were presented for a series of flight times and conditions in reference 11. Key trajectory parameters at eight times during the STS-1 entry and seven times during the STS-2 entry are compared with the nominal-design 14414.1 and the proposed STS-1 trajectories in figure 20. The two flight histories are fairly well represented by the proposed STS-1 trajectory. However, the Reynolds number, which is a key heating parameter, tends to be slightly higher than that proposed with the result that between 1100 and 1300 sec into the entry, it more nearly matches the Reynolds number predicted for the nominal-design 14414.1 entry trajectory.

The heating rates along the lower-surface center line are compared in figure 21 at the 10-, 25-, 50-, 75-, and 90-percent locations of the fuselage length. The laminar and turbulent heating rates estimated for the proposed STS-1 trajectory, as well as the values from the aerodynamic-heating design-data book, are presented for each longitudinal location. Except for the earliest STS-2 data point corresponding to 500 sec on the forward portion of the orbiter ($x/c \leq 0.50$) where nonequilibrium flow might be expected, the estimates appear to compare very favorably with the flight measurements. Fortunately, when disparities are noted, the estimated values tend to be conservative.

The heat-transfer-coefficient ratios from reference 3 were cross-plotted as functions of Reynolds number and angle of attack to determine wind-tunnel transition locations along the lower-surface center line. These indicated transition locations taken from a relatively smooth thermocouple model were then compared with estimates determined from reference 12, which was a phase-change-paint study at $\alpha = 30°$, to investigate the effect of simulated tile gaps on heating. The differences in transition locations between the two studies were insignificant. The combined data were used to predict the flight-transition times represented by the vertical lines in figure 21, with Reynolds numbers and angles of attack representative of the STS-1 projected trajectory.

At the forward fuselage location ($x/c = 0.10$), the two sets of flight data agree well with each other and with the estimates; there is no apparent indication of transition at this location from the flight data at any time depicted during entry, with

the possible exception of the last point for STS-2 at approximately 1350 sec. The wind-tunnel data indicated probable transition at approximately 1390 sec. Transition is more evident at the downstream locations. For example, transition apparently occurred at approximately 1250 sec at $x/c = 0.25$ during both the STS-1 and STS-2 entries.

The wind-tunnel data indicated that transition would occur at approximately 1360 sec. The laminar flight heating rates at this longitudinal location generally agree with the laminar estimates, and the turbulent flight heating rates agree with the turbulent estimates. This trend is generally true at other locations as well. The heating data at the 50-percent longitudinal location ($x/c = 0.50$) is noteworthy because of the differences in time at which transition appeared to occur during the two trajectories. Transition was apparently triggered a little after 1100 sec during the STS-1 entry, whereas it was delayed until almost 1300 sec during the STS-2 entry. The wind-tunnel data indicated probable transition at approximately 1270 sec. The flight heating rates prompted by the earlier transition are larger than the estimated laminar peak for the projected STS-1 entry, although they are well within the peak values of the aerodynamic-heating data book which are based on a nominal-design trajectory (14414.1). However, the extreme steepness of the estimated turbulent-heating curve indicates that if transition had occurred between 50 and 100 sec earlier, the heating rates would have exceeded the design-data-book curve as well. The transition times indicated by the wind-tunnel data for longitudinal locations greater than $x/c \approx 0.50$ were much earlier than those experienced in flight.

CONCLUDING REMARKS

An assessment of the heating on the lower surface of the Shuttle orbiter was conducted at the Langley Research Center over the nominal-design entry trajectory for aerodynamic heating (14414.1 trajectory) and the proposed STS-1 (first flight of the space transportation system) trajectory. Perfect-gas laminar radiation-equilibrium heating rates and surface temperatures were calculated based on a combination of thermocouple and phase-change-paint wind-tunnel data. Averaged data from a large number of phase-change-paint tests at identical test conditions were successfully applied in this study to predict detailed quantitative heating results which were comparable in accuracy to thermocouple measurements. Therefore, the utilization of repeated phase-change-paint tests to form a suitable data base for extracting averaged quantities should not be ignored as a viable approach for effectively analyzing heating over complex configurations.

The time histories of heating rates calculated for the nominal-design 14414.1 trajectory along the center line of the orbiter lower surface and the 40-, 55-, and 70-percent locations of maximum span were compared directly with curves contained in the aerodynamic-heating data book. Except for the 55-percent span location, the design data were approximately 40 percent higher during peak laminar heating than those determined in the present study. The design-data heating rates for the 55-percent span location were less than 10 percent higher than the laminar-heating estimates of this study.

Peak laminar heating rates during the proposed STS-1 trajectory tend to be of lesser magnitude but of somewhat longer duration than those estimated for the nominal-design 14414.1 trajectory. This result was not unexpected because for an insulator-type thermal protection system (TPS) such as that of the orbiter, the

maximum temperature is the most significant parameter. The calculated laminar heating rates of this study compare favorably with flight data from the STS-1 and STS-2 trajectories.

Turbulent heating rates were also calculated to represent a maximum heating boundary over the trajectories. Peak turbulent heating rates are estimated to occur 200 to 400 sec later into the entry than the peak laminar rates and can exceed the design data by 100 percent or more. The calculated turbulent heating rates also compare favorably with STS-1 and STS-2 flight data over those portions of the trajectories where transition has obviously occurred. Typical turbulent heating rates occurring prior to 1200 sec into the entry of either trajectory generally exceed the corresponding laminar peaks; and prior to 1100 sec, the heating rates tend to exceed the design-data peaks. Therefore, the time at which boundary-layer transition takes place has a significant impact on the TPS performance of the orbiter.

Langley Research Center
National Aeronautics and Space Administration
Hampton, VA 23665
April 22, 1983

REFERENCES

1. Fay, J. A.; and Riddell, F. R.: Theory of Stagnation Point Heat Transfer in Dissociated Air. J. Aeronaut. Sci., vol. 25, no. 2, Feb. 1958, pp. 73-85, 121.

2. Gentry, Arvel E.; and Smyth, Douglas N.: Hypersonic Arbitrary-Body Aerodynamic Computer Program (Mark III Version). Vol. II - Program Formulation and Listings. Rep. DAC 61552, Vol. II (Air Force Contract Nos. F33615 67 C 1008 and F33615 67 C 1602), McDonnell Douglas Corp., Apr. 1968. (Available from DTIC as AD 851 812.)

3. Herrera, B. J.: Results From a Convective Heat Transfer Rate Distribution Test on a 0.0175 Scale Model (22-0) of the Rockwell International Vehicle 4 Space Shuttle Configuration in the AEDC-VKF Tunnel B (OH49B).
   Volume 1. NASA CR-147,626, 1976.
   Volume 2. NASA CR-147,627, 1976.

4. Dye, W. H.: Heat Transfer Phase Change Paint Tests of 0.0175-Scale Model (No. 56-0) of the Rockwell International Space Shuttle Orbiter in the AEDC Tunnel B Hypersonic Wind Tunnel (Test OH25B). NASA CR-151063, 1977.

5. Dye, W. H.: Heat Transfer Phase Change Paint Tests of 0.0175-Scale Models (Nos. 21-0 and 46-0) of the Rockwell International Space Shuttle Orbiter in the AEDC Tunnel B Hypersonic Wind Tunnel (Test OH25A). NASA CR-141546, 1975.

6. Goodrich, W. D.; Li, C. P.; Houston, C. K.; Chiu, P. B.; and Olmedo, L.: Numerical Computations of Orbiter Flowfields and Laminar Heating Rates. J. Spacecr. & Rockets, vol. 14, no. 5, May 1977, pp. 257-264.

7. Jones, Robert A.; and Hunt, James L.: Use of Fusible Temperature Indicators for Obtaining Quantitative Aerodynamic Heat-Transfer Data. NASA TR R-230, 1966.

8. Ames Research Staff: Equations, Tables, and Charts for Compressible Flow. NACA Rep. 1135, 1953. (Supersedes NACA TN 1428.)

9. Pittman, Jimmy L. (appendix by C. L. W. Edwards): Application of Supersonic Linear Theory and Hypersonic Impact Methods to Three Nonslender Hypersonic Airplane Concepts at Mach Numbers From 1.10 to 2.86. NASA TP-1539, 1979.

10. Hunt, James L.; and Souders, Sue W.: Normal- and Oblique-Shock Flow Parameters in Equilibrium Air Including Attached-Shock Solutions for Surfaces at Angles of Attack, Sweep, and Dihedral. NASA SP-3093, 1975.

11. Hamilton, H. Harris, II: Approximate Method of Predicting Heating on the Windward side of Space Shuttle Orbiter and Comparisons With Flight Data. AIAA-82-0823, June 1982.

12. Quan, M.: Phase Change Paint Tests To Investigate Effects of TPS Tiles on Heating Rates of Rockwell Space Shuttle Orbiter (Test OH4C, Model 21-0). NASA CR-141505, 1975.

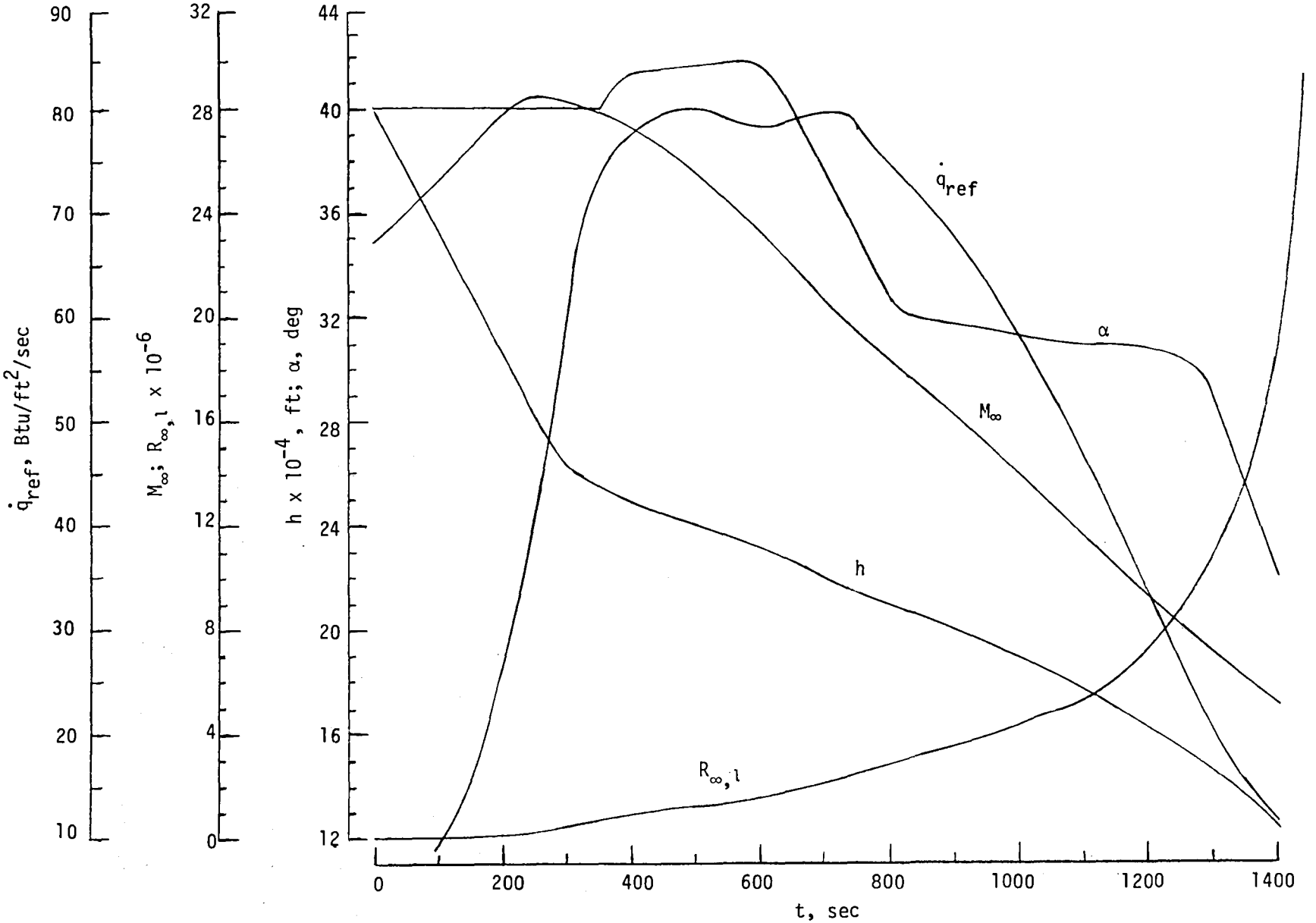

(a) 14414.1 nominal-design entry trajectory.

Figure 1.- Graphical representation of trajectories.

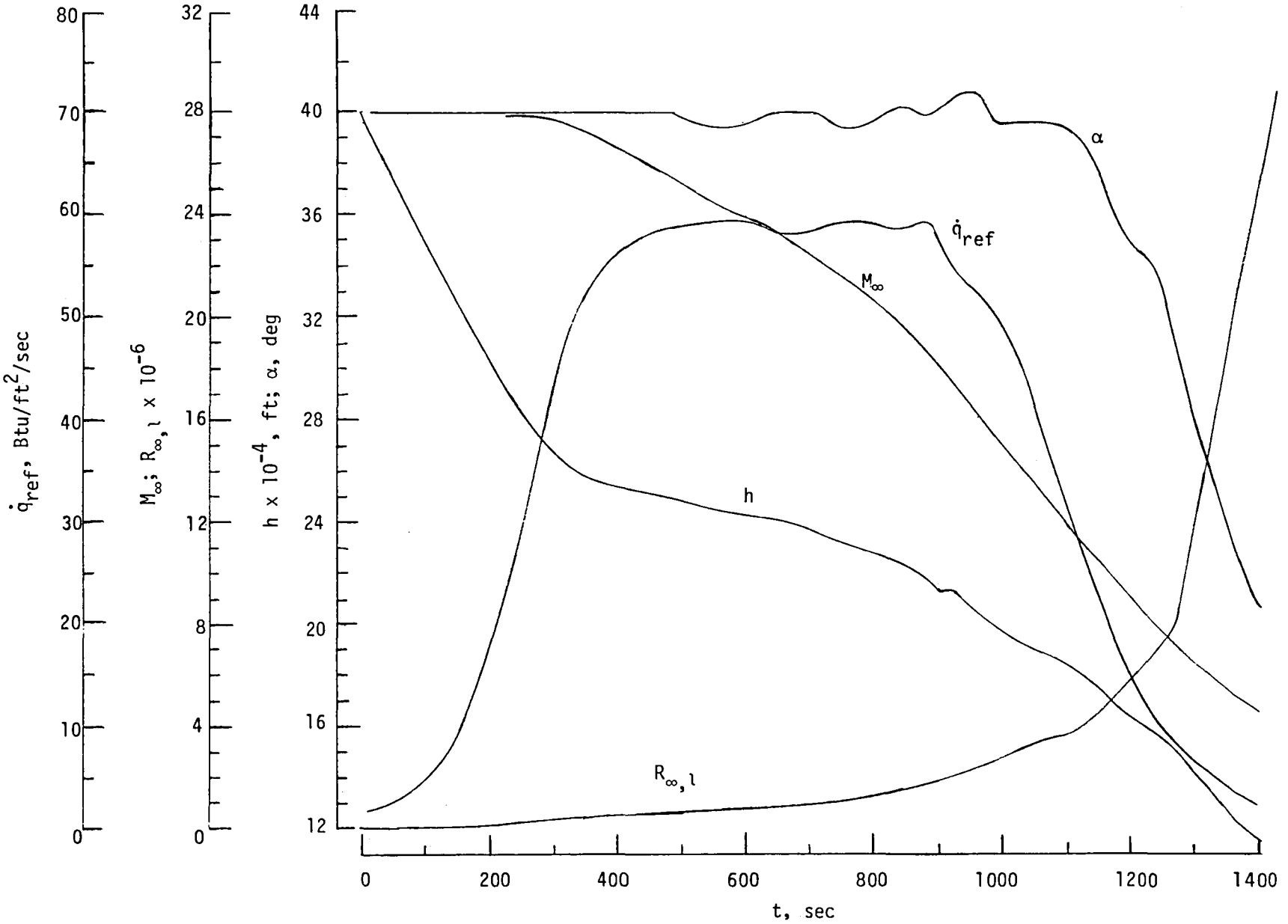

(b) Proposed STS-1 entry trajectory.

Figure 1.- Concluded.

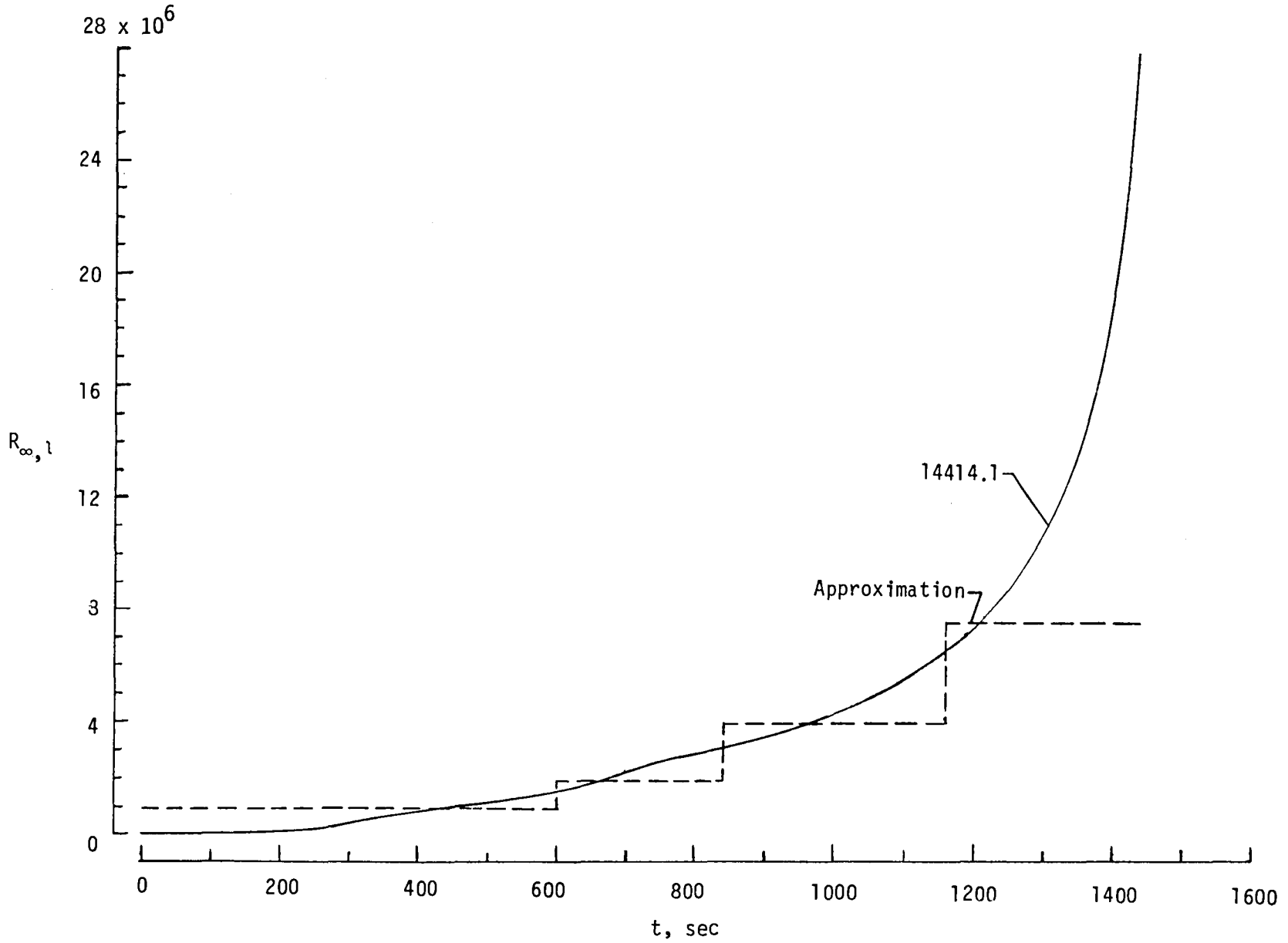

(a) 14414.1 nominal-design entry trajectory.

Figure 2.- Wind-tunnel-data approximations of trajectory Reynolds numbers.

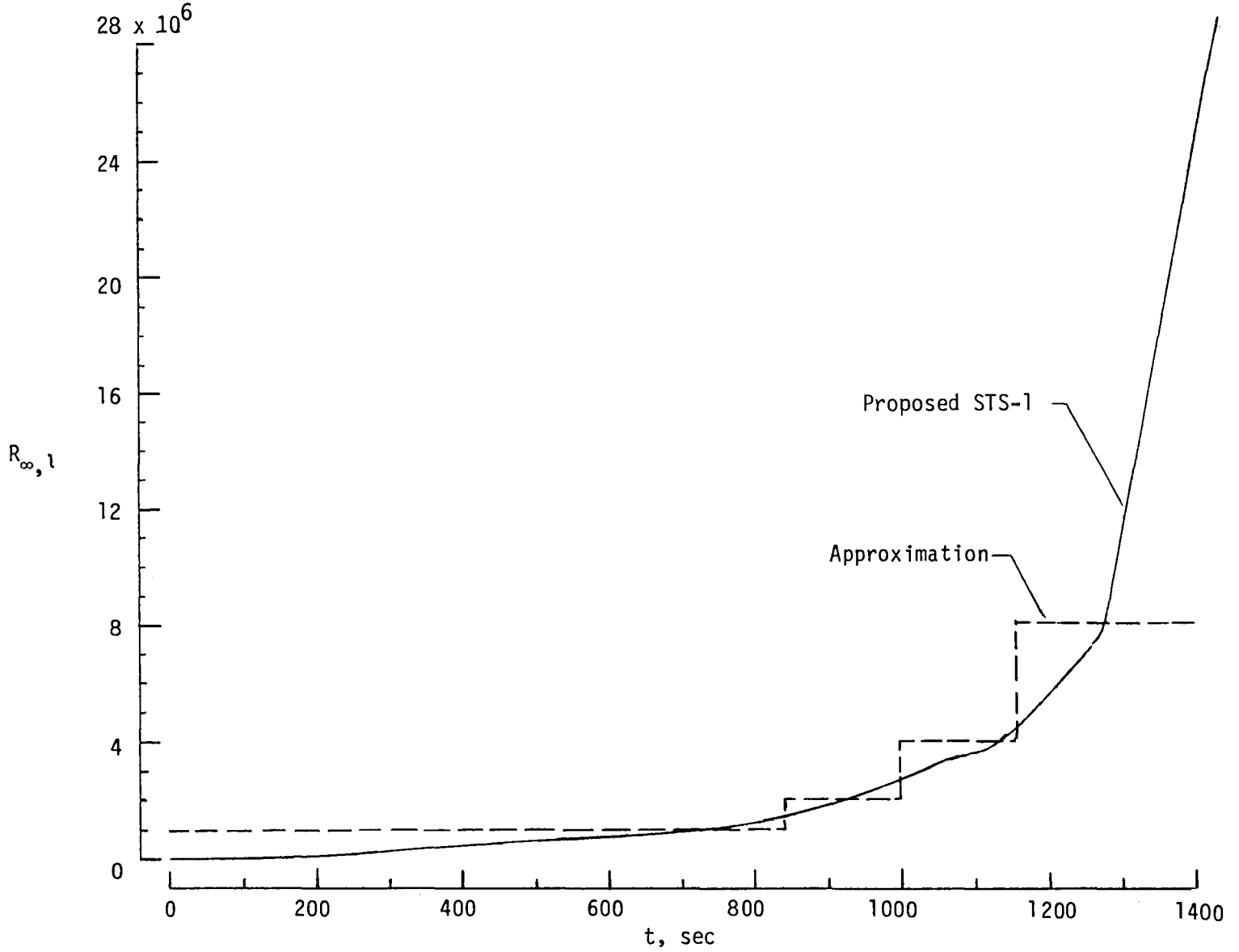

(b) Proposed STS-1 entry trajectory.

Figure 2.- Concluded.

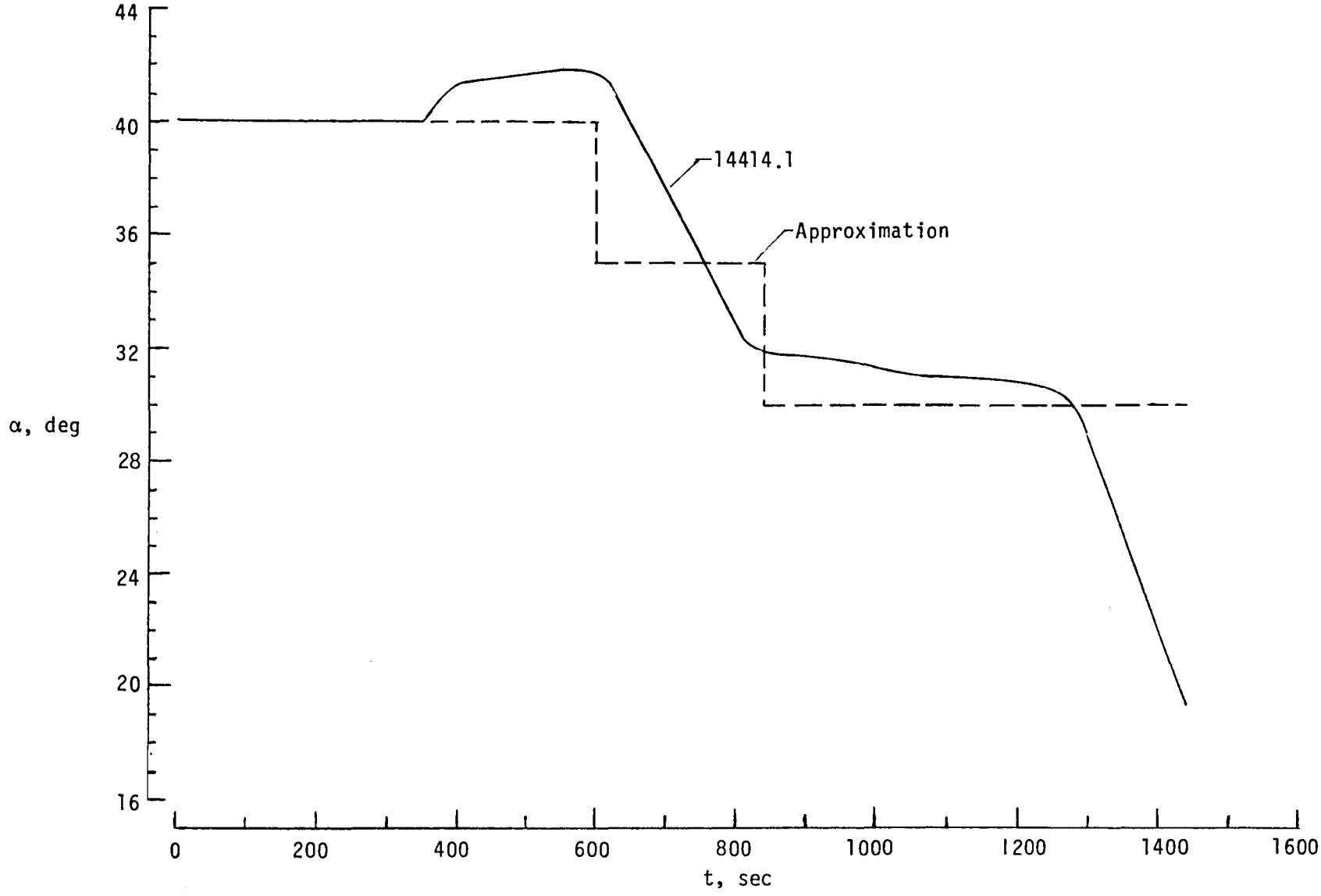

(a) 14414.1 nominal-design entry trajectory.

Figure 3.- Wind-tunnel data of orbiter angles of attack.

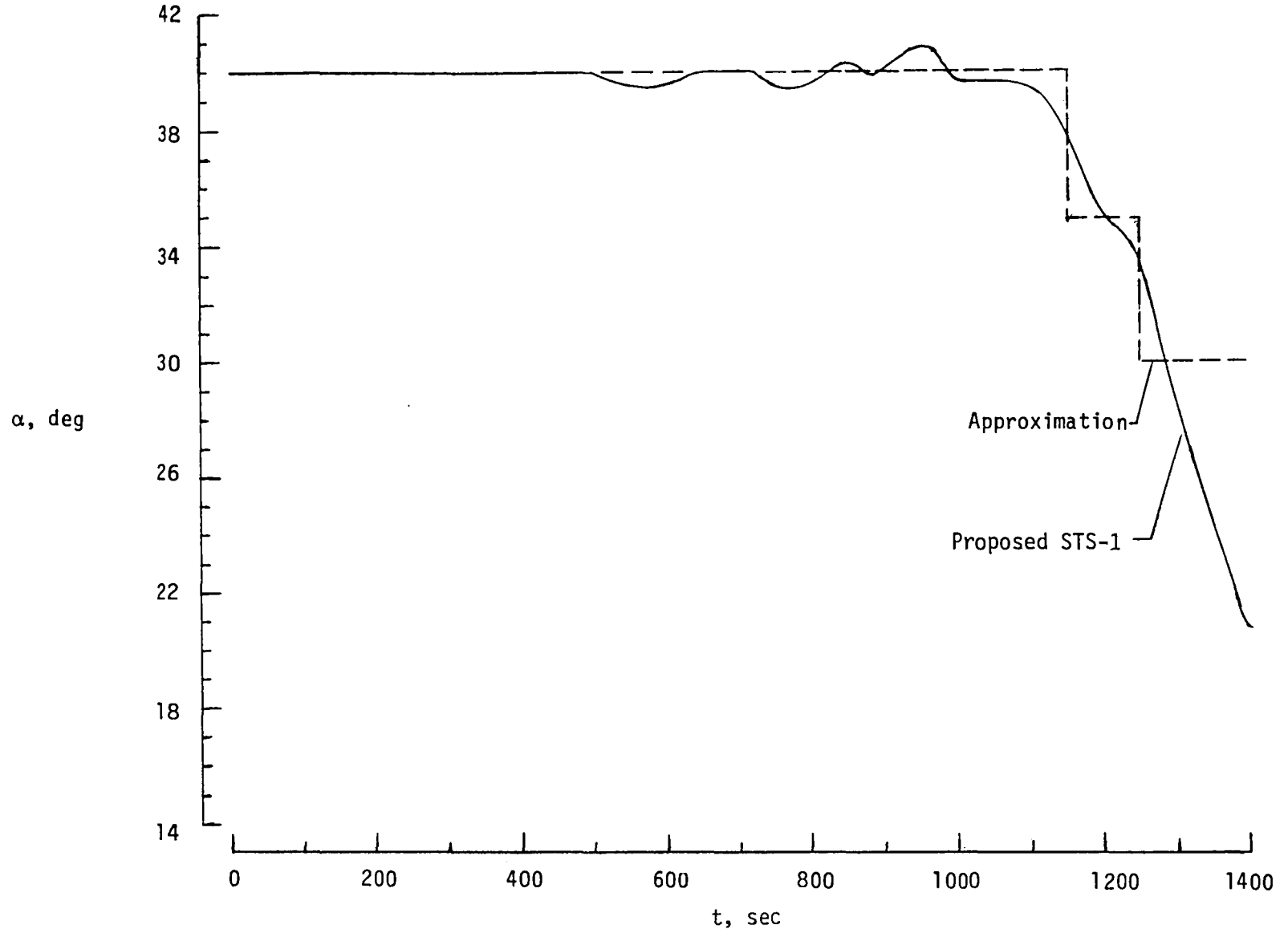

(b) Proposed STS-1 entry trajectory.

Figure 3.- Concluded.

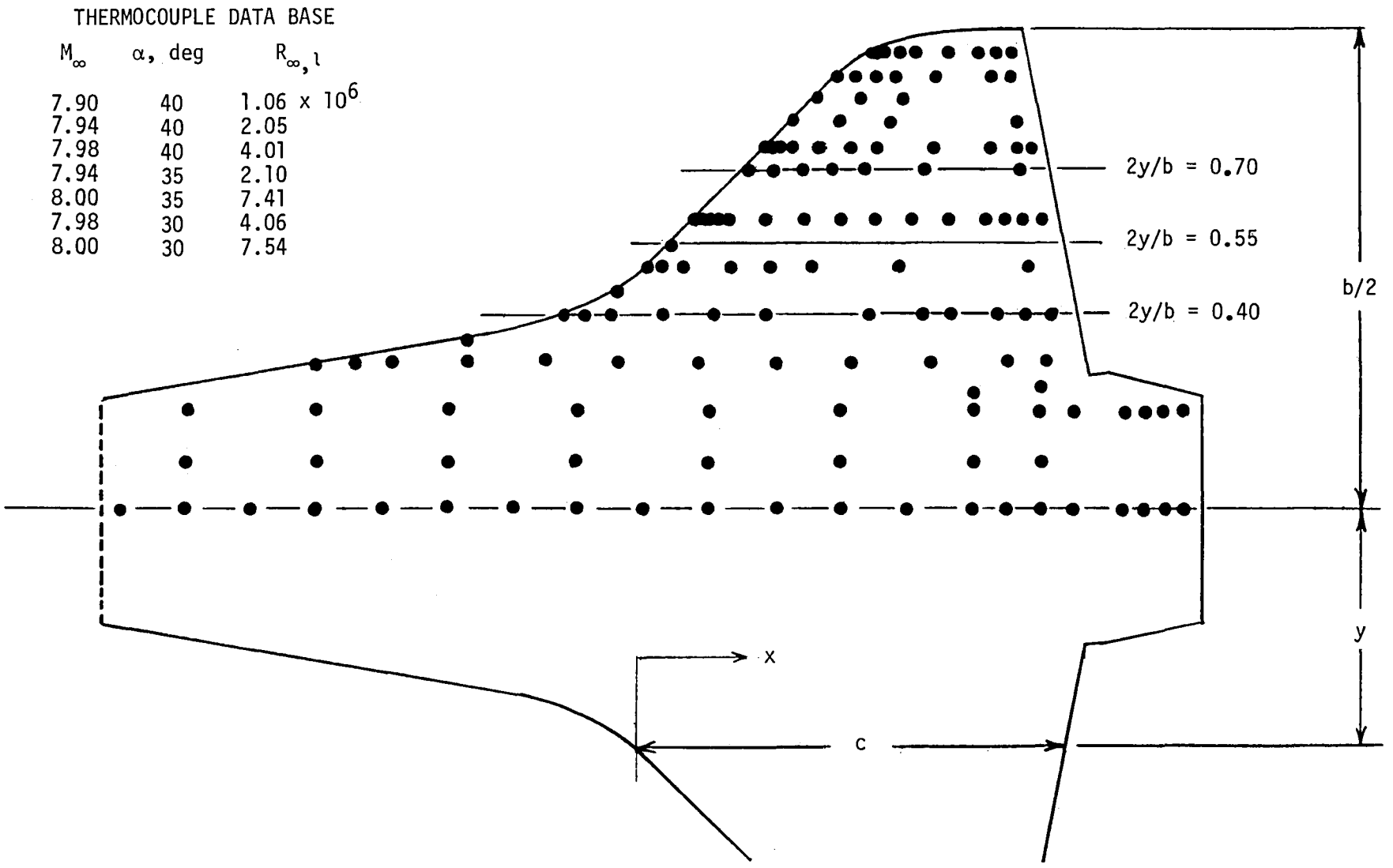

Figure 4.- Thermocouple locations on lower surface of orbiter.

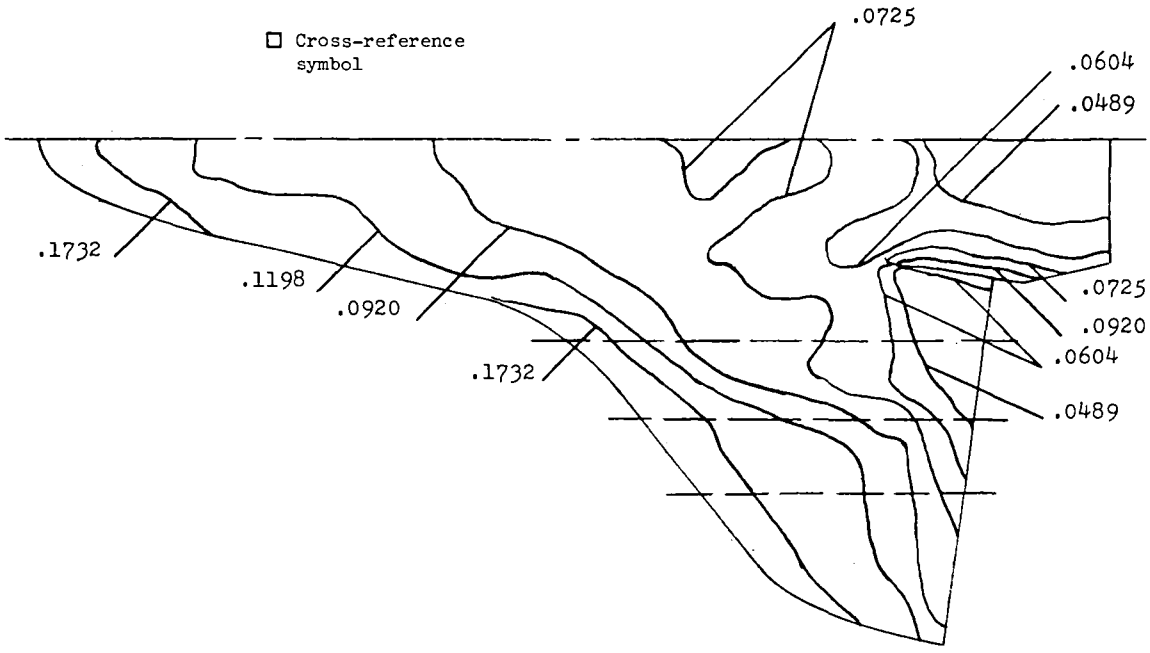

(a) $M_\infty = 7.88$; $\alpha = 40.01°$; $R_{\infty,l} = 0.937 \times 10^6$; $T_{pc} = 131°F$; data taken from reference 4.

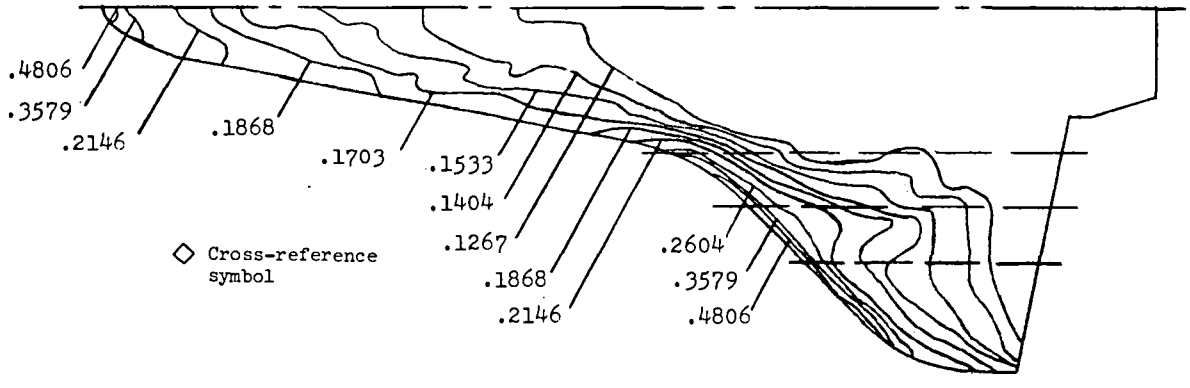

(b) $M_\infty = 7.90$; $\alpha = 40.00°$; $R_{\infty,l} = 1.03 \times 10^6$; $T_{pc} = 250°F$; data taken from reference 5.

Figure 5.- Phase-change-paint heat-transfer-coefficient ratios U/U_{ref} for $\alpha \approx 40°$ and $R_{\infty,l} \approx 1 \times 10^6$.

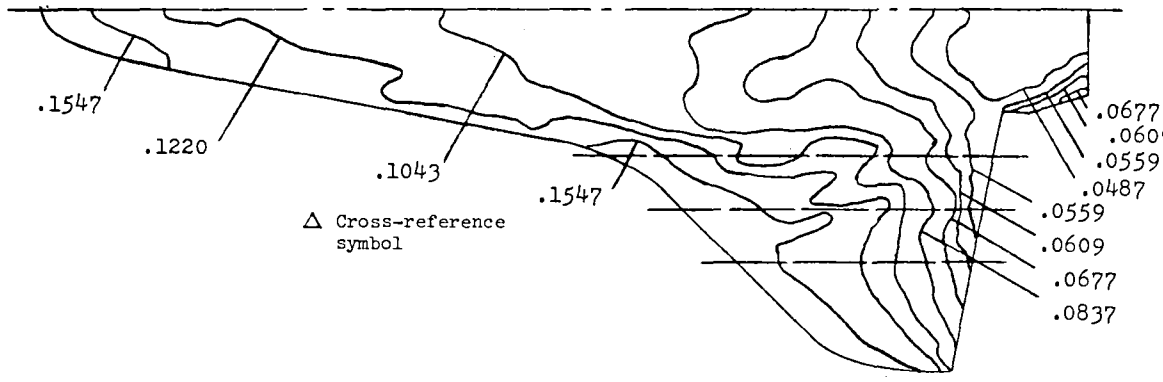

(c) $M_\infty = 7.90$; $\alpha = 40.03°$; $R_{\infty,l} = 1.03 \times 10^6$; $T_{pc} = 131°F$; data taken from reference 5.

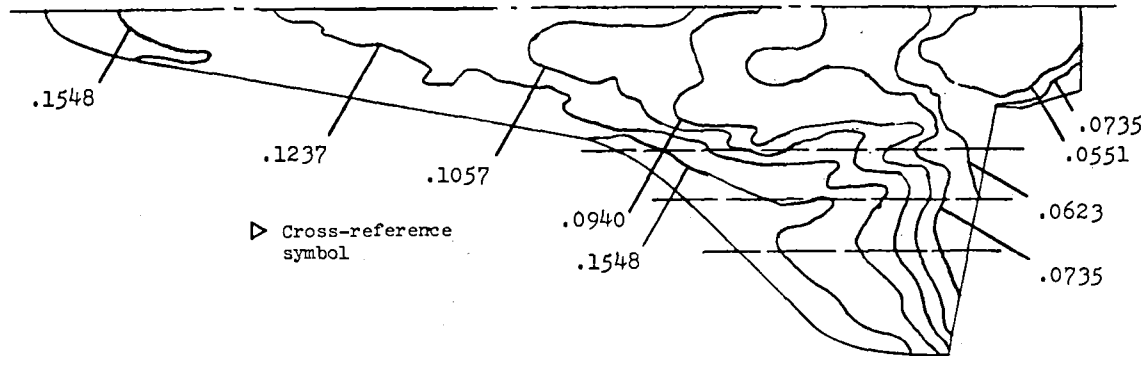

(d) $M_\infty = 7.90$; $\alpha = 40.02°$; $R_{\infty,l} = 1.04 \times 10^6$; $T_{pc} = 131°F$; data taken from reference 5.

Figure 5.- Continued.

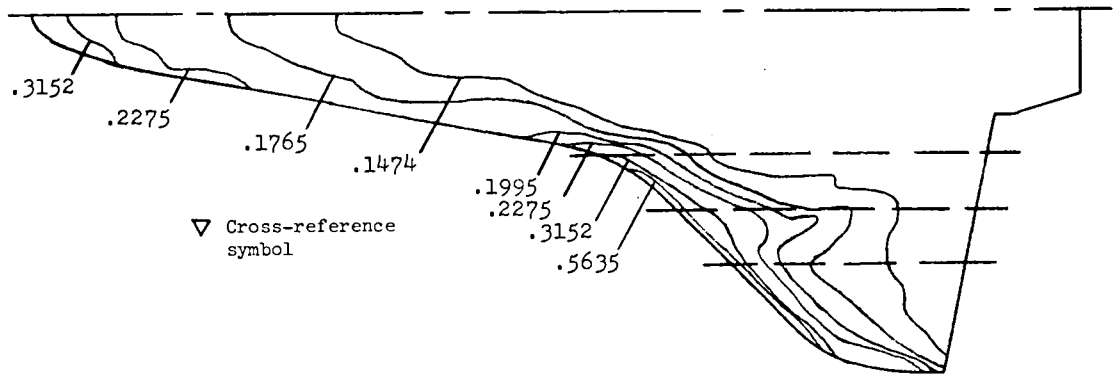

(e) $M_\infty = 7.90$; $\alpha = 40.03°$; $R_{\infty,l} = 1.04 \times 10^6$; $T_{pc} = 250°F$; data taken from reference 5.

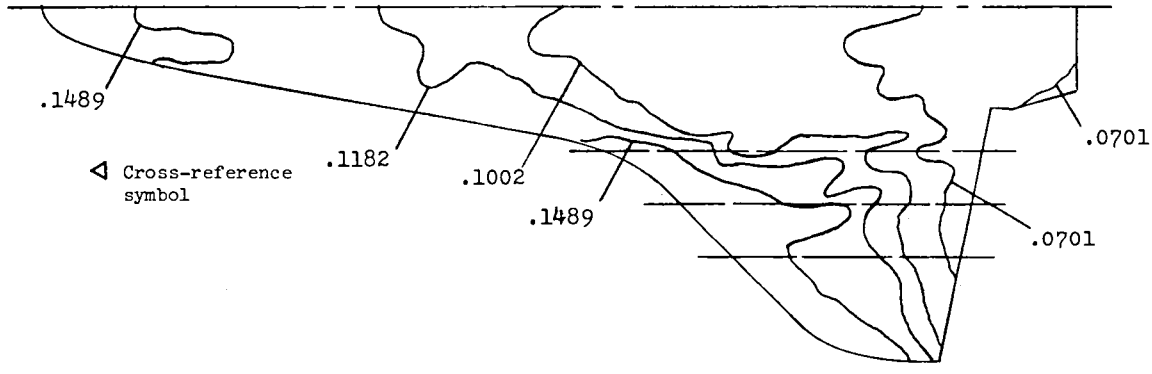

(f) $M_\infty = 7.90$; $\alpha = 40.03°$; $R_{\infty,l} = 1.05 \times 10^6$; $T_{pc} = 131°F$; data taken from reference 5.

Figure 5.- Continued.

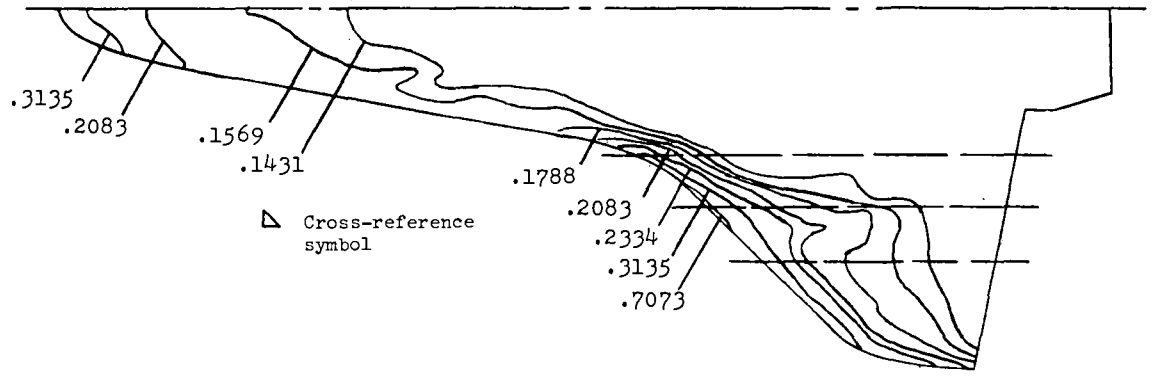

(g) $M_\infty = 7.90$; $\alpha = 40.03°$; $R_{\infty,l} = 1.03 \times 10^6$; $T_{pc} = 250°F$; data taken from reference 5.

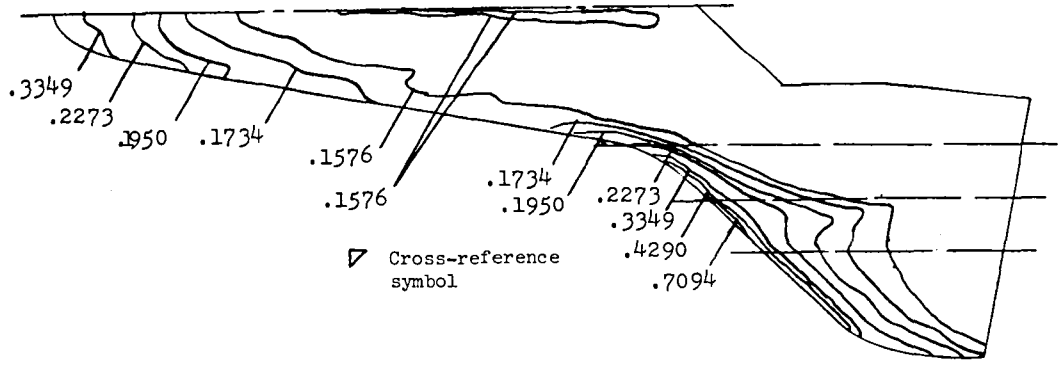

(h) $M_\infty = 7.90$; $\alpha = 40.03°$; $R_{\infty,l} = 1.05 \times 10^6$; $T_{pc} = 250°F$; data taken from reference 5.

Figure 5.- Continued.

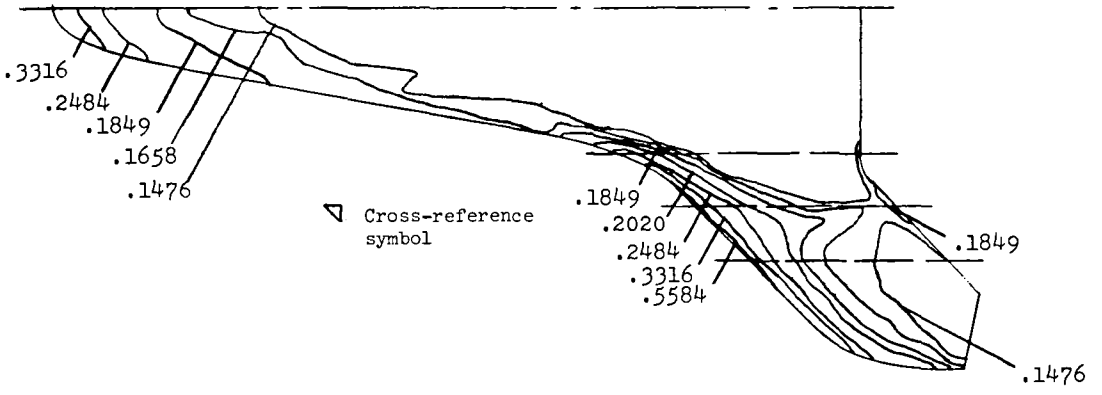

(i) $M_\infty = 7.90$; $\alpha = 40.04°$; $R_{\infty,l} = 1.03 \times 10^6$; $T_{pc} = 250°F$; data taken from reference 5.

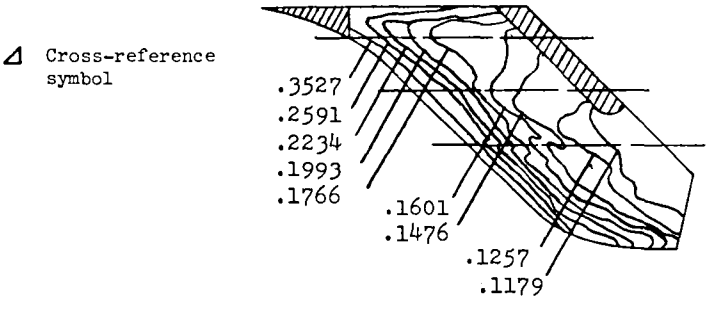

(j) $M_\infty = 7.90$; $\alpha = 40.01°$; $R_{\infty,l} = 1.05 \times 10^6$; $T_{pc} = 225°F$; data taken from reference 5.

Figure 5.- Concluded.

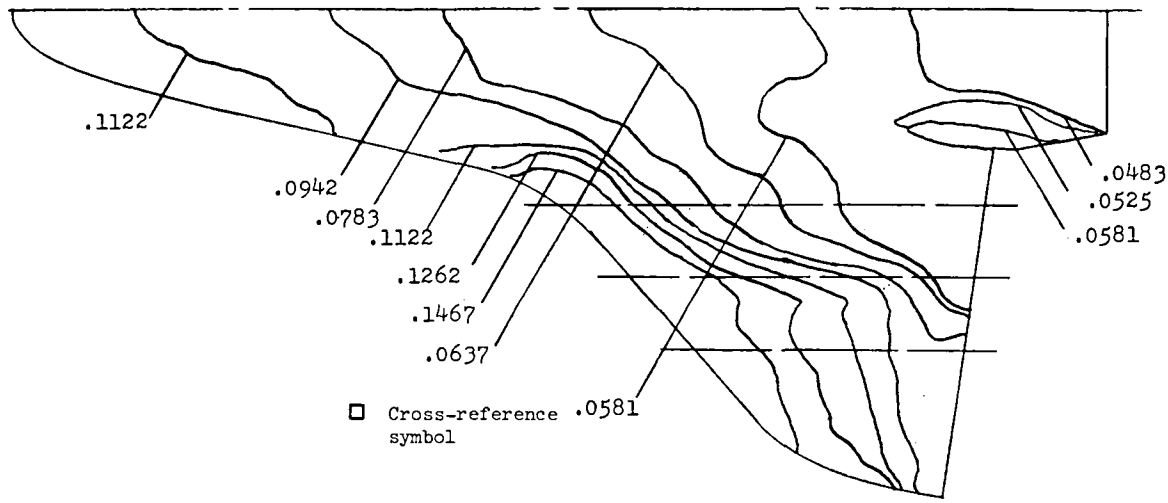

Figure 6.- Phase-change-paint heat-transfer-coefficient ratios U/U_{ref} for $\alpha = 35°$ and $R_{\infty,l} \approx 1.79 \times 10^6$. $M_\infty = 7.94$; $T_{pc} = 150°F$; data taken from reference 4.

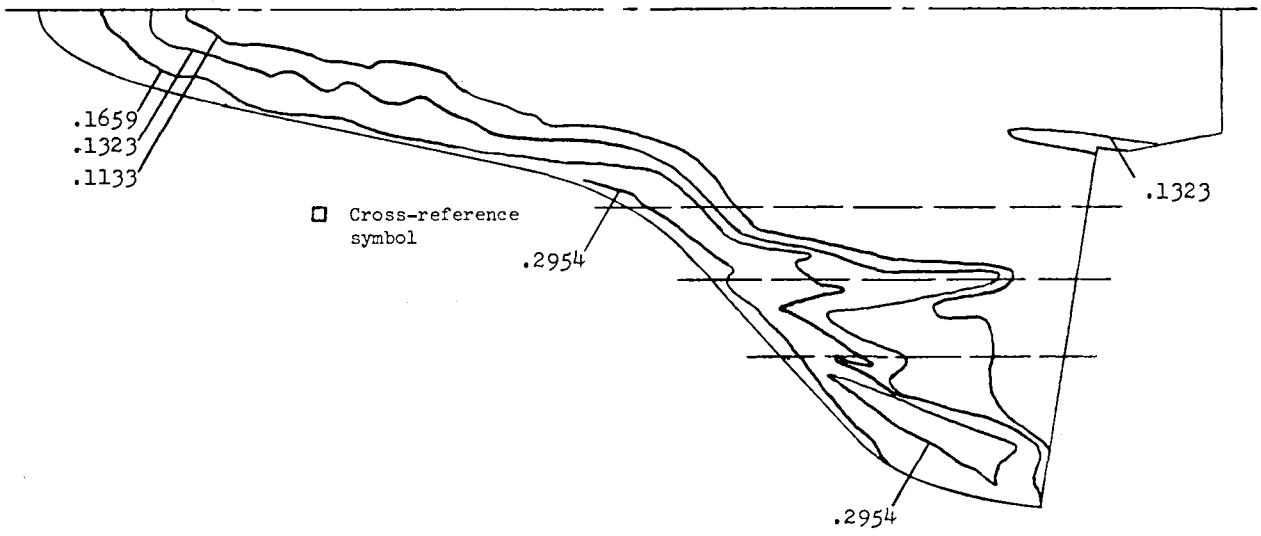

(a) $M_\infty = 7.98$; $\alpha = 30.01°$; $R_{\infty,l} = 3.73 \times 10^6$; $T_{pc} = 250°F$; data taken from reference 4.

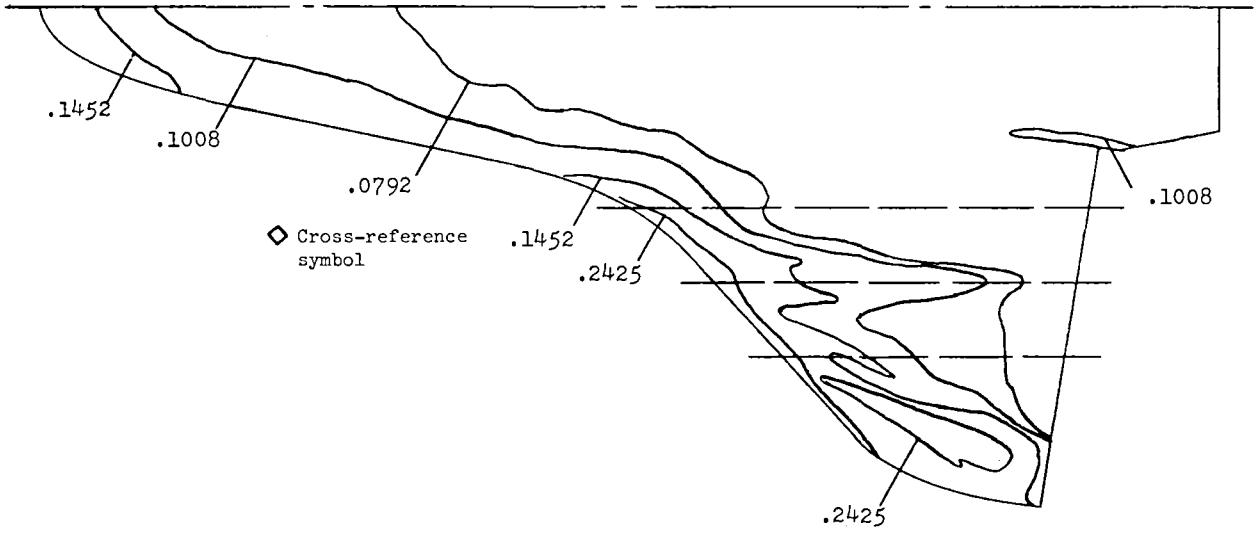

(b) $M_\infty = 7.98$; $\alpha = 29.99°$; $R_{\infty,l} = 3.70 \times 10^6$; $T_{pc} = 200°F$; data taken from reference 4.

Figure 7.- Phase-change-paint heat-transfer-coefficient ratios U/U_{ref} for $\alpha \approx 30°$ and $R_{\infty,l} \approx 3.75 \times 10^6$.

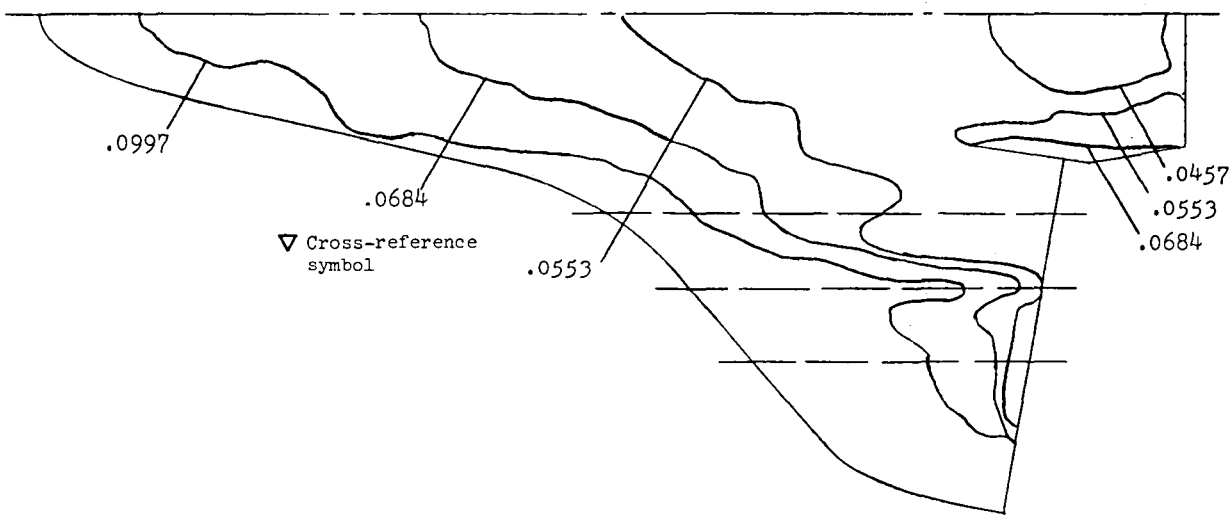

(c) $M_\infty = 7.98$; $\alpha = 30.11°$; $R_{\infty,l} = 3.68 \times 10^6$; $T_{pc} = 150°F$; data taken from reference 4.

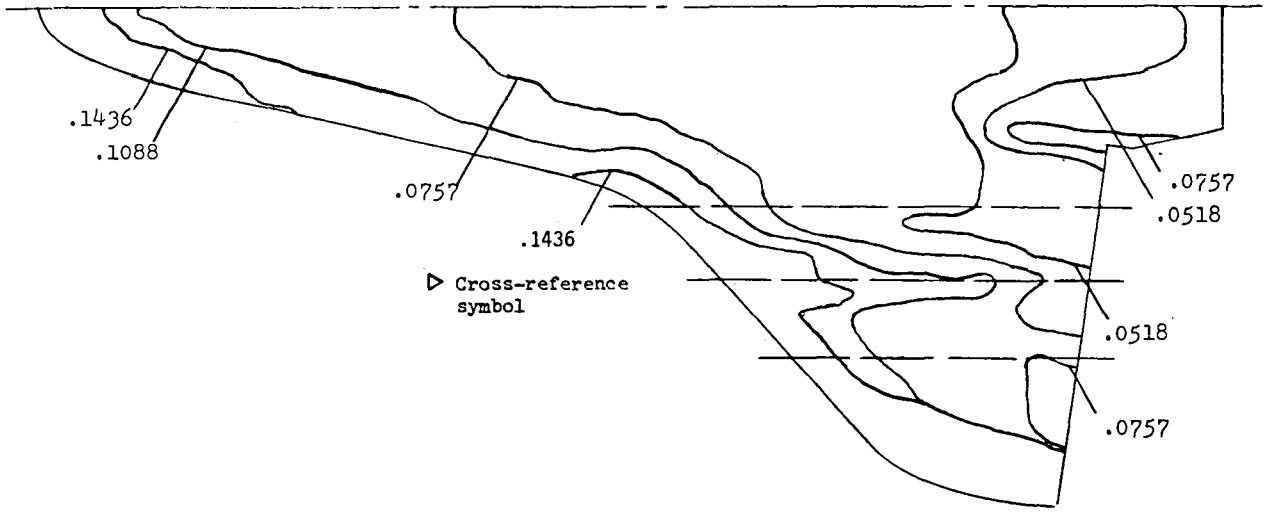

(d) $M_\infty = 7.98$; $\alpha = 30.00°$; $R_{\infty,l} = 3.67 \times 10^6$; $T_{pc} = 175°F$; data taken from reference 4.

Figure 7.- Continued.

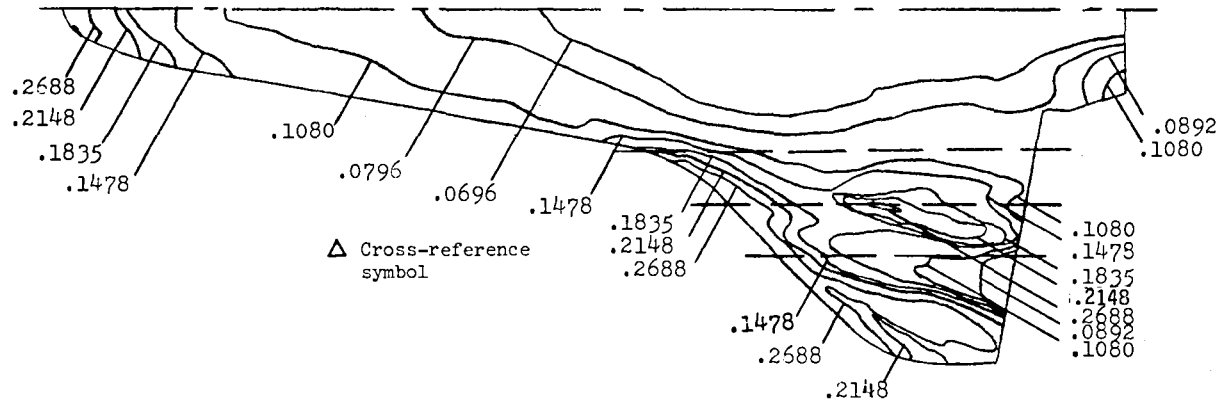

(e) $M_\infty = 7.98$; $\alpha = 30.01°$; $R_{\infty,l} = 3.70 \times 10^6$; $T_{pc} = 225°F$; data taken from reference 5.

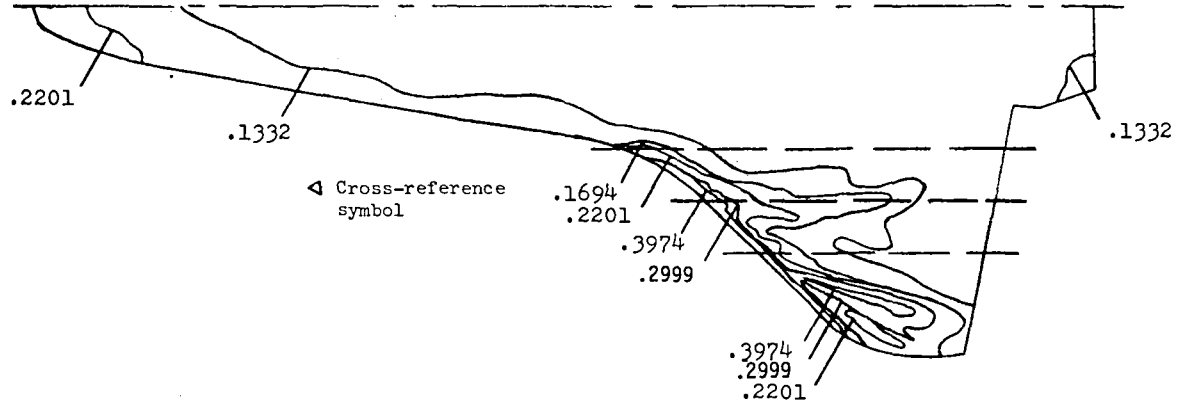

(f) $M_\infty = 7.98$; $\alpha = 30.03°$; $R_{\infty,l} = 3.75 \times 10^6$; $T_{pc} = 300°F$; data taken from reference 5.

Figure 7.- Continued.

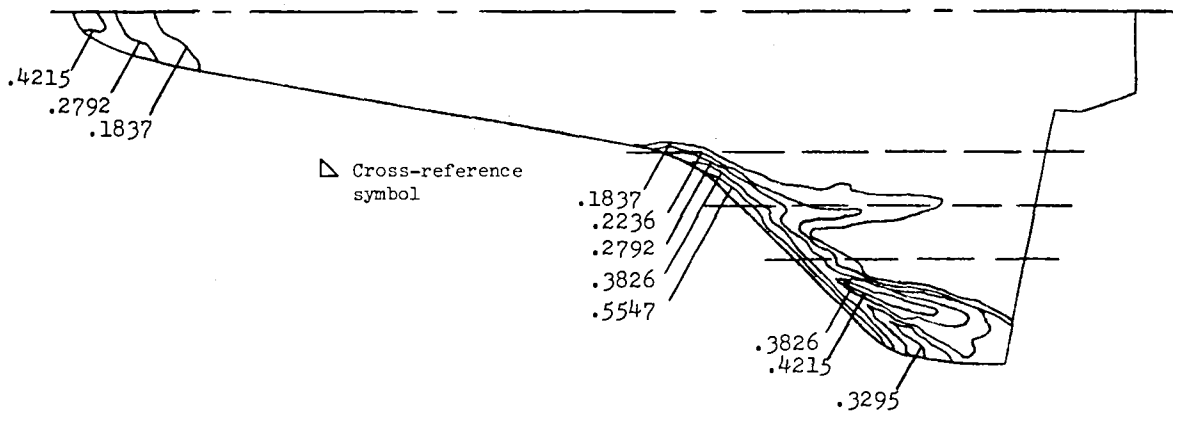

(g) $M_\infty = 7.98$; $\alpha = 30.03°$; $R_{\infty,l} = 3.80 \times 10^6$; $T_{pc} = 350°F$; data taken from reference 5.

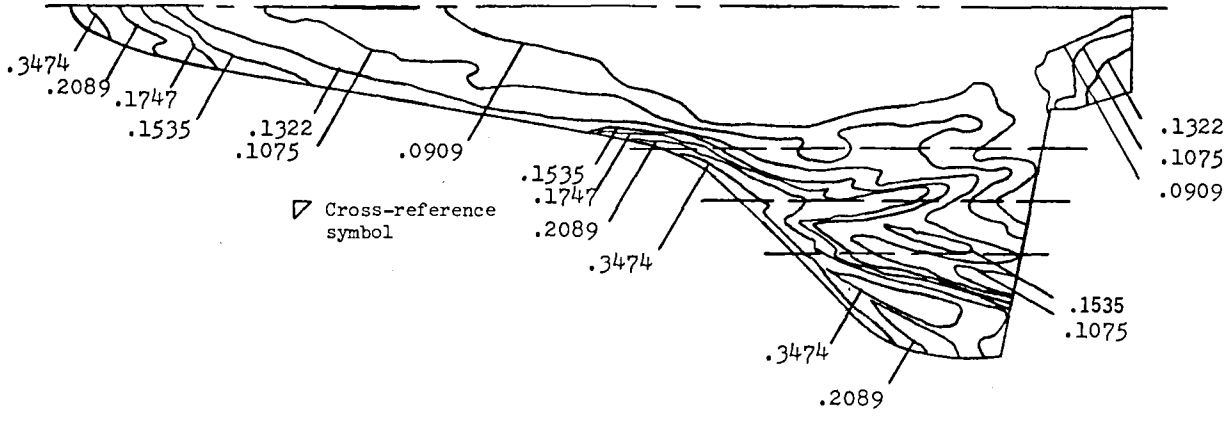

(h) $M_\infty = 7.98$; $\alpha = 30.01°$; $R_{\infty,l} = 3.72 \times 10^6$; $T_{pc} = 250°F$; data taken from reference 5.

Figure 7.- Continued.

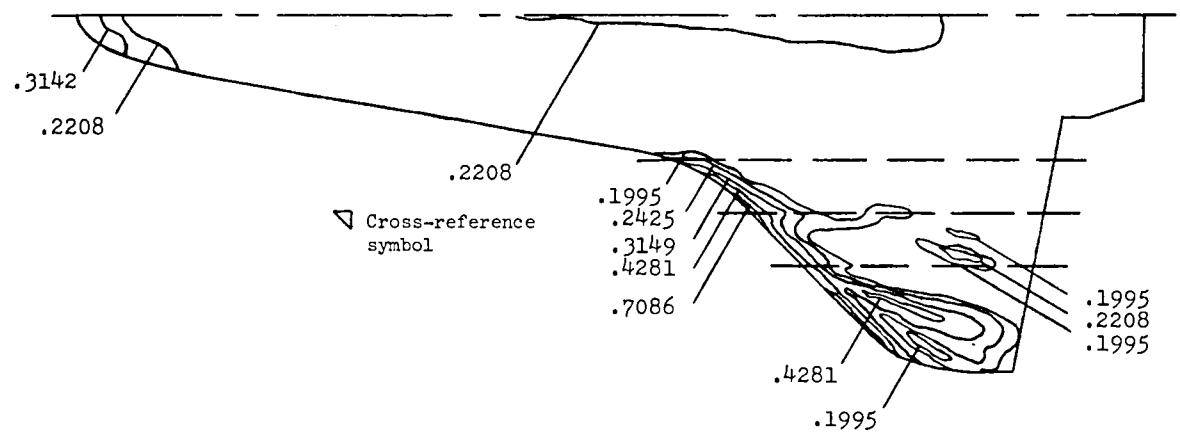

(i) $M_\infty = 7.98$; $\alpha = 30.01°$; $R_{\infty,l} = 3.80 \times 10^6$; $T_{pc} = 350°F$; data taken from reference 5.

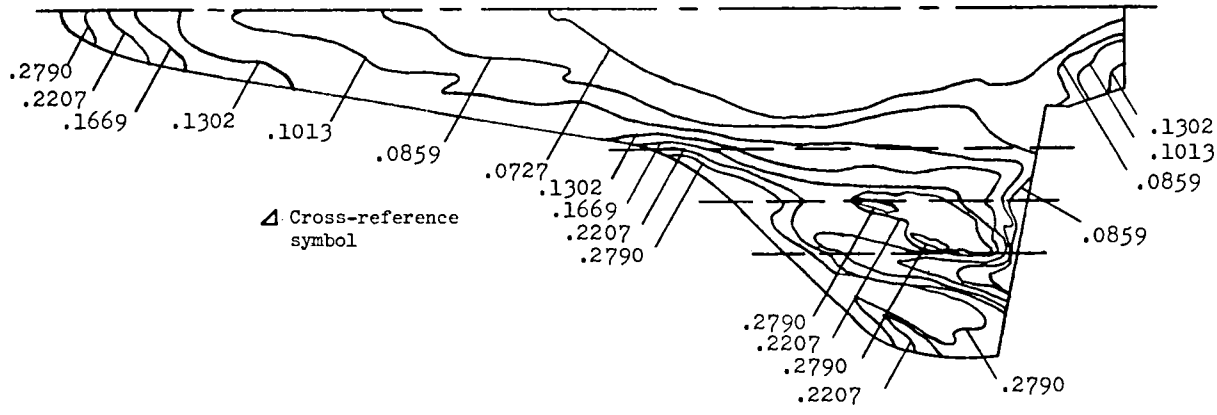

(j) $M_\infty = 7.98$; $\alpha = 30.01°$; $R_{\infty,l} = 3.75 \times 10^6$; $T_{pc} = 225°F$; data taken from reference 5.

Figure 7.- Continued.

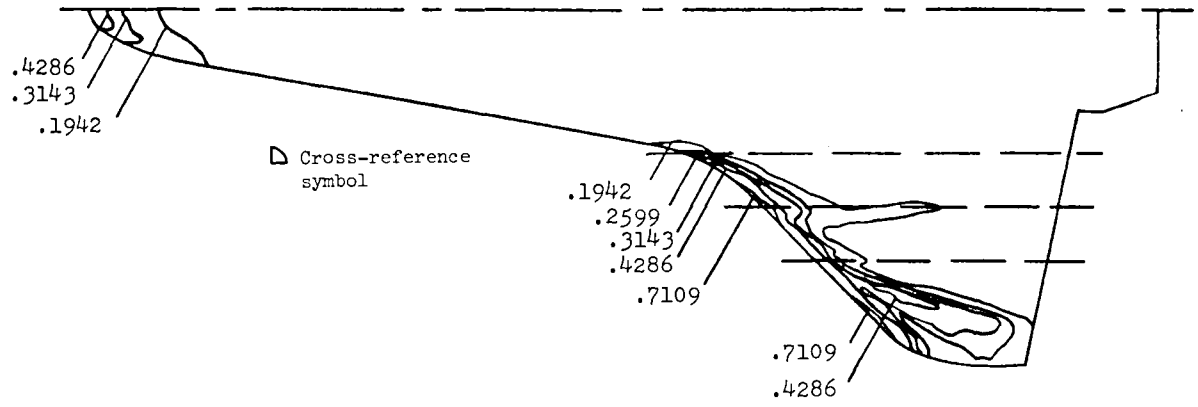

(k) $M_\infty = 7.98$; $\alpha = 30.01°$; $R_{\infty,l} = 3.79 \times 10^6$; $T_{pc} = 350°F$; data taken from reference 5.

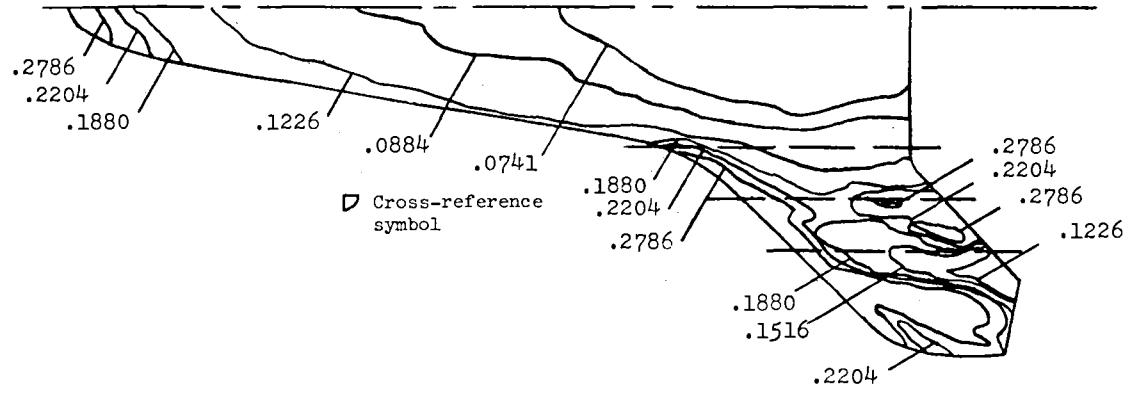

(l) $M_\infty = 7.98$; $\alpha = 30.01°$; $R_{\infty,l} = 3.73 \times 10^6$; $T_{pc} = 225°F$; data taken from reference 5.

Figure 7.- Continued.

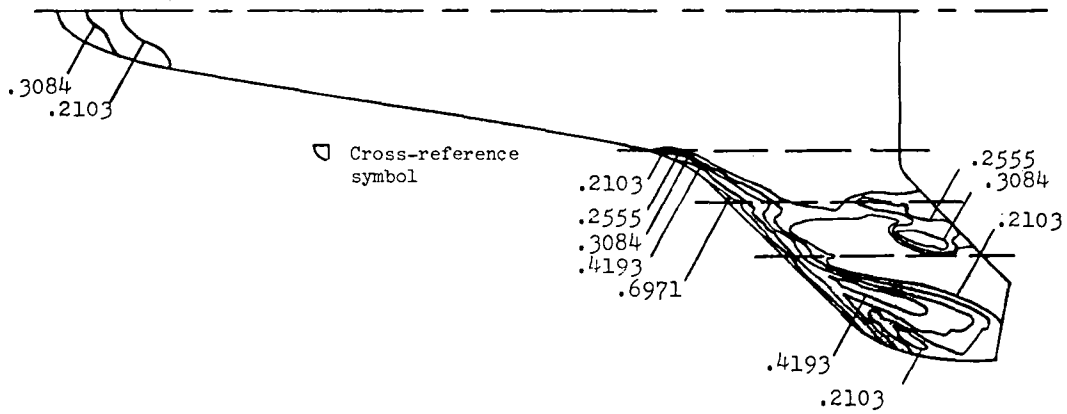

(m) $M_\infty = 7.98$; $\alpha = 30.01°$; $R_{\infty,l} = 3.77 \times 10^6$; $T_{pc} = 350°F$; data taken from reference 5.

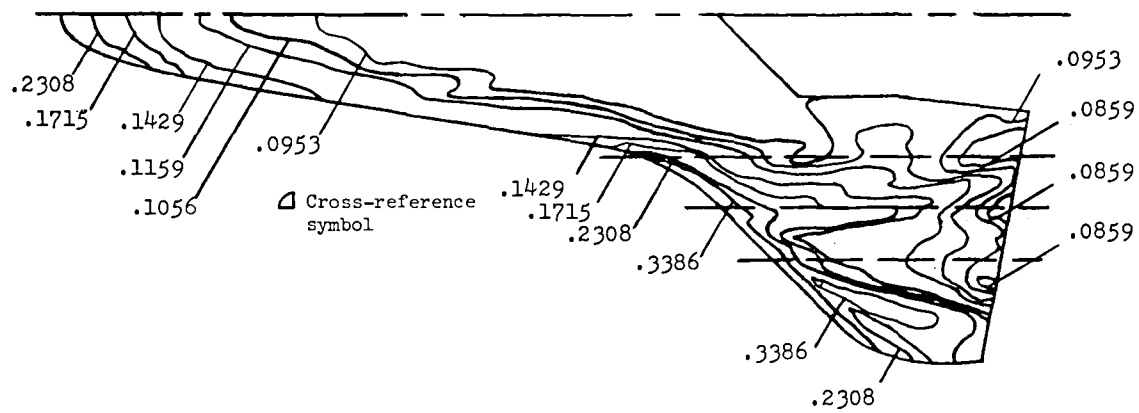

(n) $M_\infty = 7.98$; $\alpha = 30.00°$; $R_{\infty,l} = 3.74 \times 10^6$; $T_{pc} = 250°F$; data taken from reference 5.

Figure 7.- Continued.

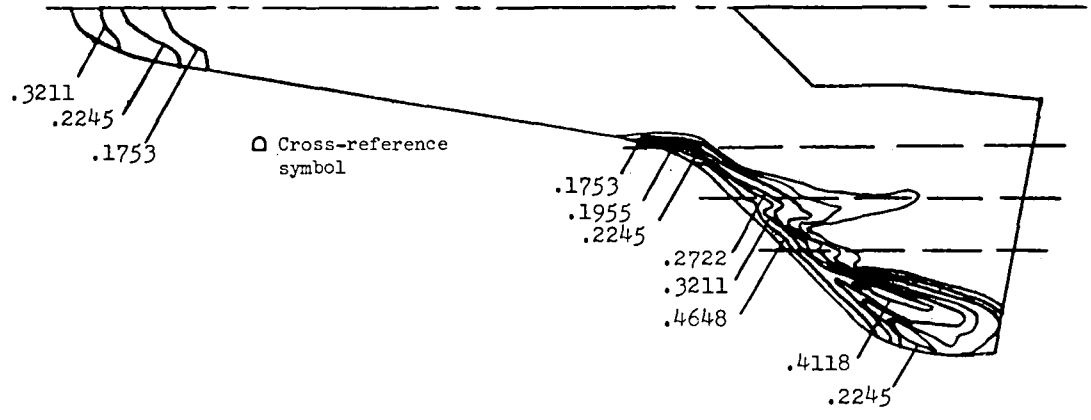

(o) $M_\infty = 7.98$; $\alpha = 30.01°$; $R_{\infty,l} = 3.74 \times 10^6$; $T_{pc} = 350°F$; data taken from reference 5.

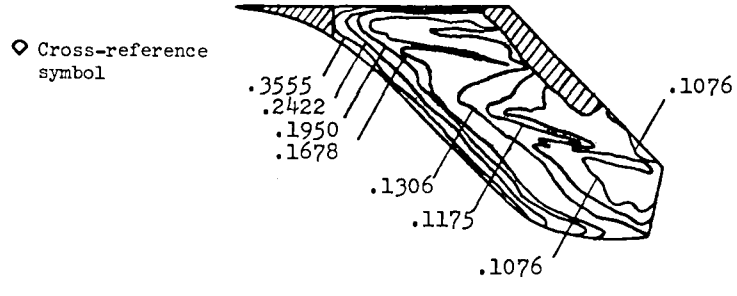

(p) $M_\infty = 7.98$; $\alpha = 30.01°$; $R_{\infty,l} = 3.76 \times 10^6$; $T_{pc} = 250°F$; data taken from reference 5.

Figure 7.- Continued.

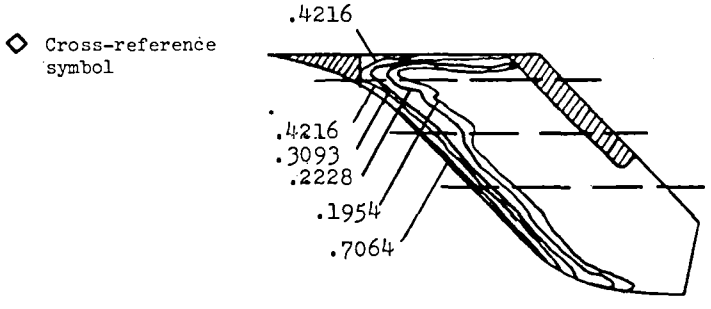

(q) $M_\infty = 7.98$; $\alpha = 30.03°$; $R_{\infty,l} = 3.78 \times 10^6$; $T_{pc} = 350°F$; data taken from reference 5.

Figure 7.- Concluded.

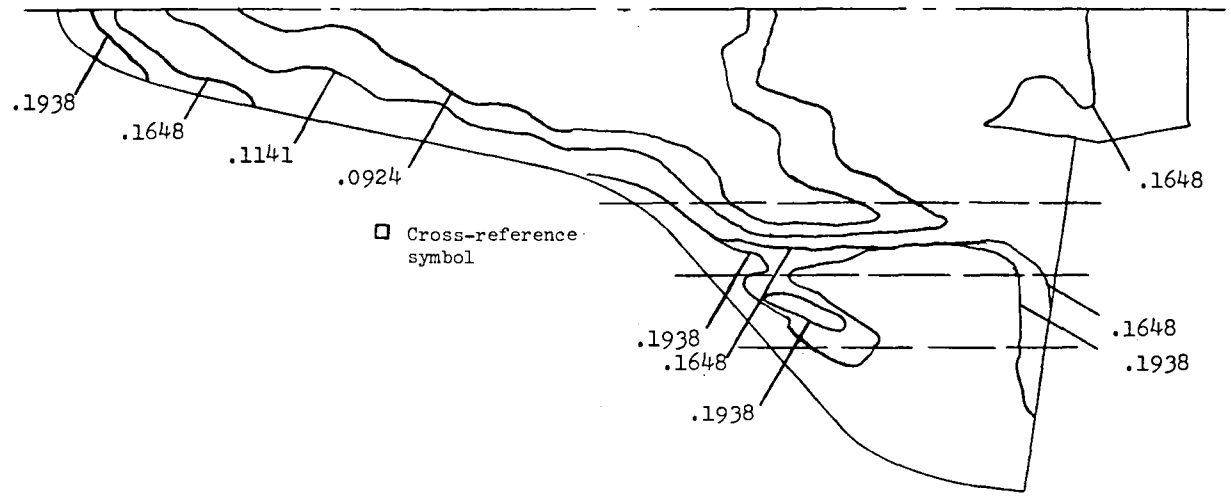

(a) $M_\infty = 8.00$; $\alpha = 30.14°$; $R_{\infty,l} = 7.08 \times 10^6$; $T_{pc} = 250°F$; data taken from reference 4.

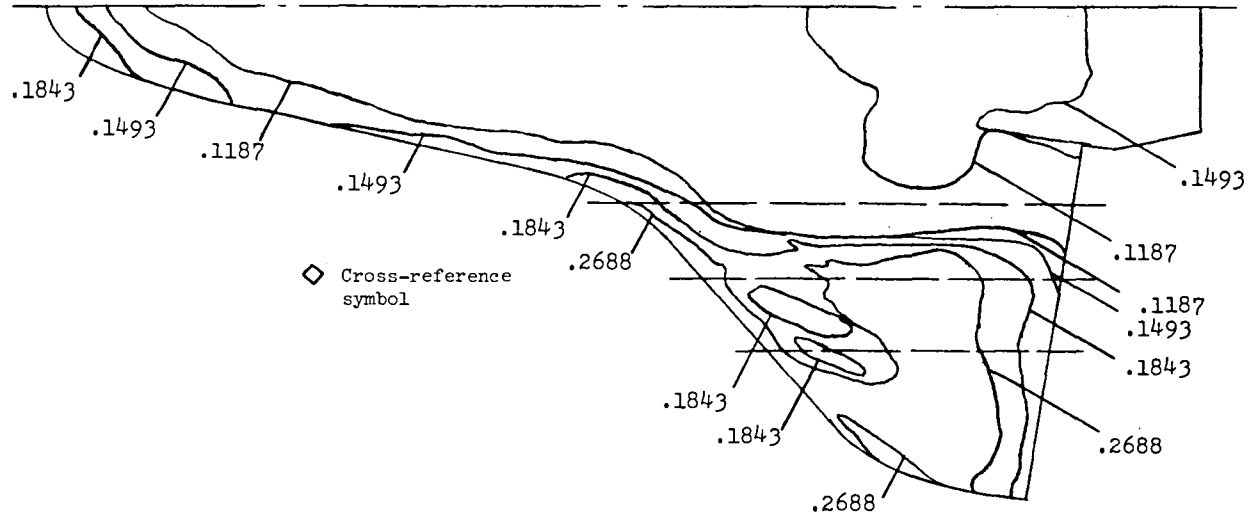

(b) $M_\infty = 8.00$; $\alpha = 30.04°$; $R_{\infty,l} = 7.10 \times 10^6$; $T_{pc} = 300°F$; data taken from reference 4.

Figure 8.- Phase-change-paint heat-transfer-coefficient ratios U/U_{ref} for $\alpha \approx 30°$ and $R_{\infty,l} \approx 7 \times 10^6$.

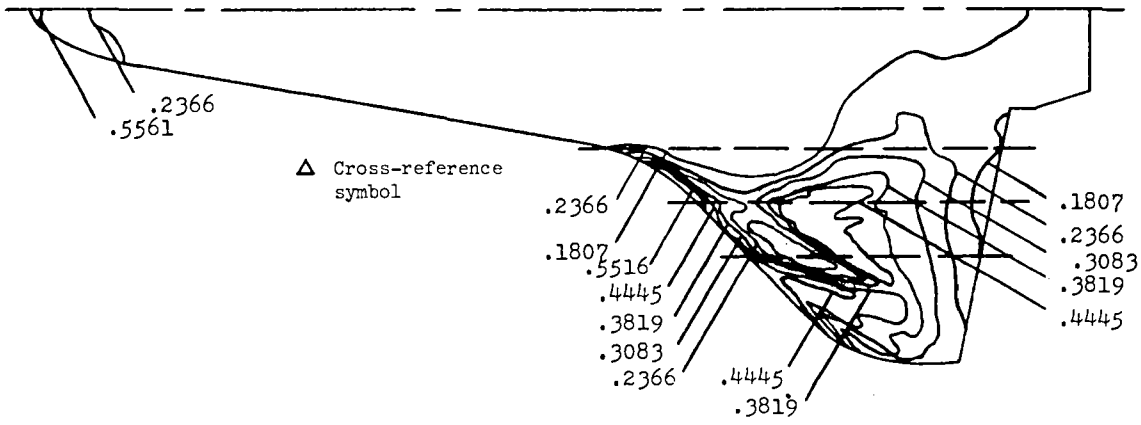

(c) $M_\infty = 8.00$; $\alpha = 30.03°$; $R_{\infty,l} = 6.93 \times 10^6$; $T_{pc} = 400°F$; data taken from reference 5.

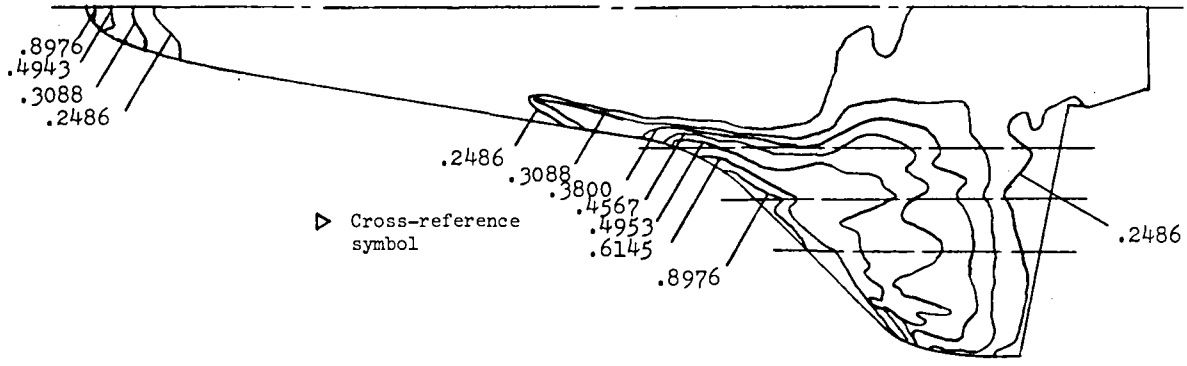

(d) $M_\infty = 8.00$; $\alpha = 30.00°$; $R_{\infty,l} = 6.90 \times 10^6$; $T_{pc} = 500°F$; data taken from reference 5.

Figure 8.- Continued.

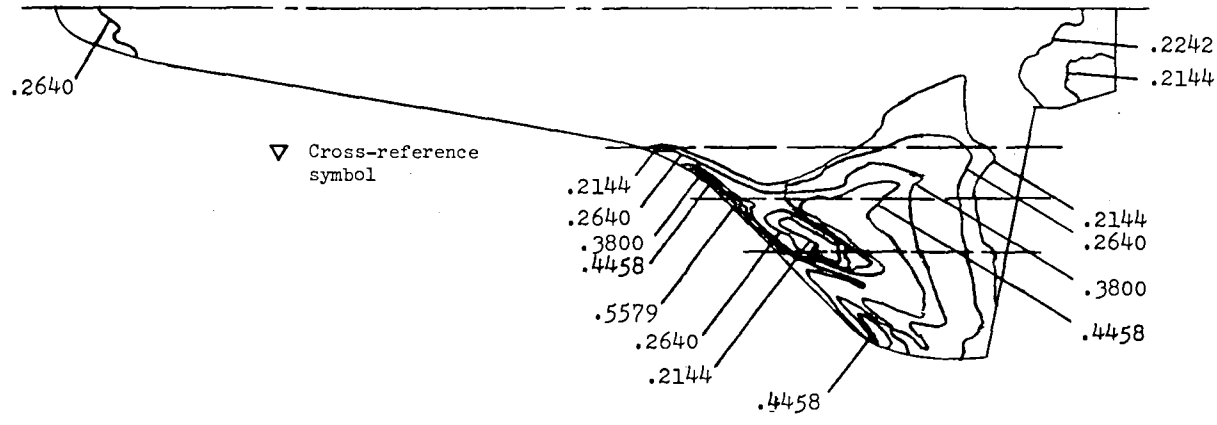

(e) $M_\infty = 8.00$; $\alpha = 30.00°$; $R_{\infty,l} = 6.94 \times 10^6$; $T_{pc} = 400°F$; data taken from reference 5.

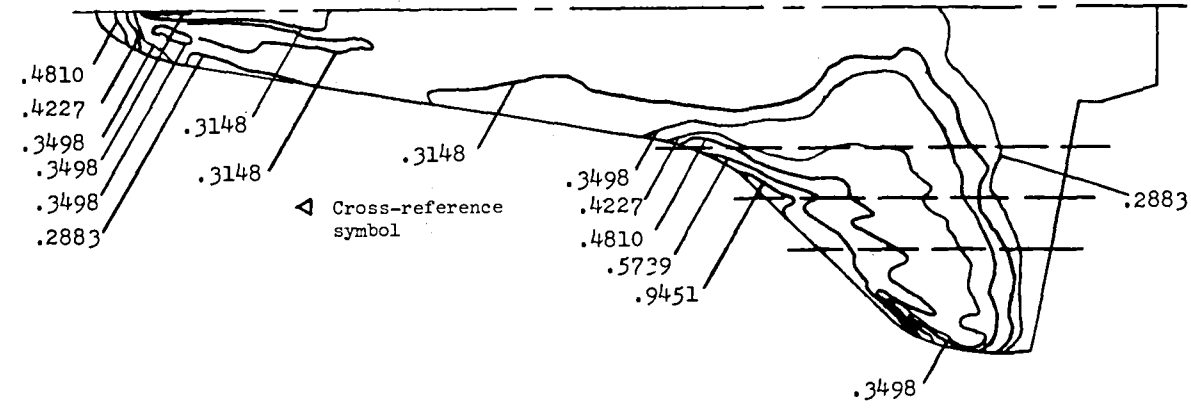

(f) $M_\infty = 8.00$; $\alpha = 30.02°$; $R_{\infty,l} = 6.96 \times 10^6$; $T_{pc} = 500°F$; data taken from reference 5.

Figure 8.- Continued.

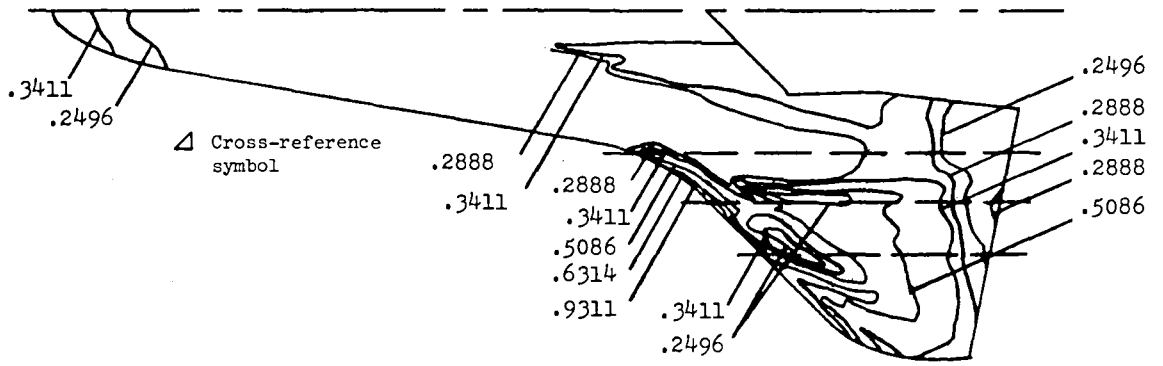

(g) $M_\infty = 8.00$; $\alpha = 30.01°$; $R_{\infty,l} = 6.91 \times 10^6$; $T_{pc} = 500°F$; data taken from reference 5.

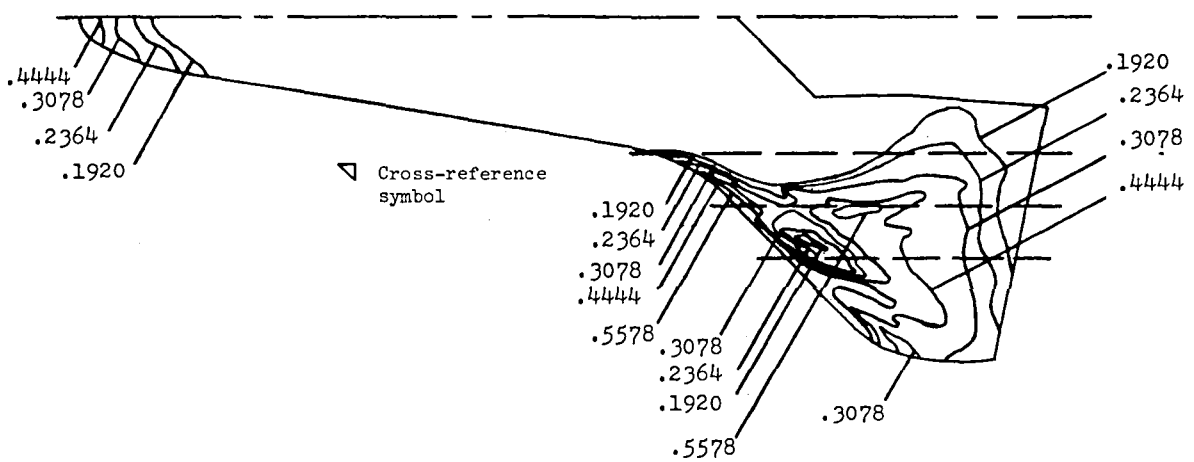

(h) $M_\infty = 8.00$; $\alpha = 30.00°$; $R_{\infty,l} = 6.97 \times 10^6$; $T_{pc} = 400°F$; data taken from reference 5.

Figure 8.- Continued.

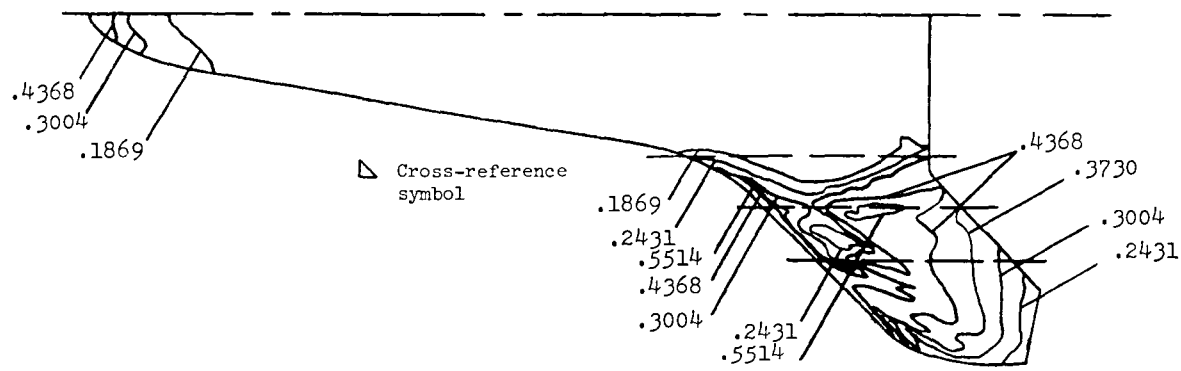

(i) $M_\infty = 8.00$; $\alpha = 30.00°$; $R_{\infty,l} = 6.91 \times 10^6$; $T_{pc} = 400°F$; data taken from reference 5.

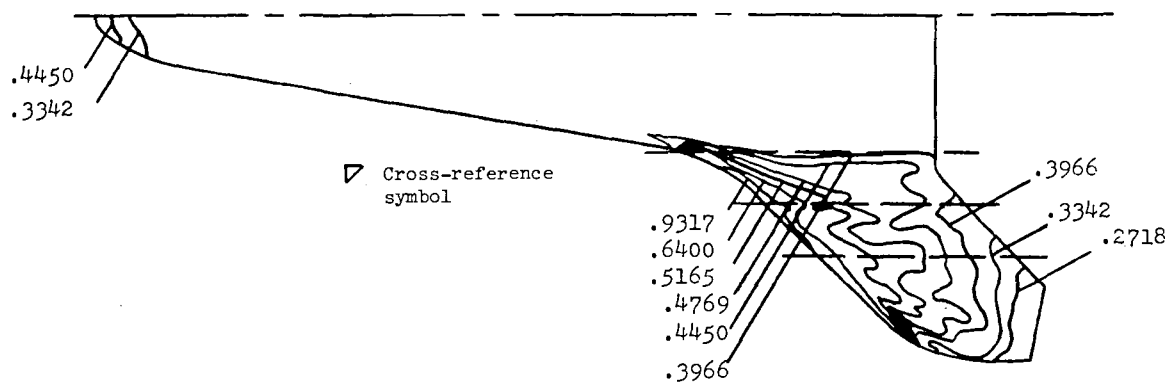

(j) $M_\infty = 8.00$; $\alpha = 30.01°$; $R_{\infty,l} = 6.93 \times 10^6$; $T_{pc} = 500°F$; data taken from reference 5.

Figure 8.- Concluded.

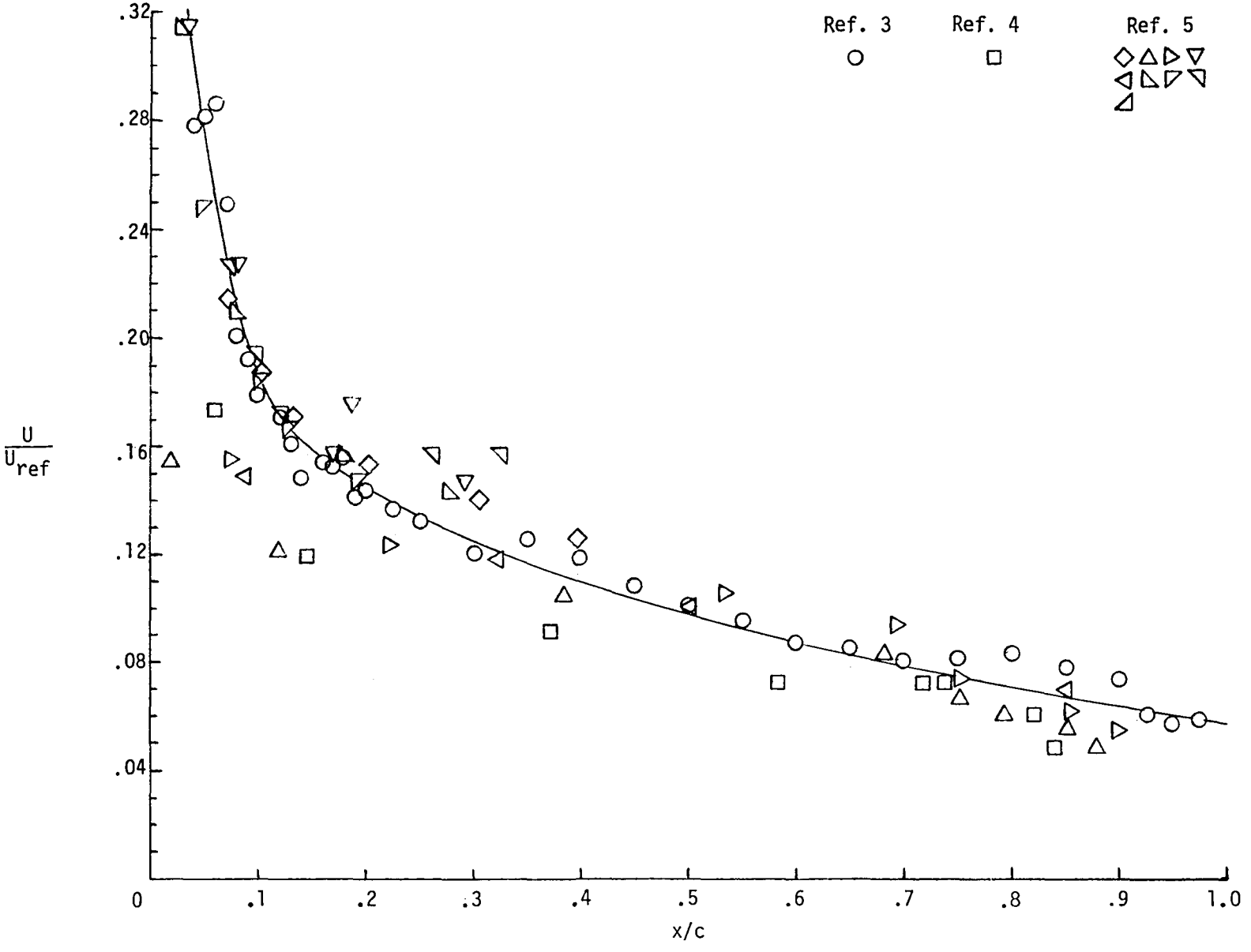

(a) 2y/b = 0.00.

Figure 9.- Wind-tunnel experimental heat-transfer-coefficient ratios from references 3, 4, and 5 applied to nominal-design 14414.1 trajectory between 0 and 600 sec of entry and to proposed STS-1 trajectory between 0 and 850 sec of entry. $M_\infty \approx 8$; $\alpha \approx 40°$; $R_{\infty,1} \approx 1 \times 10^6$.

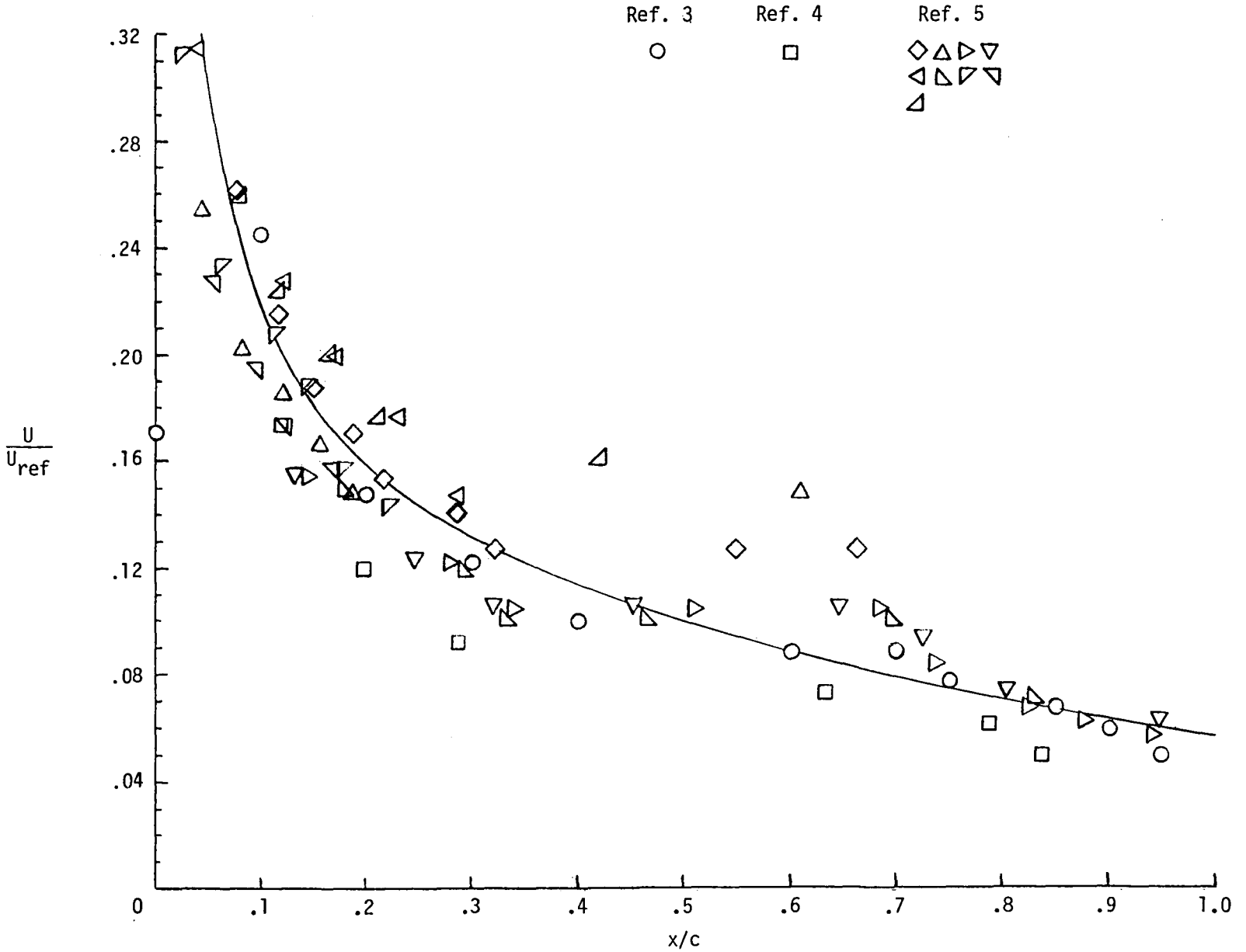

(b) 2y/b = 0.40.

Figure 9.- Continued.

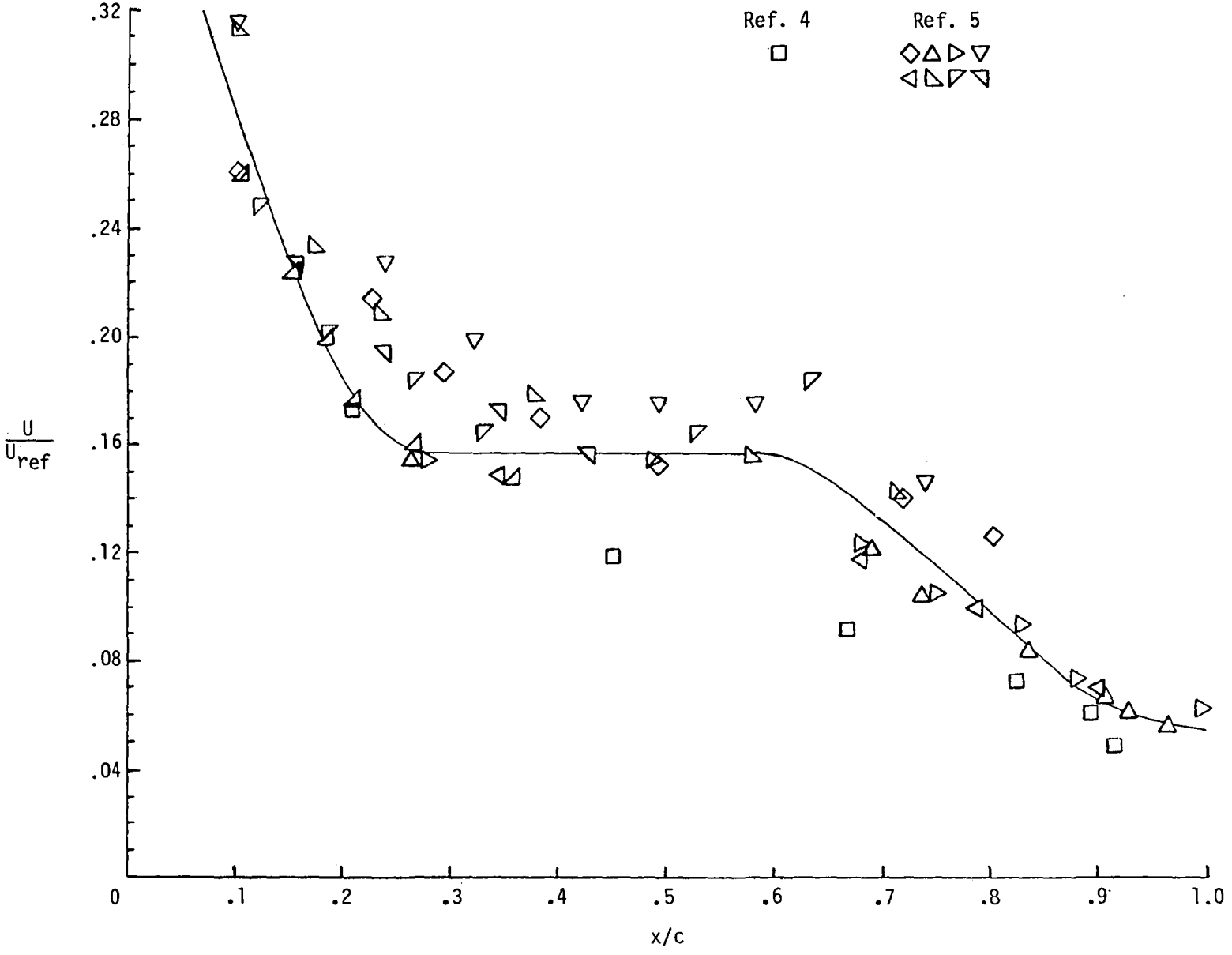

(c) 2y/b = 0.55.

Figure 9.- Continued.

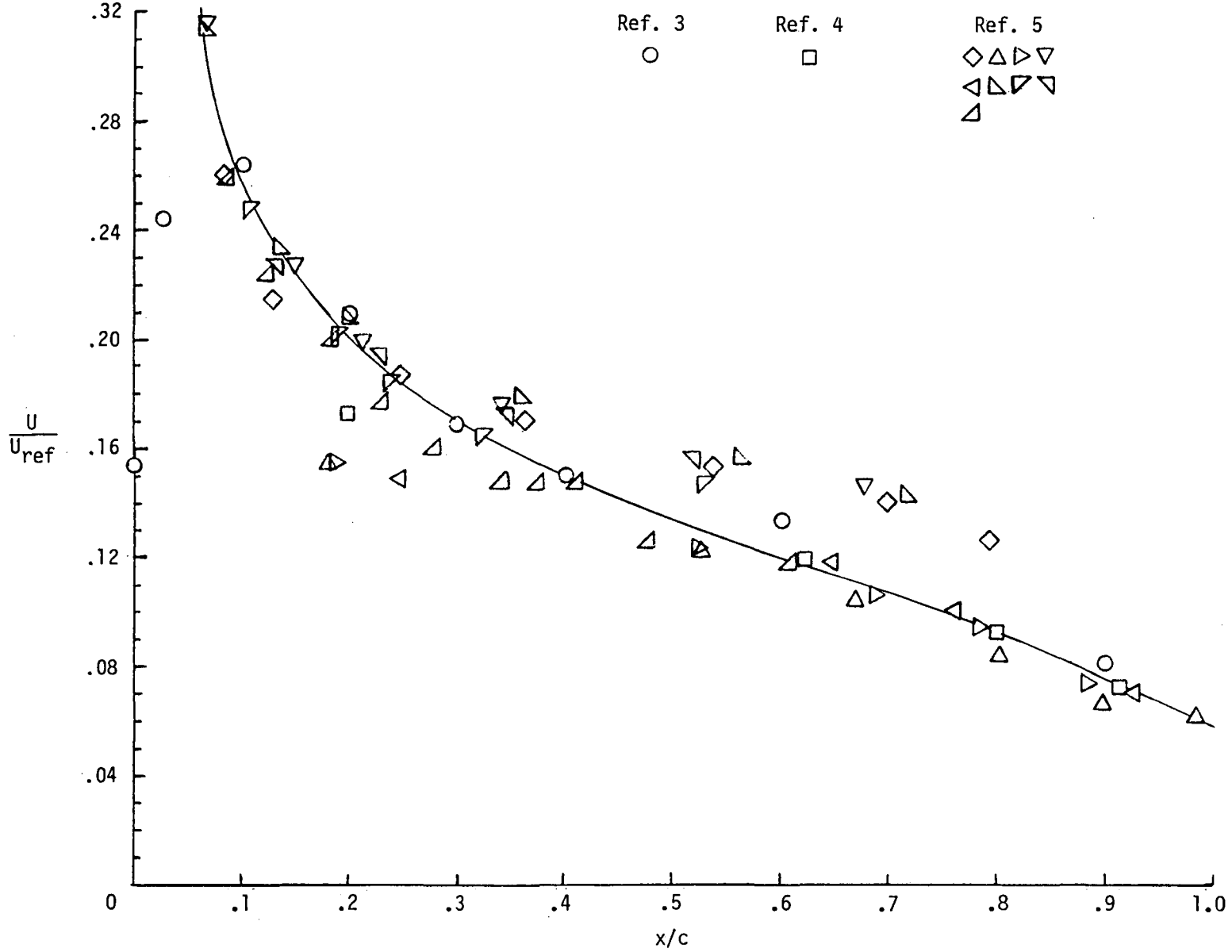

(d) 2y/b = 0.70.

Figure 9.- Concluded.

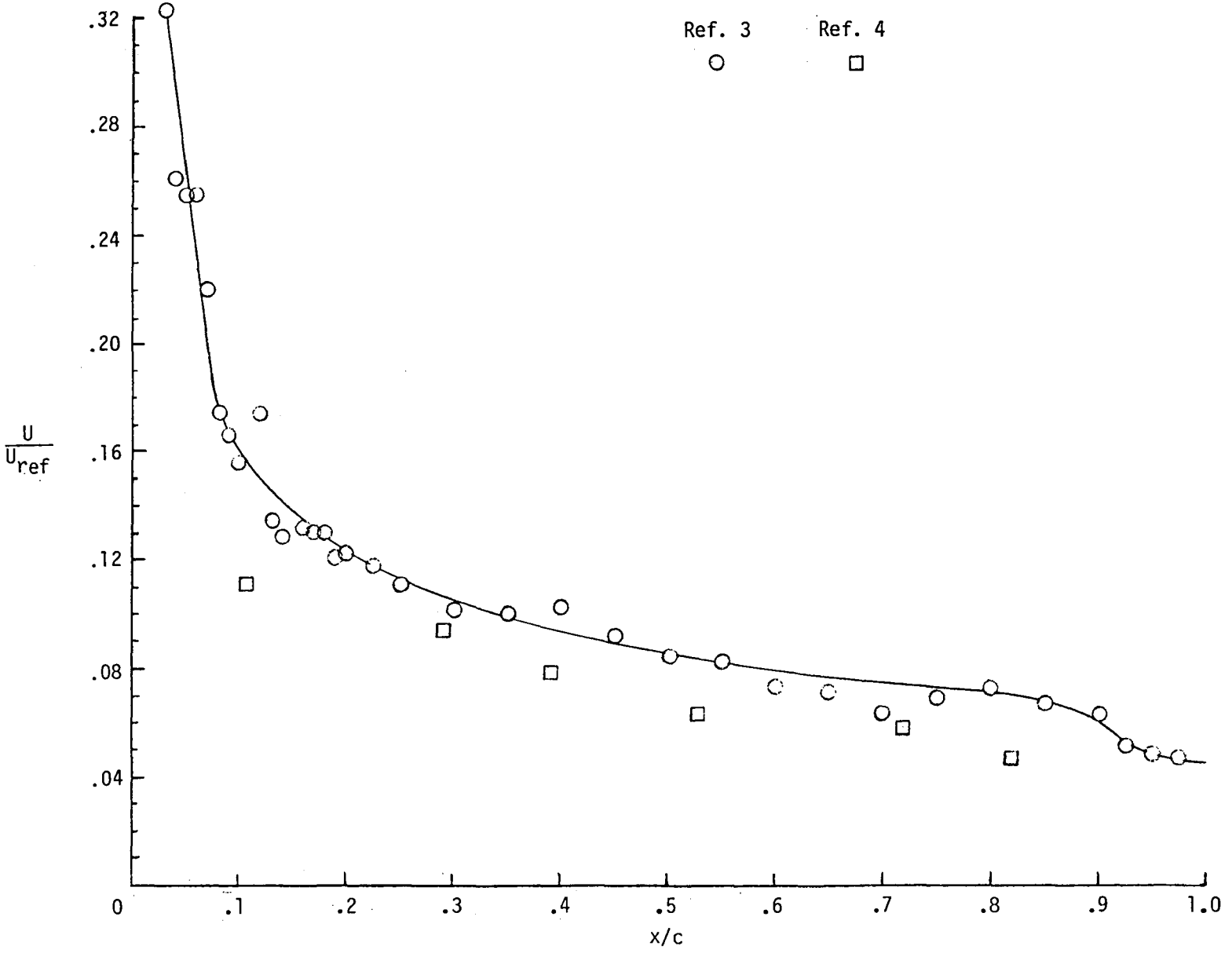

(a) 2y/b = 0.00.

Figure 10.- Wind-tunnel experimental heat-transfer-coefficient ratios from references 3 and 4 applied to nominal-design 14414.1 trajectory between 600 and 850 sec of entry. $M_\infty \approx 8$; $\alpha \approx 35°$; $R_{\infty,l} \approx 2 \times 10^6$.

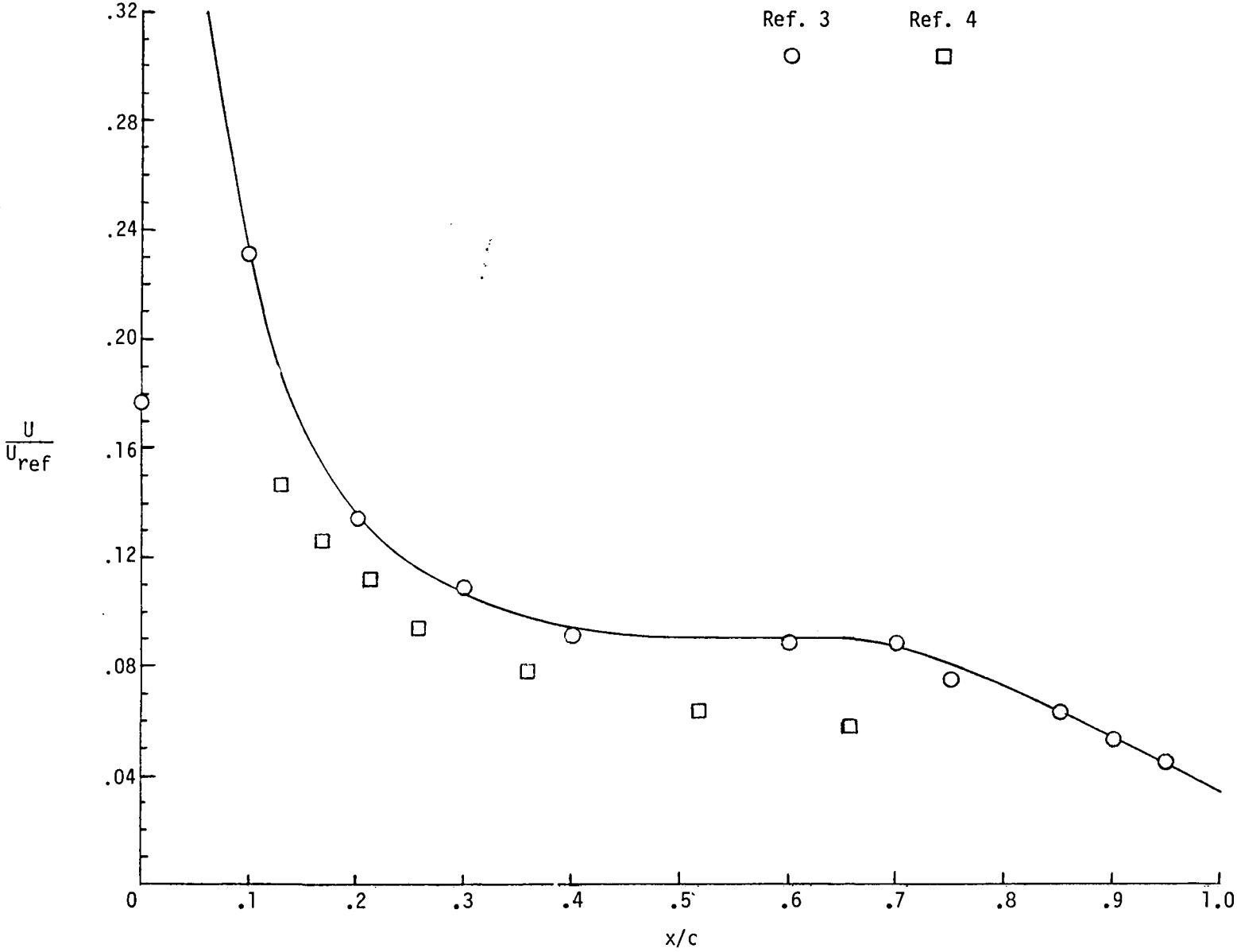

(b) 2y/b = 0.40.

Figure 10.- Continued.

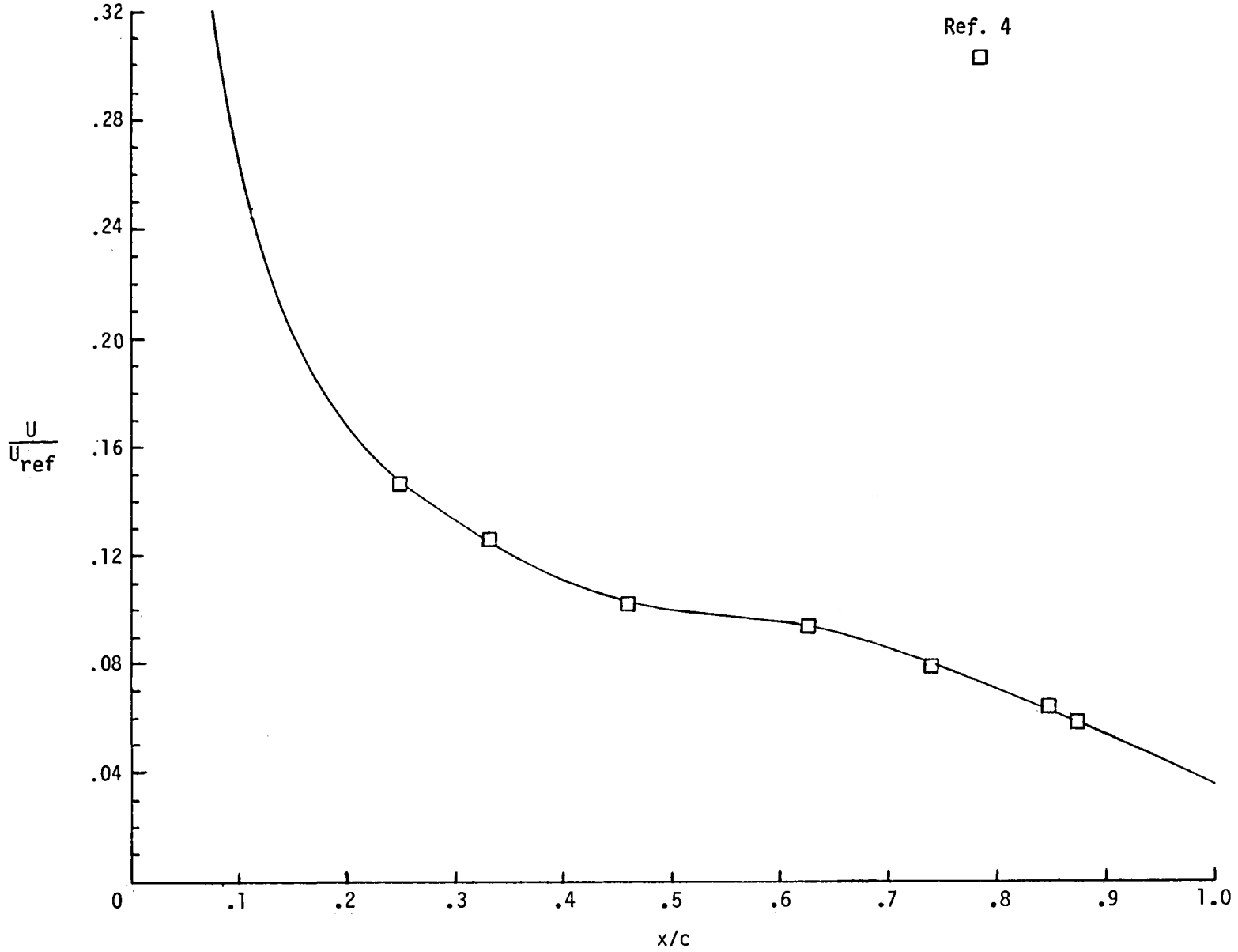

(c) 2y/b = 0.55.

Figure 10.- Continued.

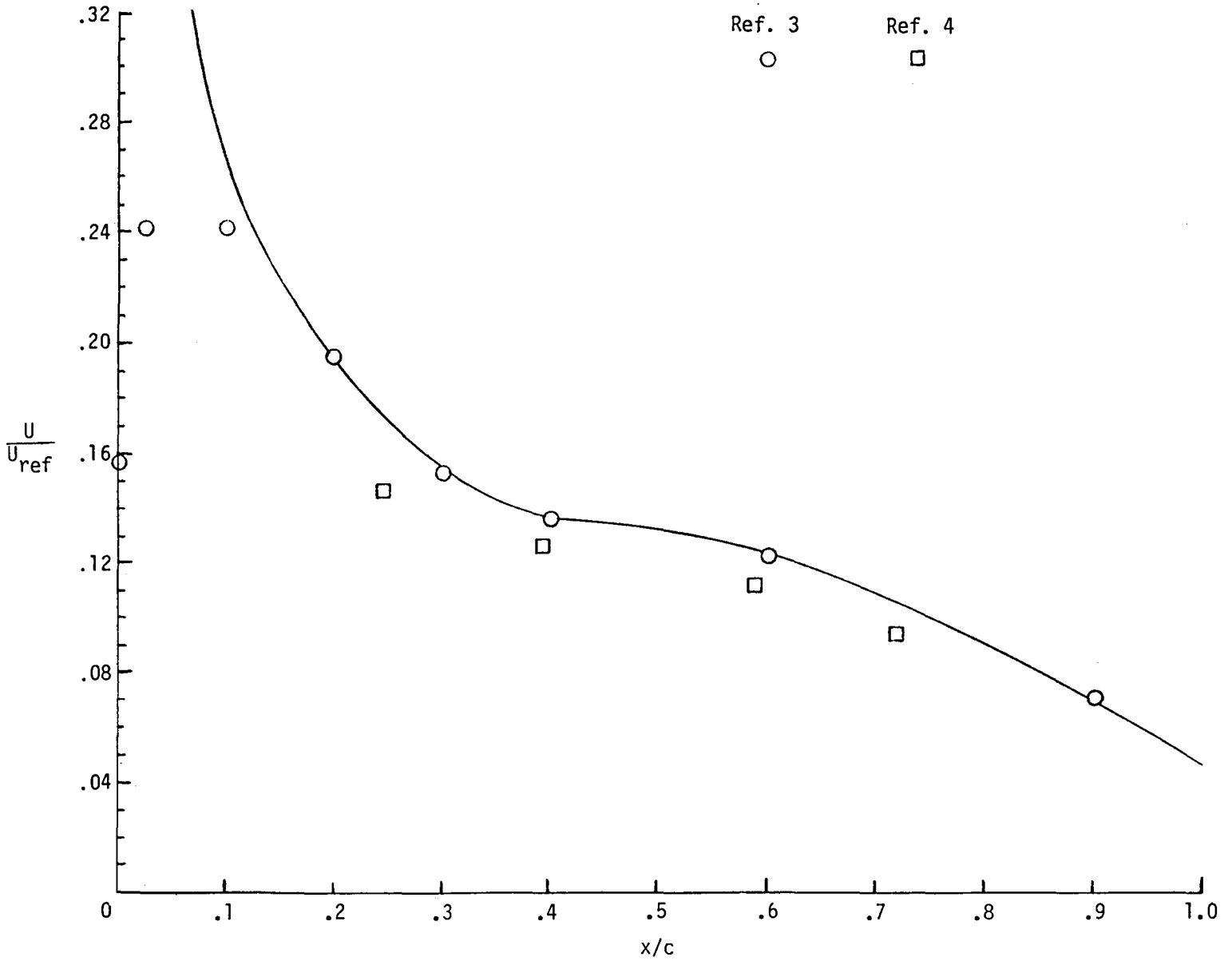

(d) 2y/b = 0.70.

Figure 10.- Concluded.

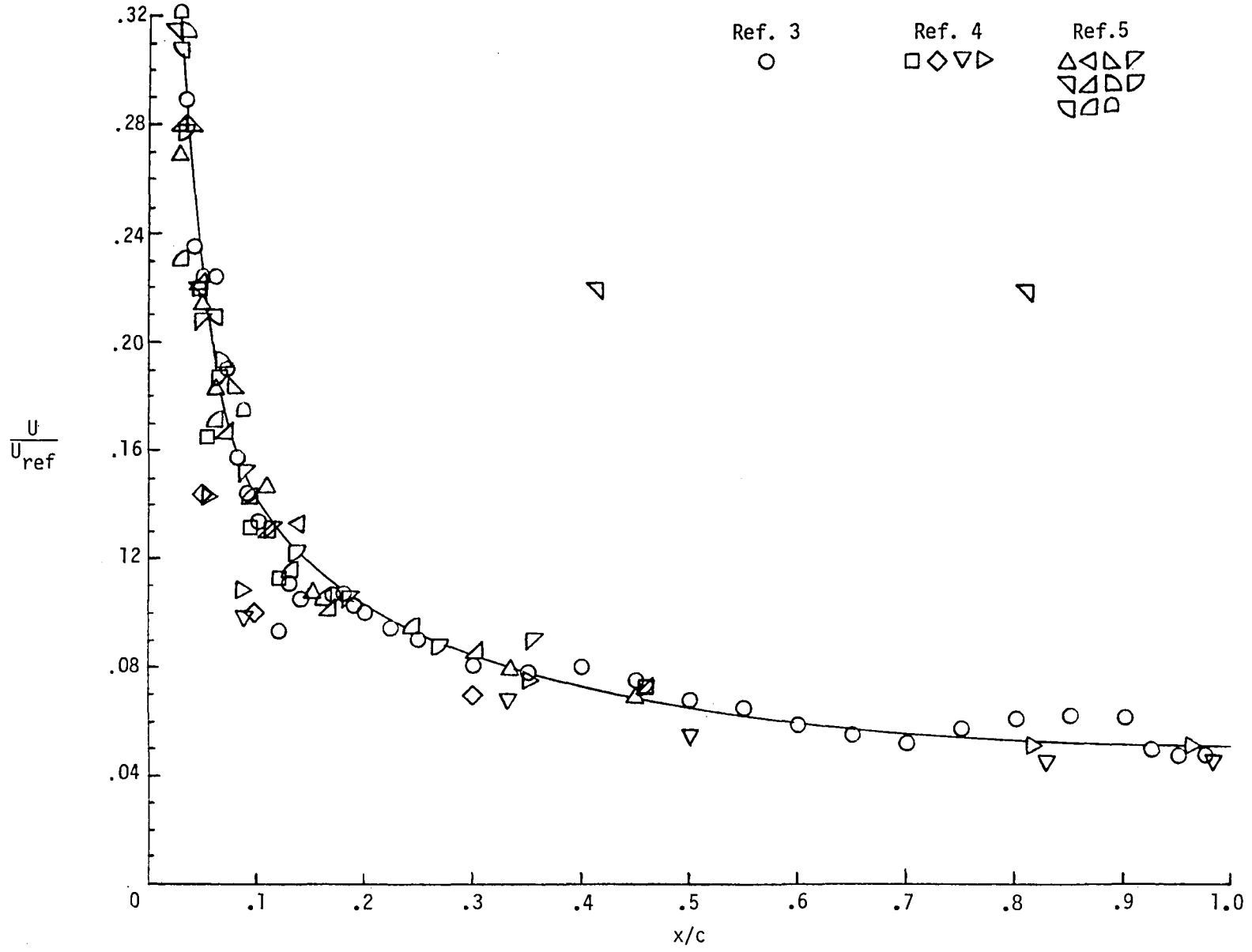

(a) 2y/b = 0.00.

Figure 11.- Wind-tunnel experimental heat-transfer-coefficient ratios from references 3, 4, and 5 applied to nominal-design 14414.1 trajectory between 850 and 1050 sec of entry. $M_\infty \approx 8$; $\alpha \approx 30°$; $R_{\infty,l} \approx 4 \times 10^6$.

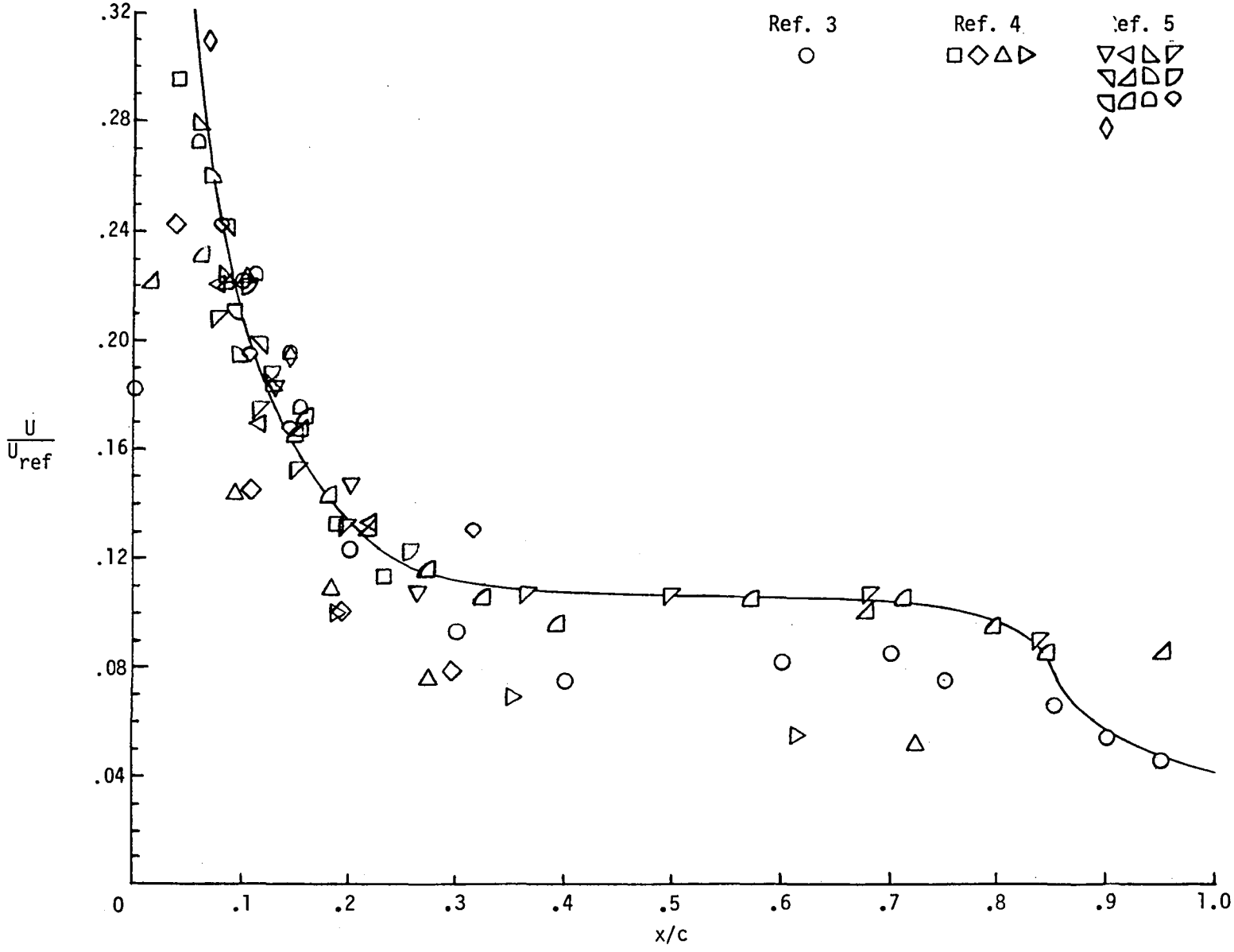

(b) 2y/b = 0.40.

Figure 11.- Continued.

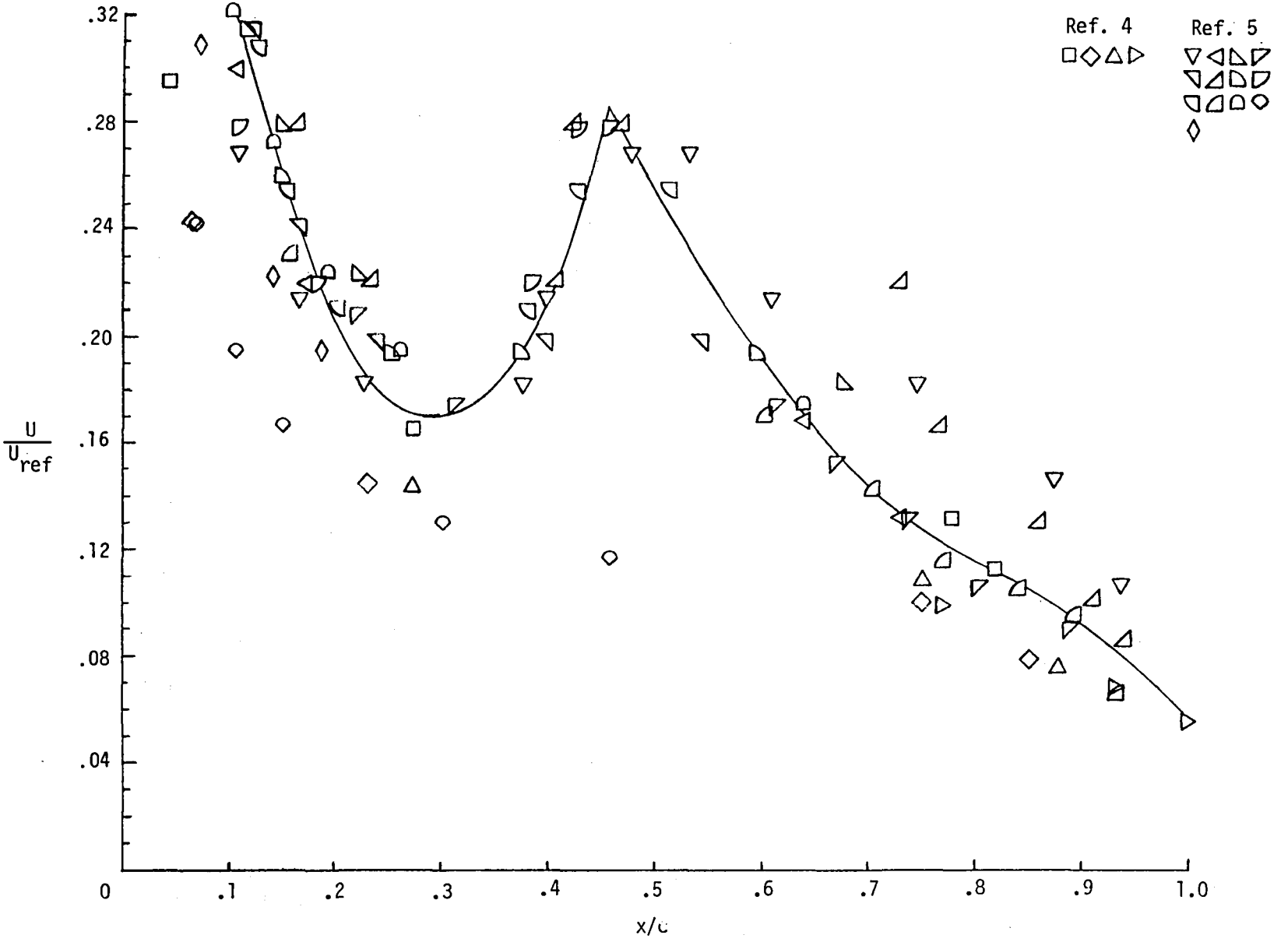

(c) 2y/b = 0.55.

Figure 11.- Continued.

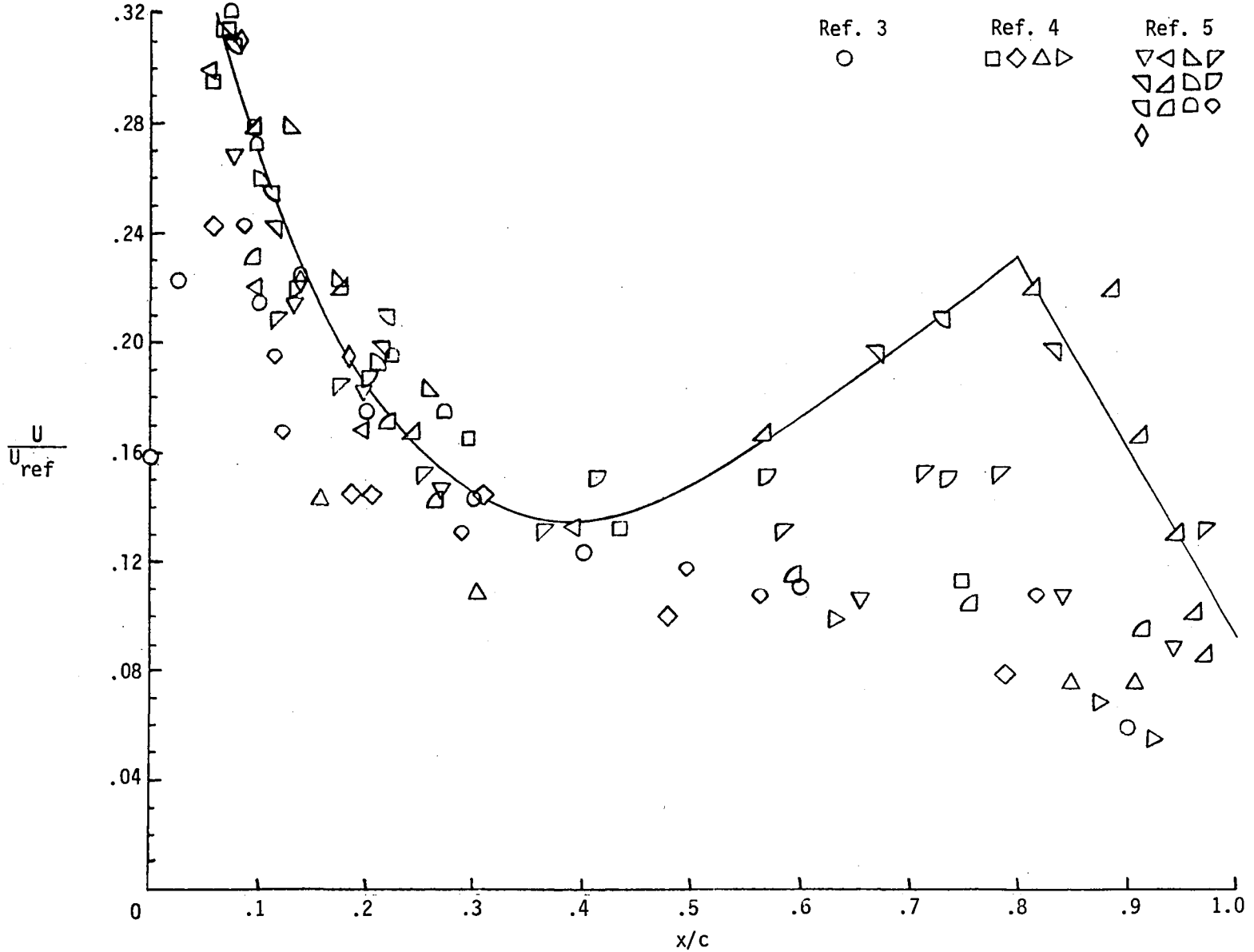

(d) 2y/b = 0.70.

Figure 11.- Concluded.

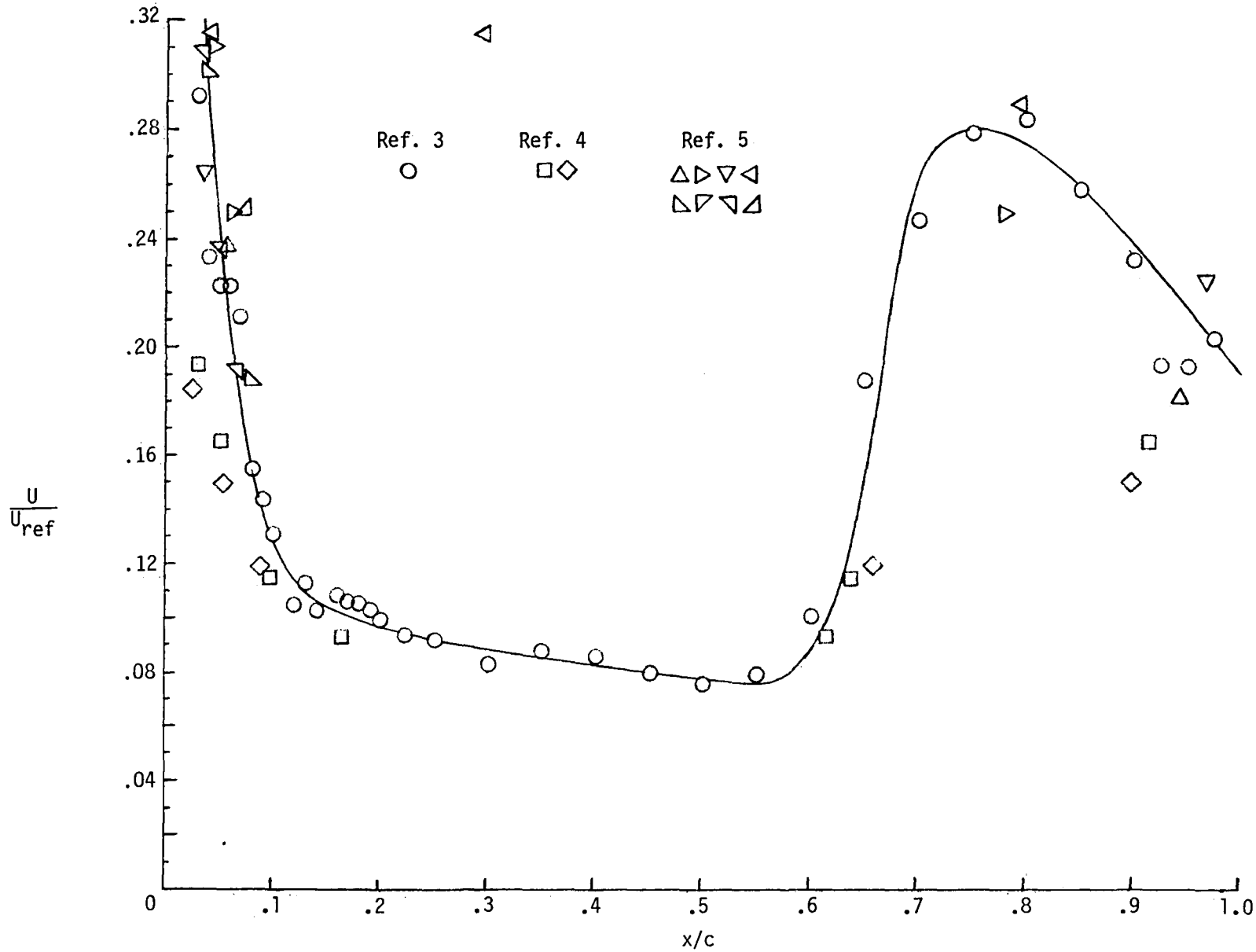

(a) 2y/b = 0.00.

Figure 12.- Wind-tunnel experimental heat-transfer-coefficient ratios from references 3, 4, and 5 applied to nominal-design 14414.1 trajectory between 1050 and 1450 sec of entry and to proposed STS-1 trajectory between 1250 and 1450 sec of entry. $M_\infty \approx 8$; $\alpha \approx 30°$; $R_{\infty,l} \approx 8 \times 10^6$.

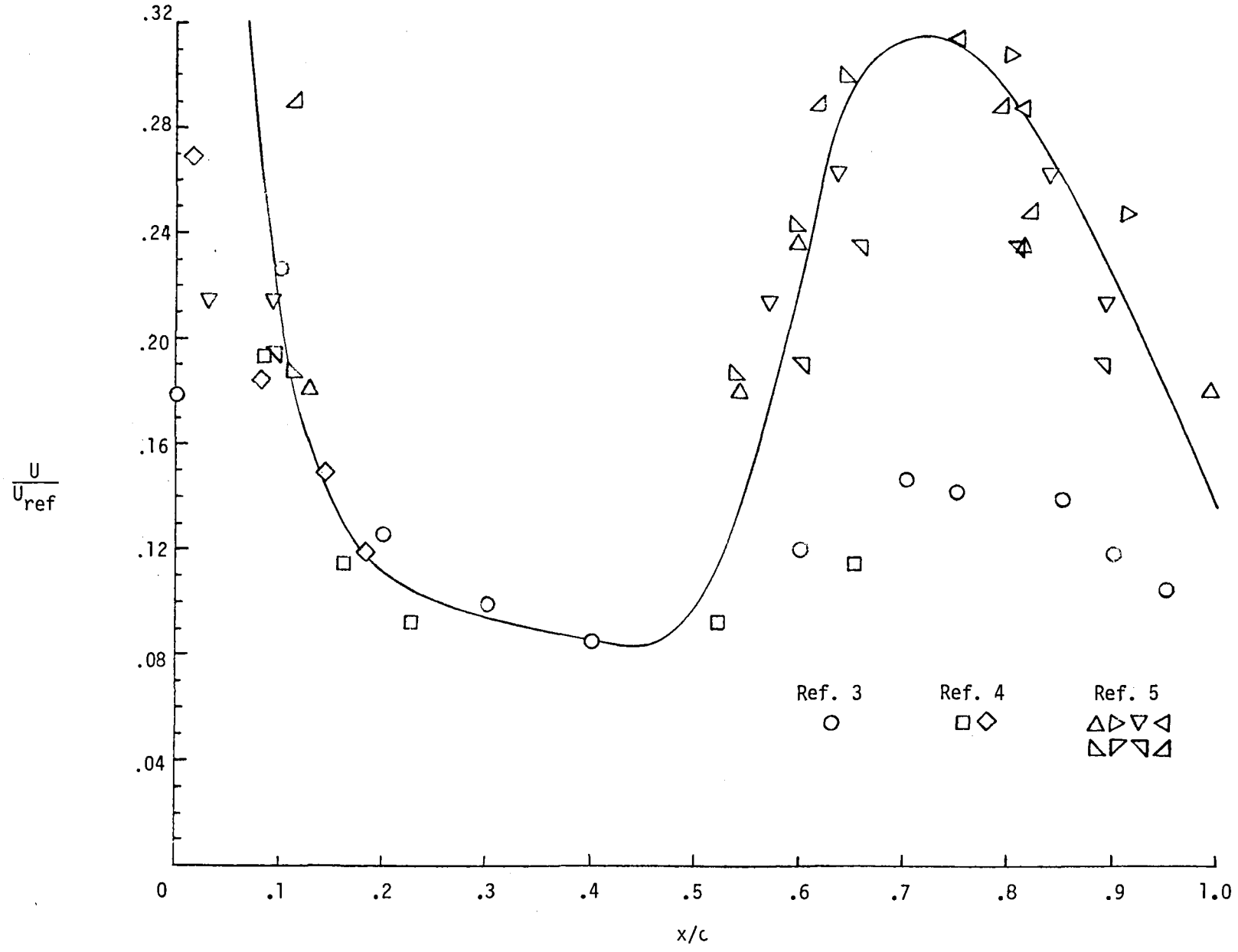

(b) 2y/b = 0.40.

Figure 12.- Continued.

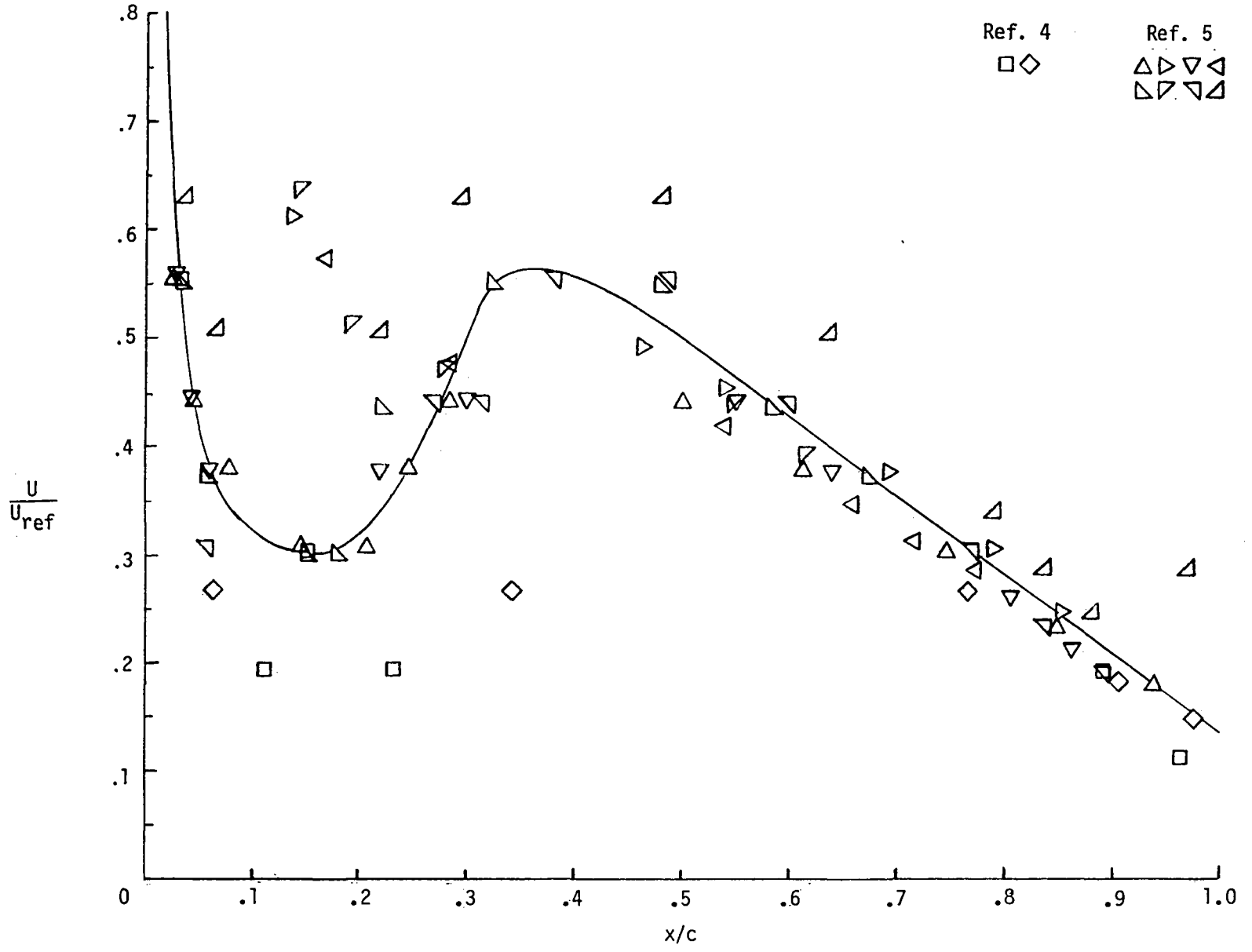

(c) 2y/b = 0.55.

Figure 12.- Continued.

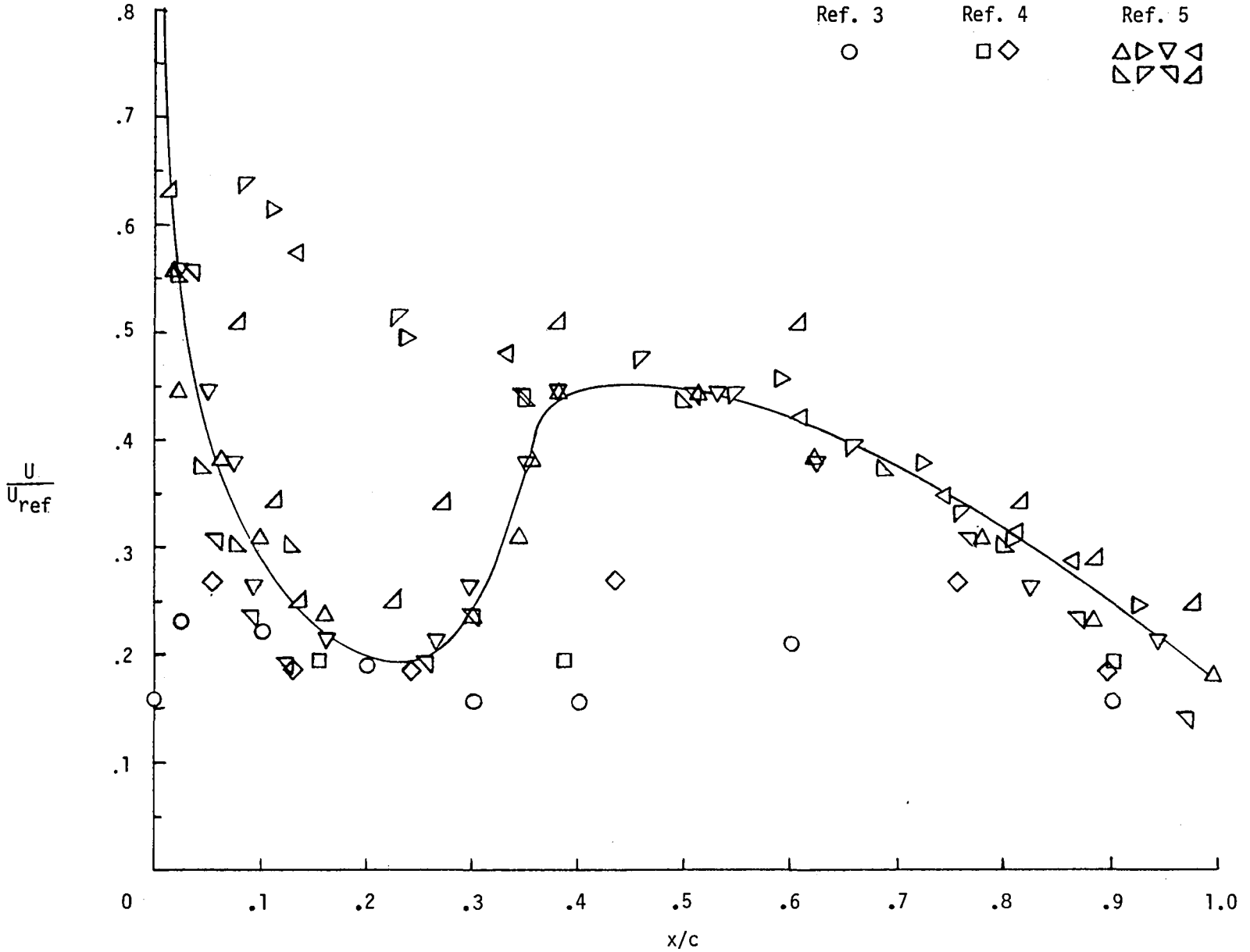

(d) 2y/b = 0.70.

Figure 12.- Concluded.

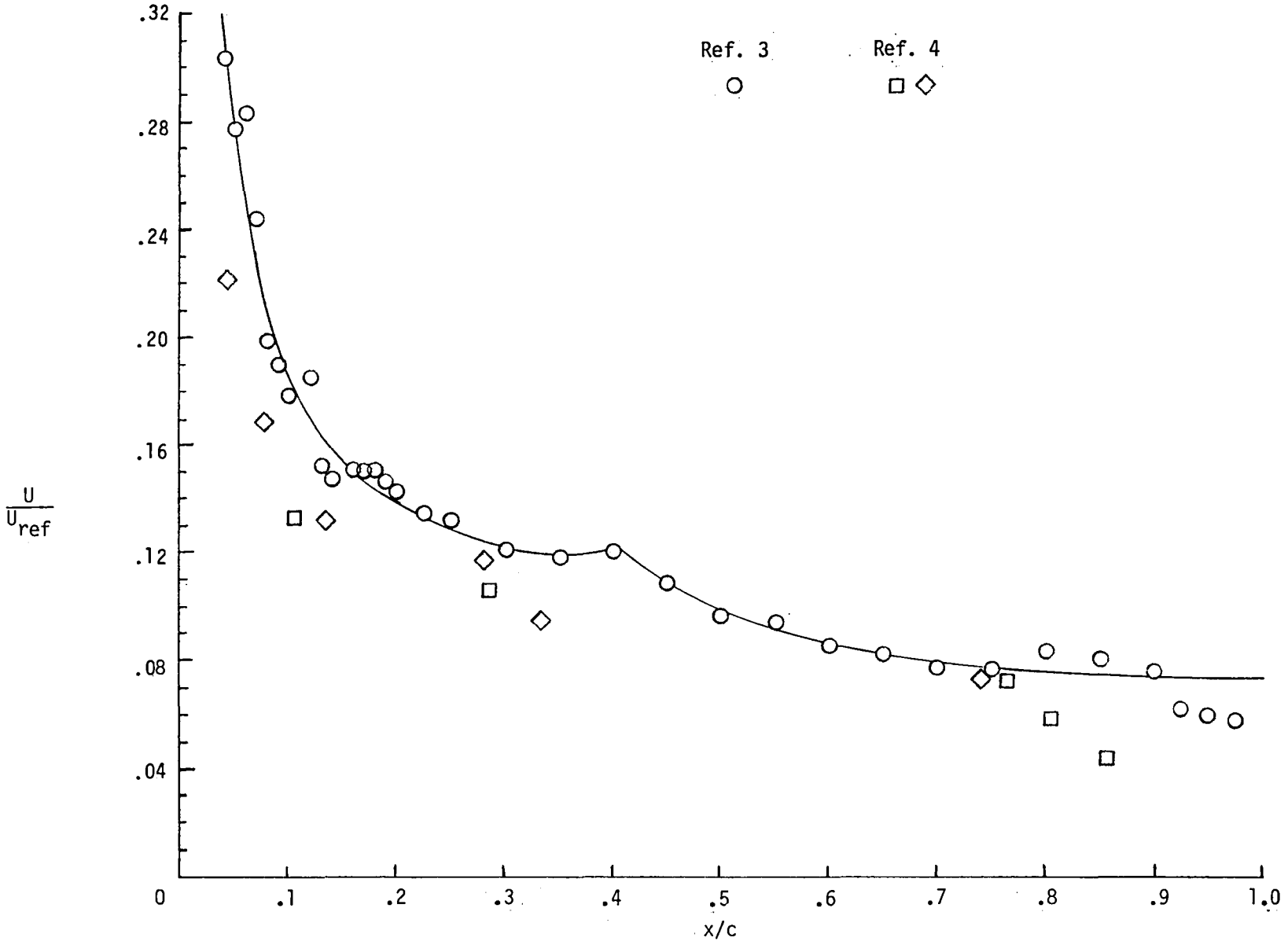

(a) 2y/b = 0.00.

Figure 13.- Wind-tunnel experimental heat-transfer-coefficient ratios from references 3 and 4 applied to proposed STS-1 trajectory between 850 and 1000 sec of entry. $M_\infty \approx 8$; $\alpha \approx 40°$; $R_{\infty,l} \approx 2 \times 10^6$.

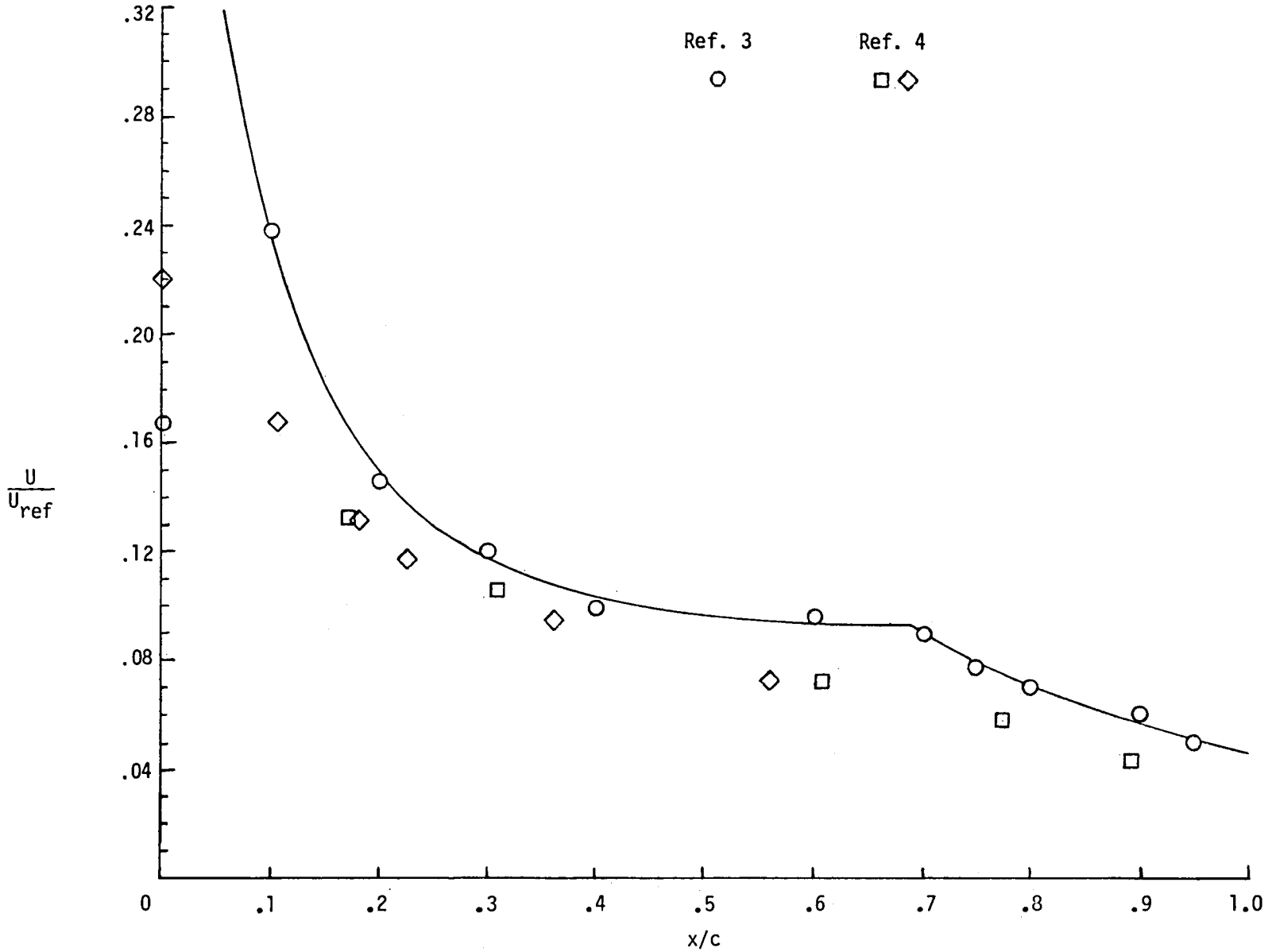

(b) 2y/b = 0.40.

Figure 13.- Continued.

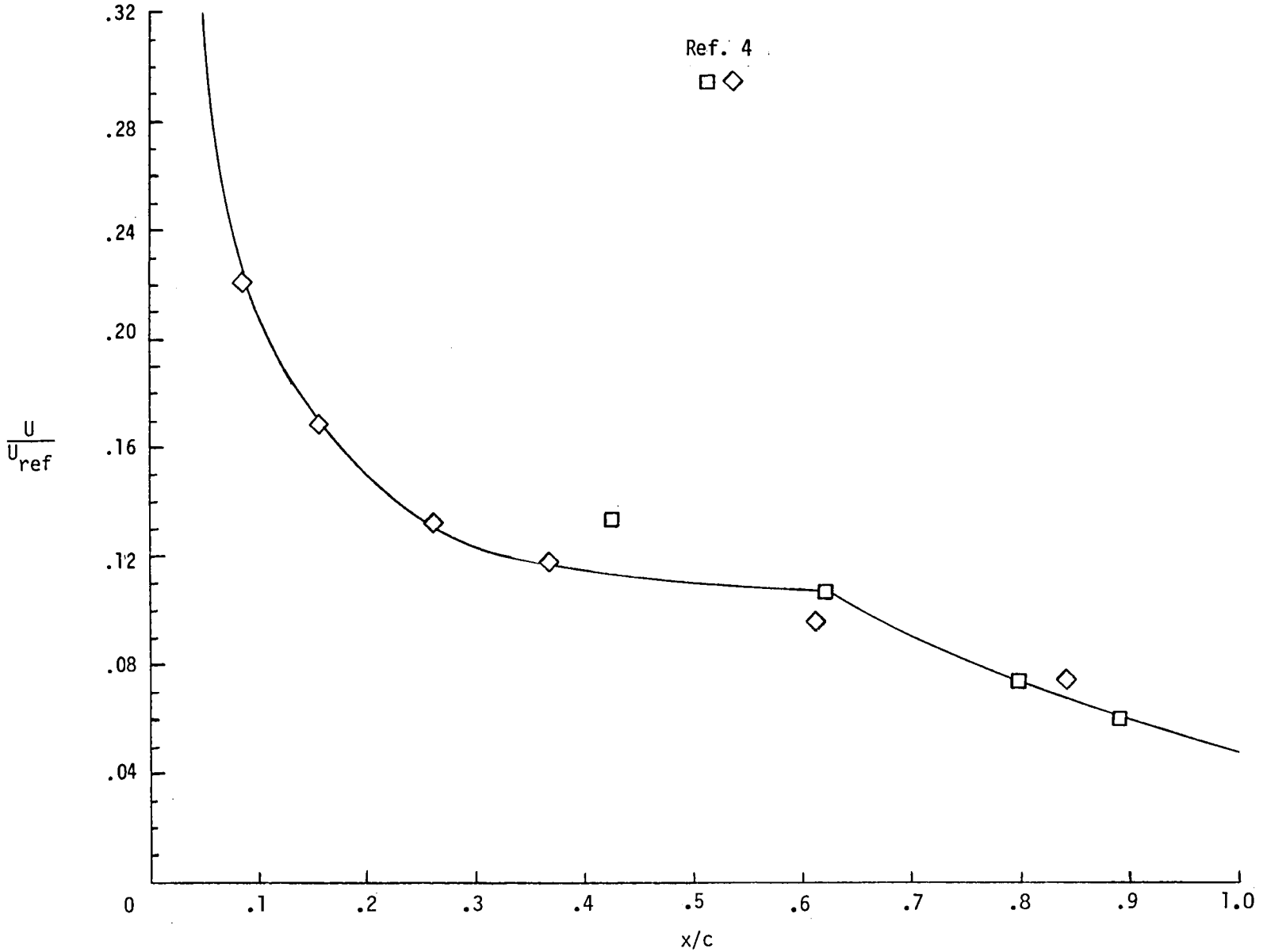

(c) 2y/b = 0.55.

Figure 13.- Continued.

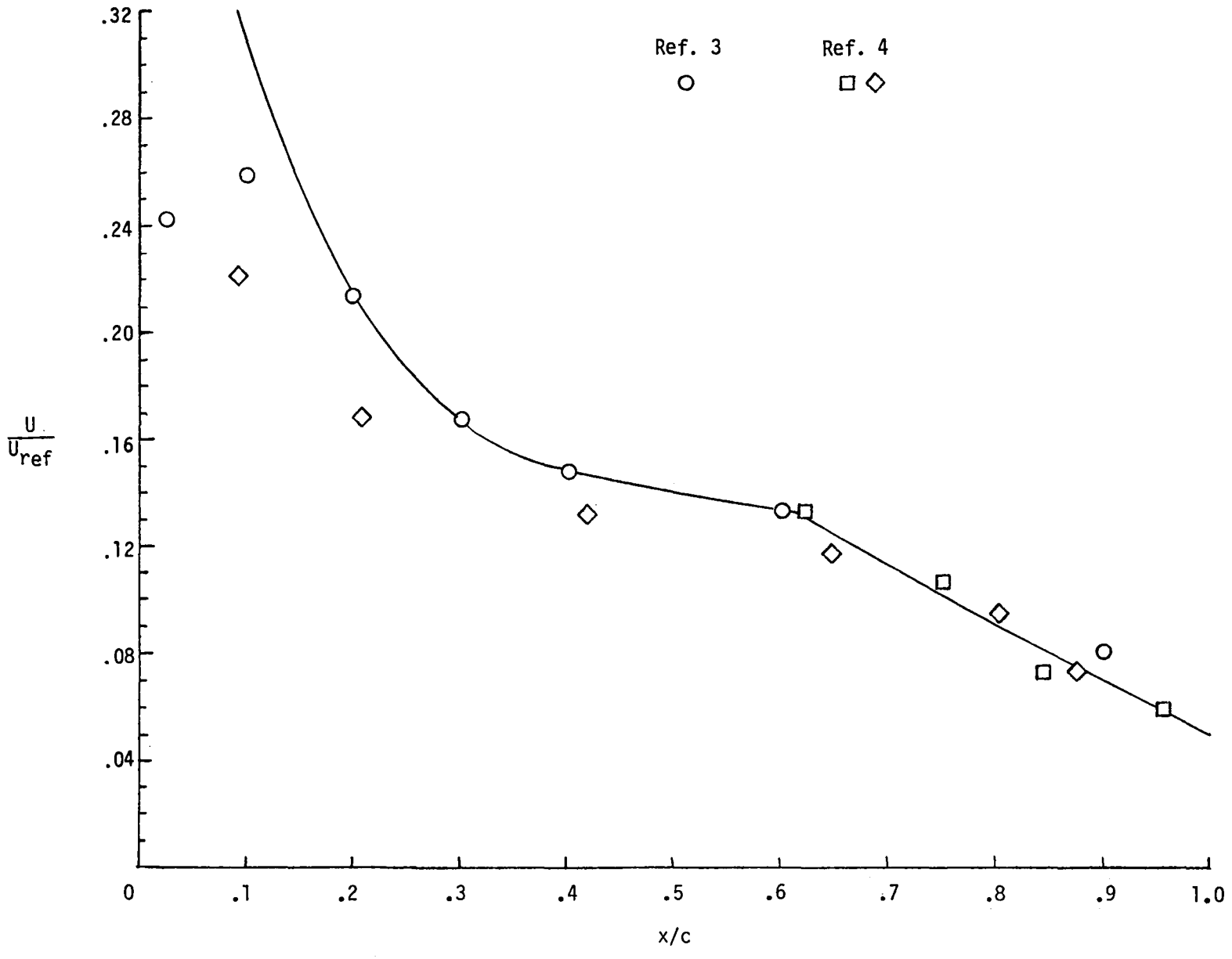

(d) 2y/b = 0.70.

Figure 13.- Concluded.

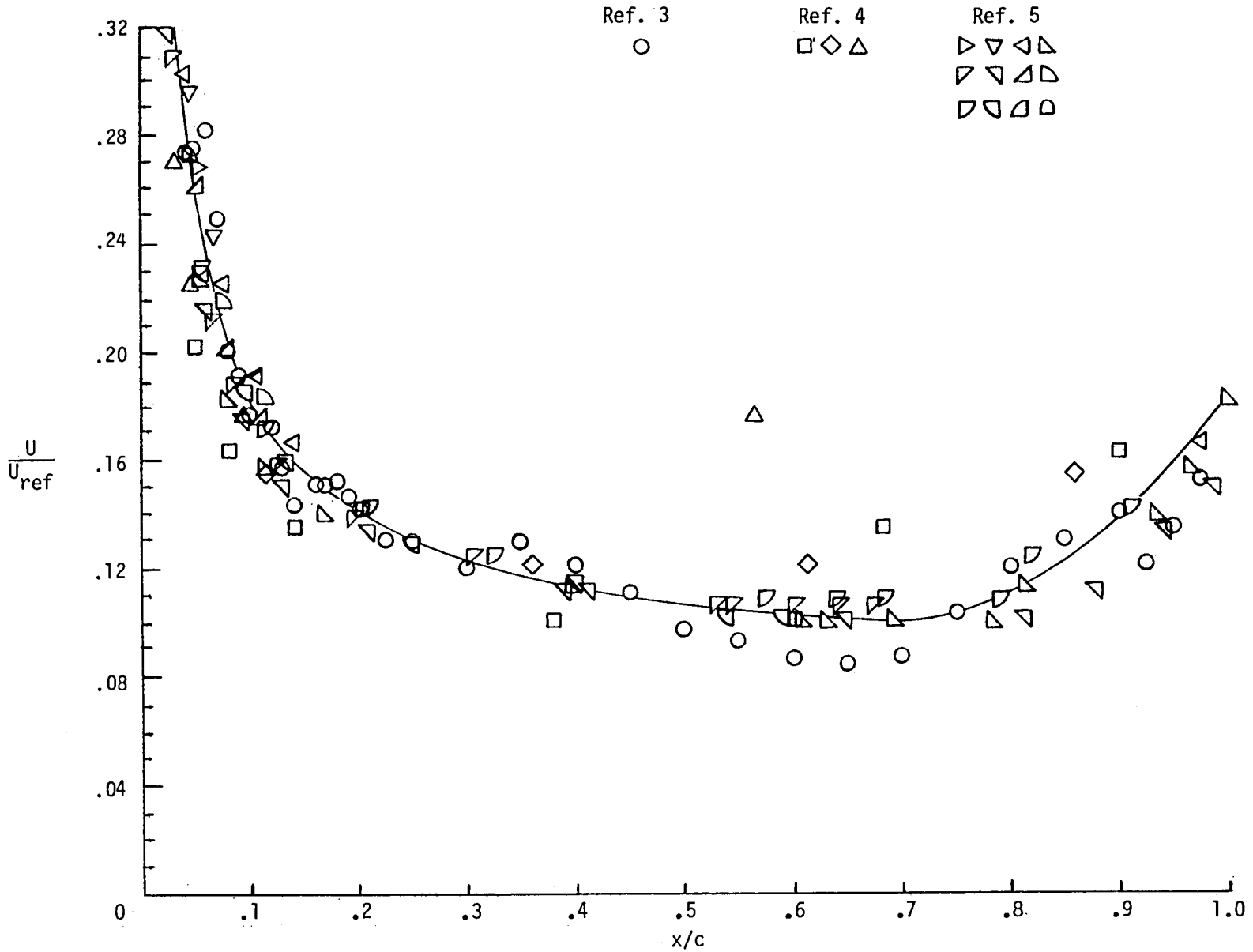

(a) 2y/b = 0.00.

Figure 14.- Wind-tunnel experimental heat-transfer-coefficient ratios from references 3, 4, and 5 applied to proposed STS-1 trajectory between 1000 and 1150 sec of entry. $M_\infty \approx 8$; $\alpha \approx 40°$; $R_{\infty,l} \approx 4 \times 10^6$.

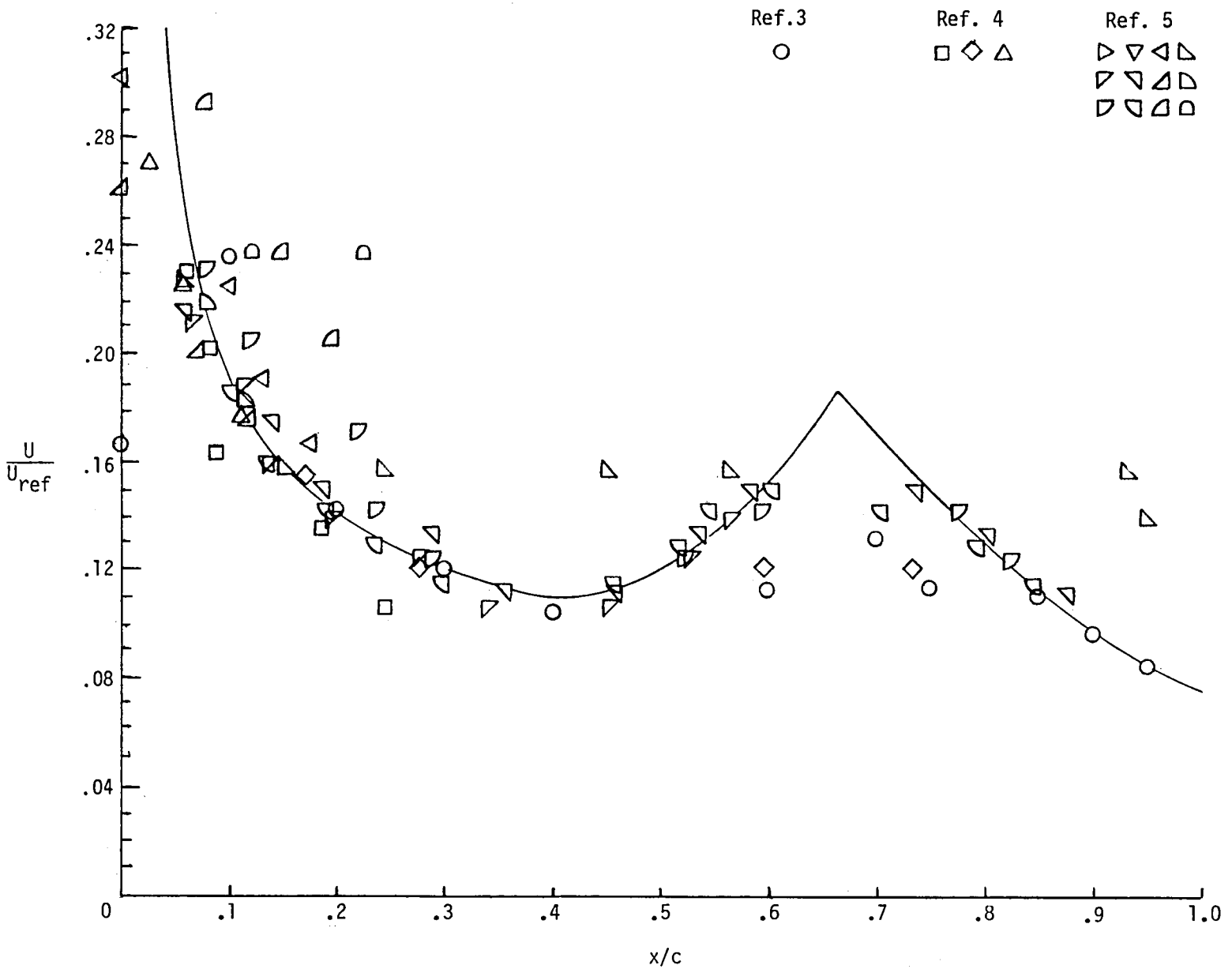

(b) 2y/b = 0.40.

Figure 14.- Continued.

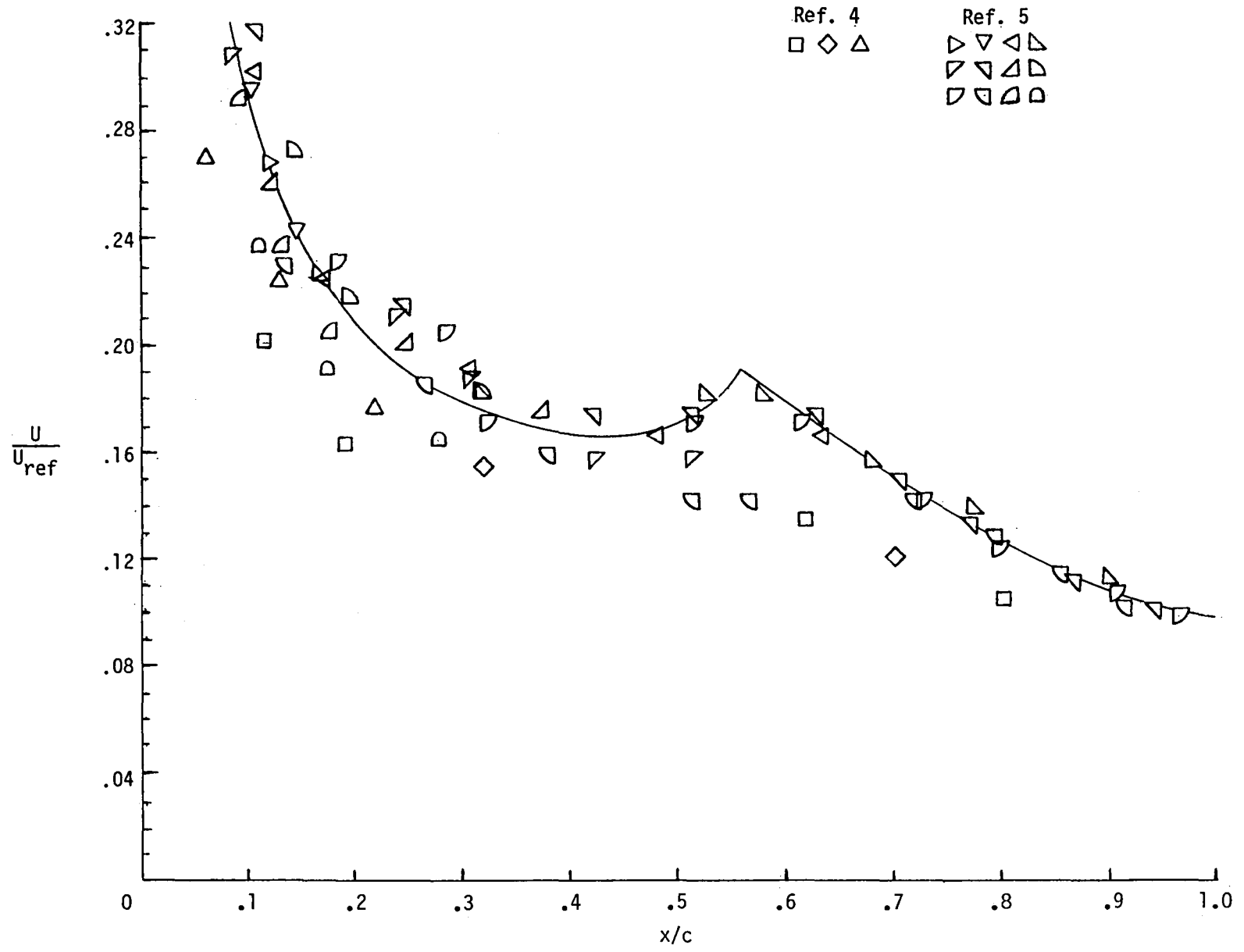

(c) 2y/b = 0.55.

Figure 14.- Continued.

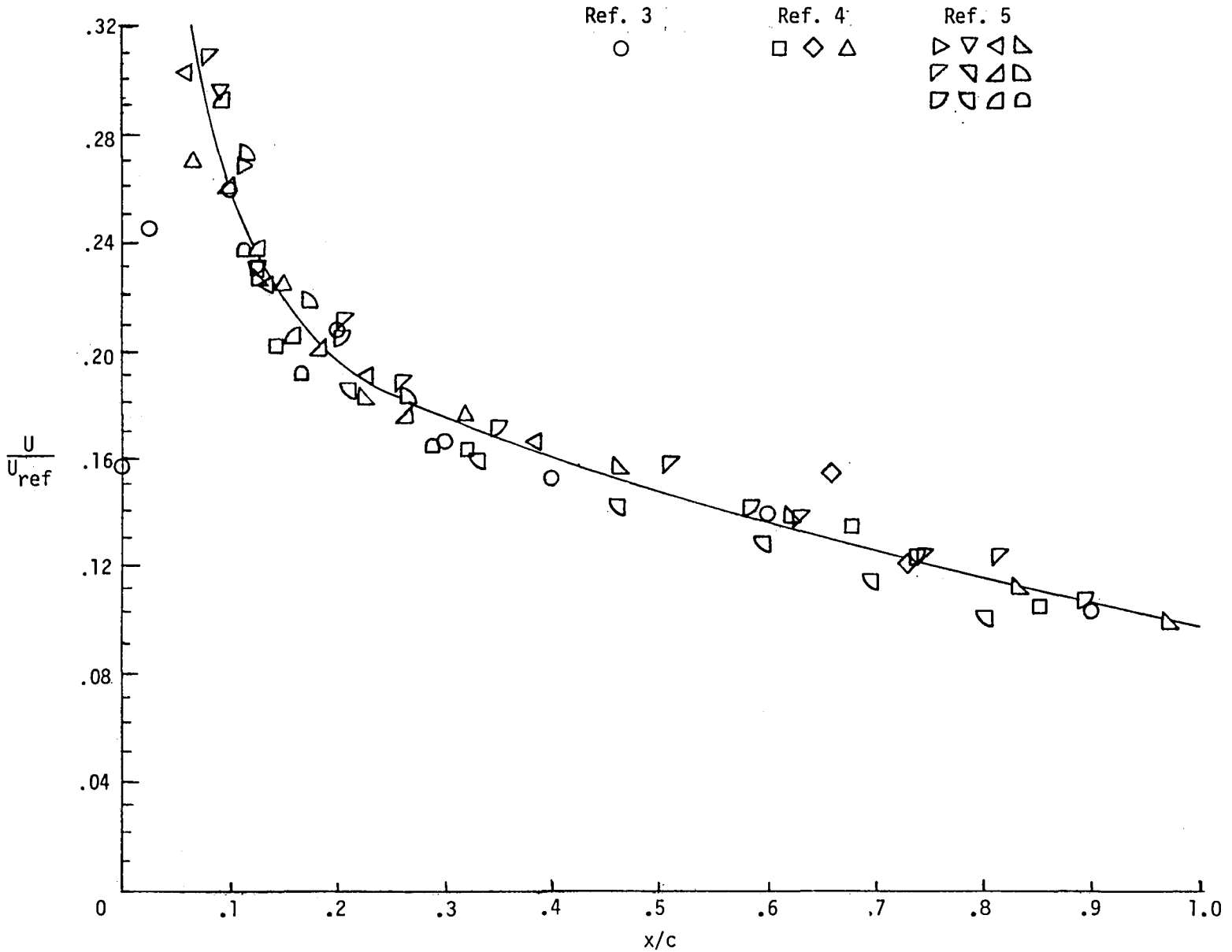

(d) 2y/b = 0.70.

Figure 14.- Concluded.

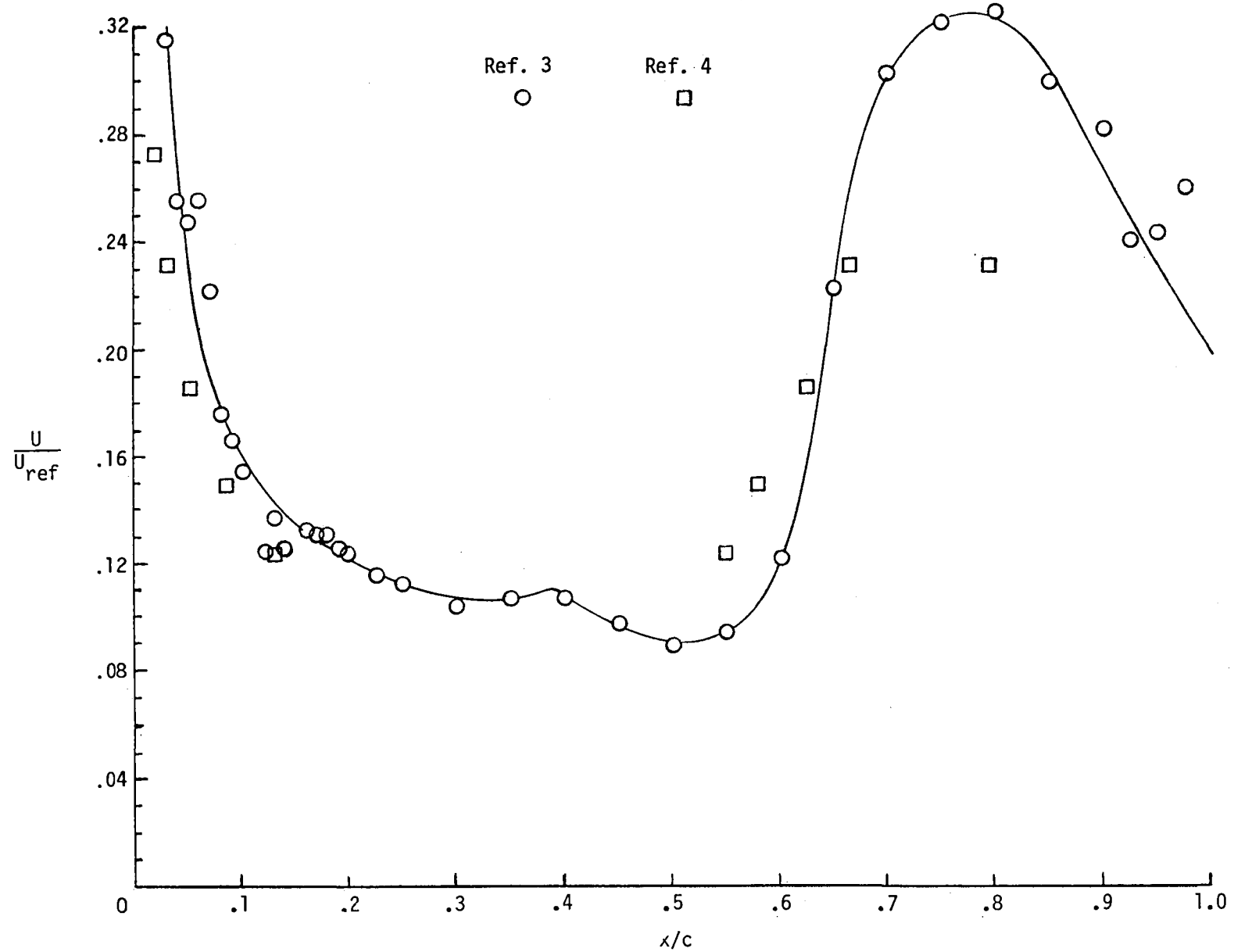

(a) 2y/b = 0.00.

Figure 15.- Wind-tunnel experimental heat-transfer-coefficient ratios from references 3 and 4 applied to proposed STS-1 trajectory between 1150 and 1250 sec of entry. $M_\infty \approx 8$; $\alpha \approx 35°$; $R_{\infty,l} \approx 8 \times 10^6$.

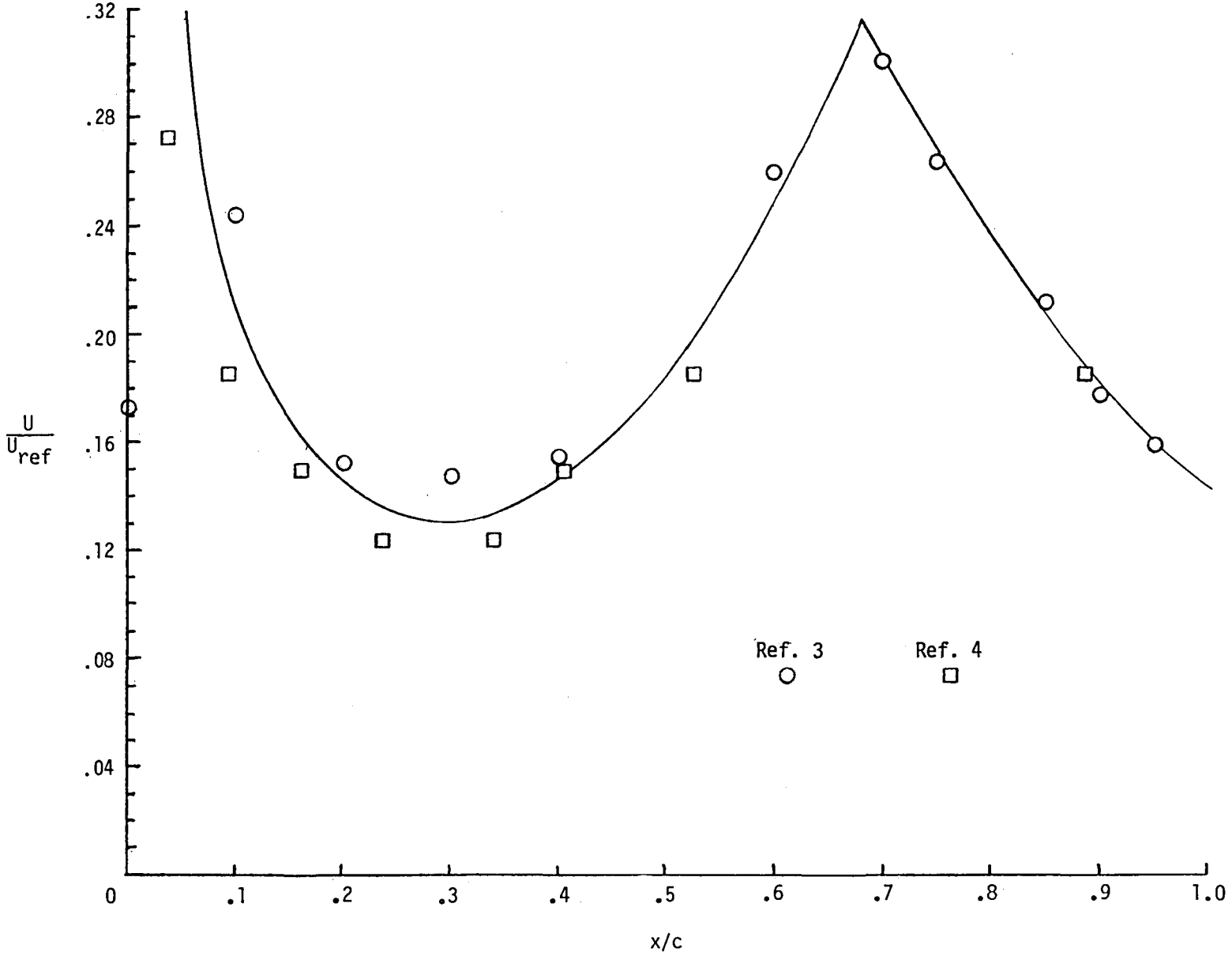

(b) 2y/b = 0.40.

Figure 15.- Continued.

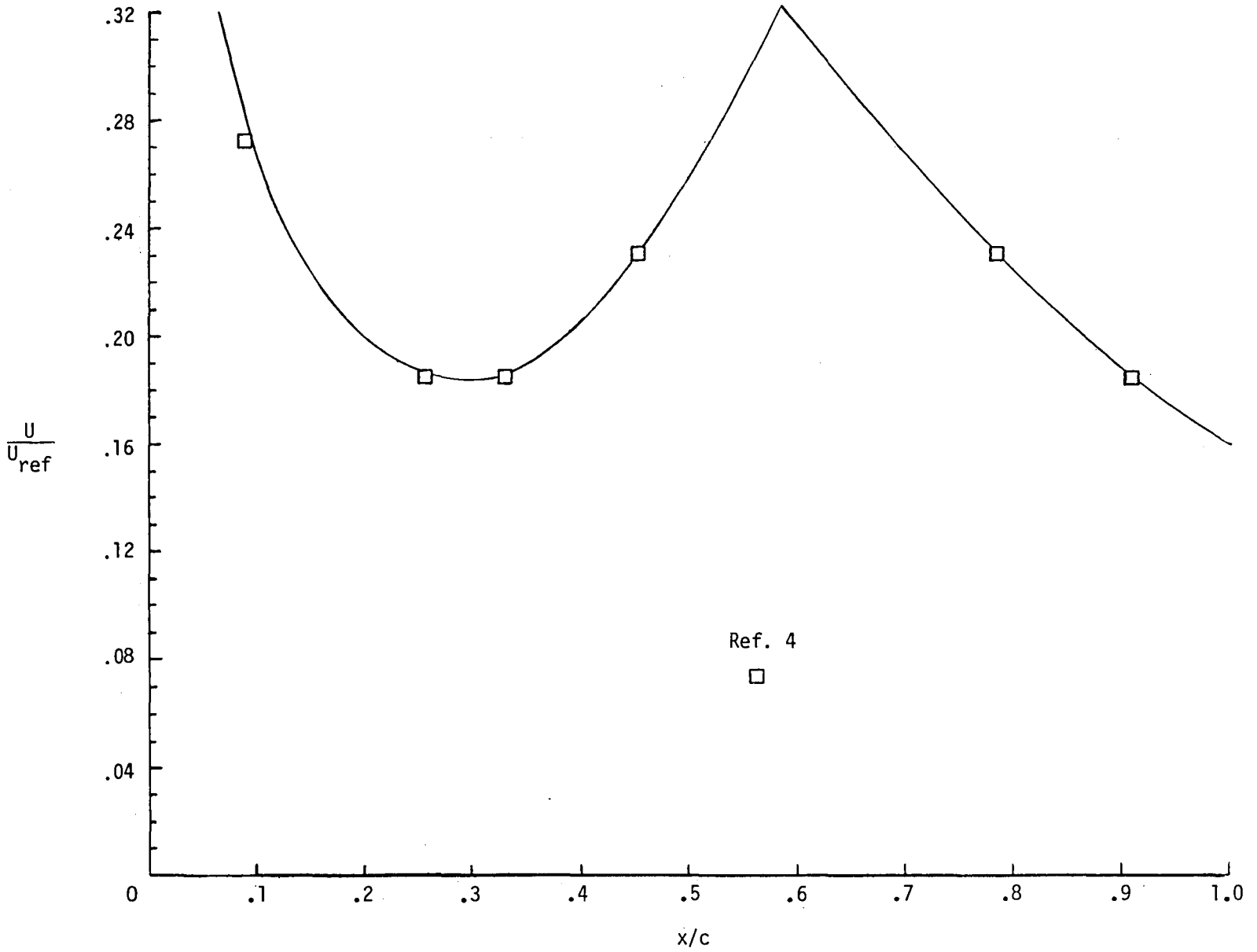

(c) 2y/b = 0.55.

Figure 15.- Continued.

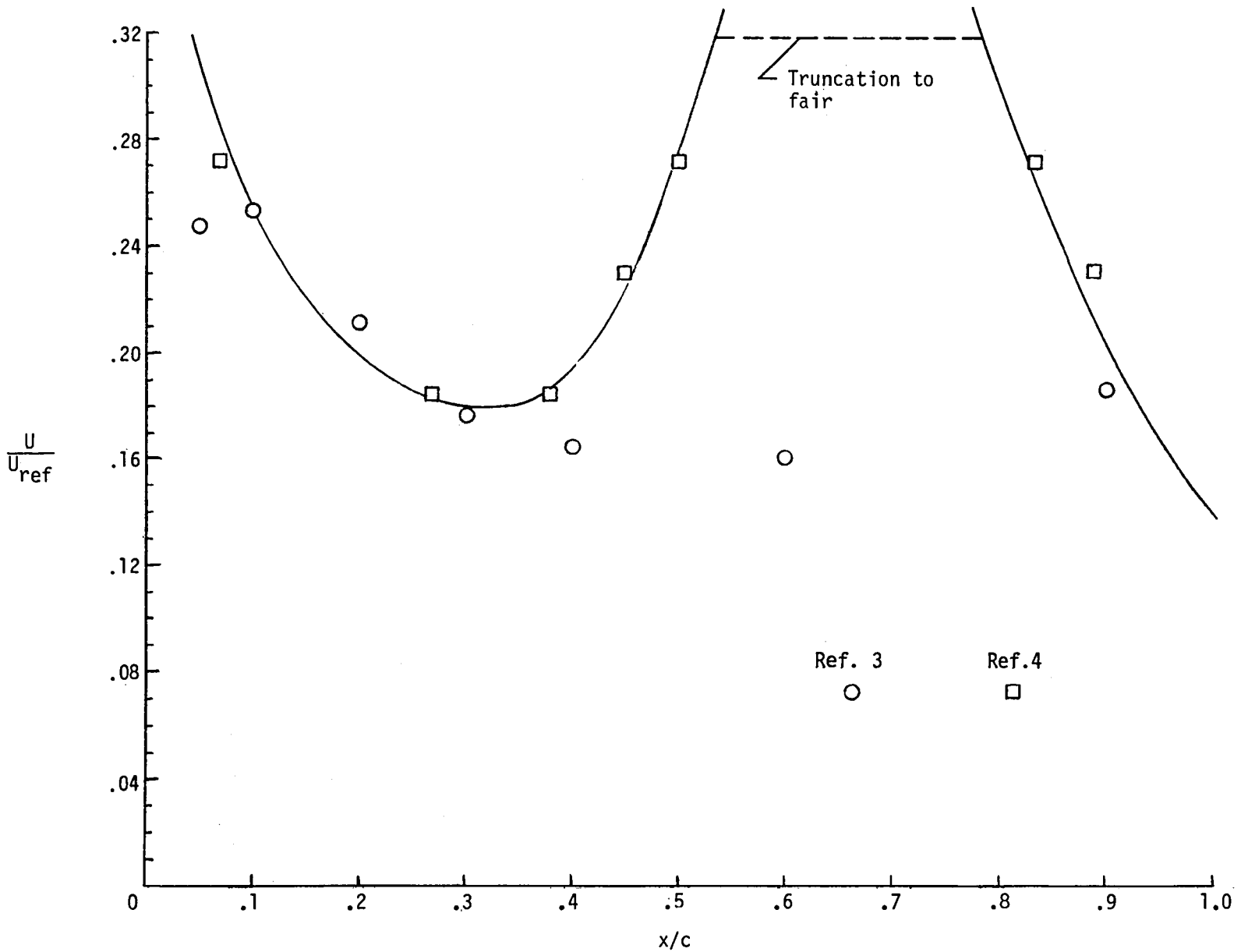

(d) 2y/b = 0.70.

Figure 15.- Concluded.

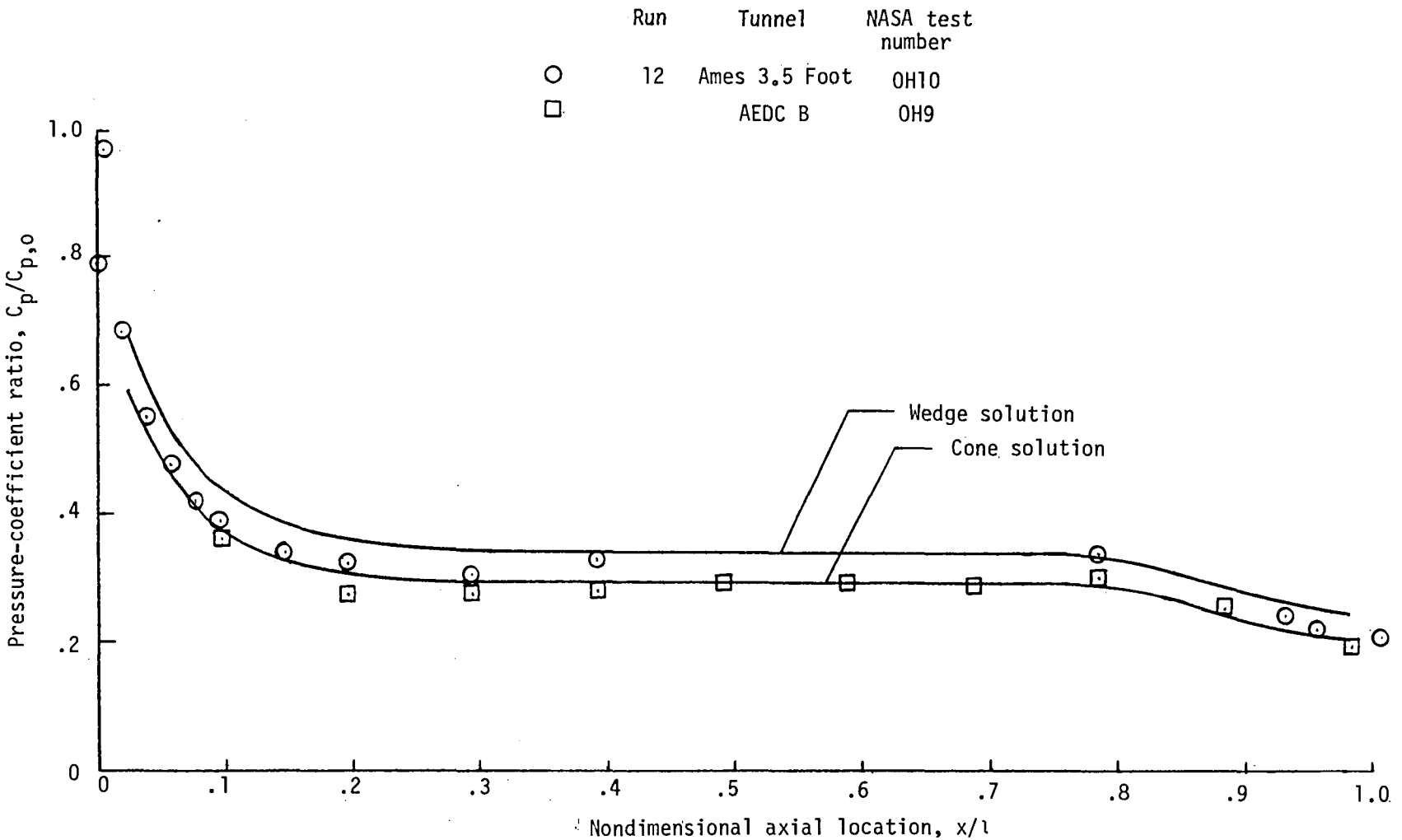

Figure 16.- Pressure-coefficient comparisons from fuselage lower-surface center line. Tests were made in the AEDC Tunnel B and the Ames 3.5-Foot Hypersonic Wind Tunnel.

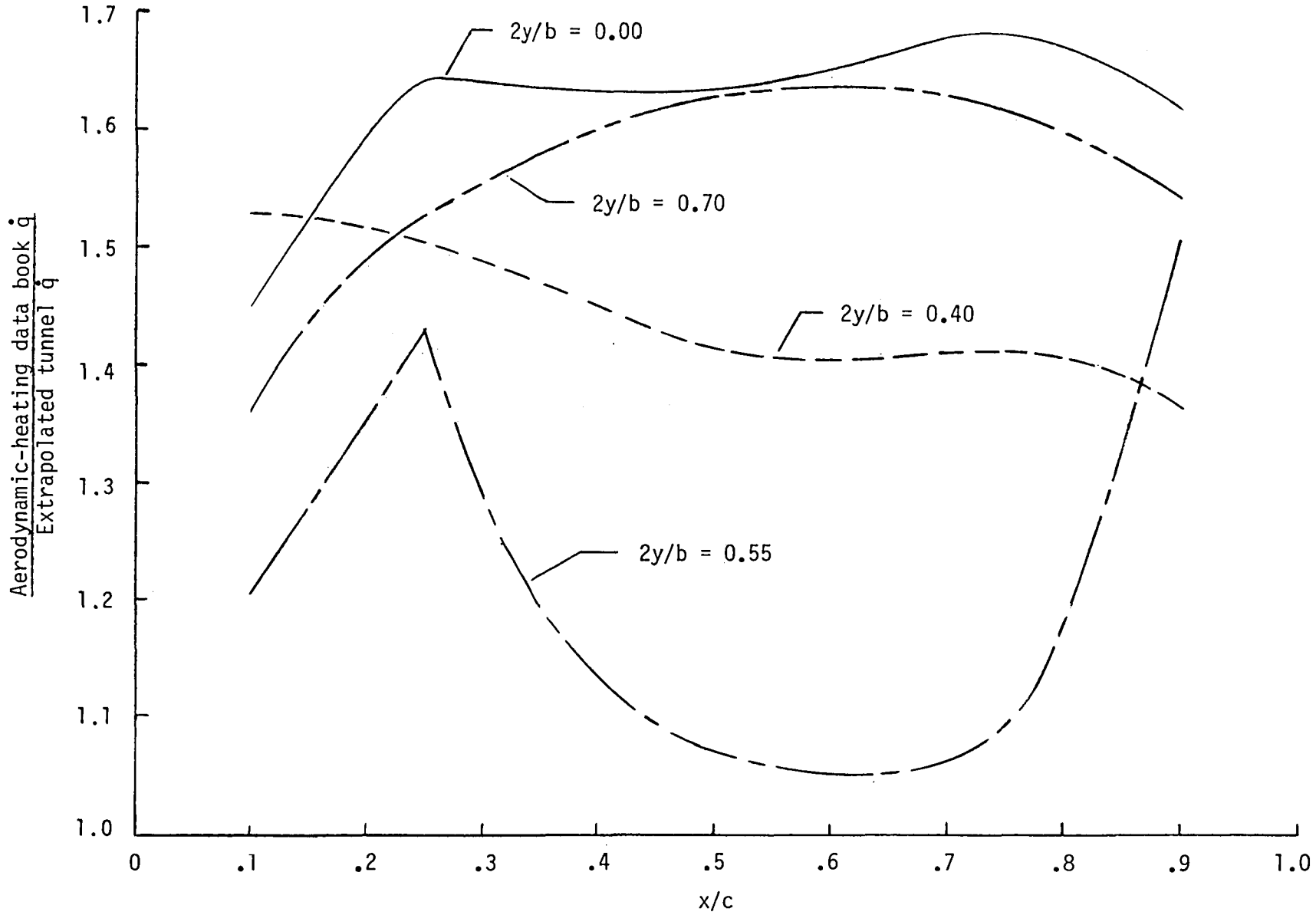

Figure 17.- Comparison of peak laminar heating rates from wind-tunnel extrapolations and aerodynamic-heating data book for nominal-design 14414.1 entry trajectory.

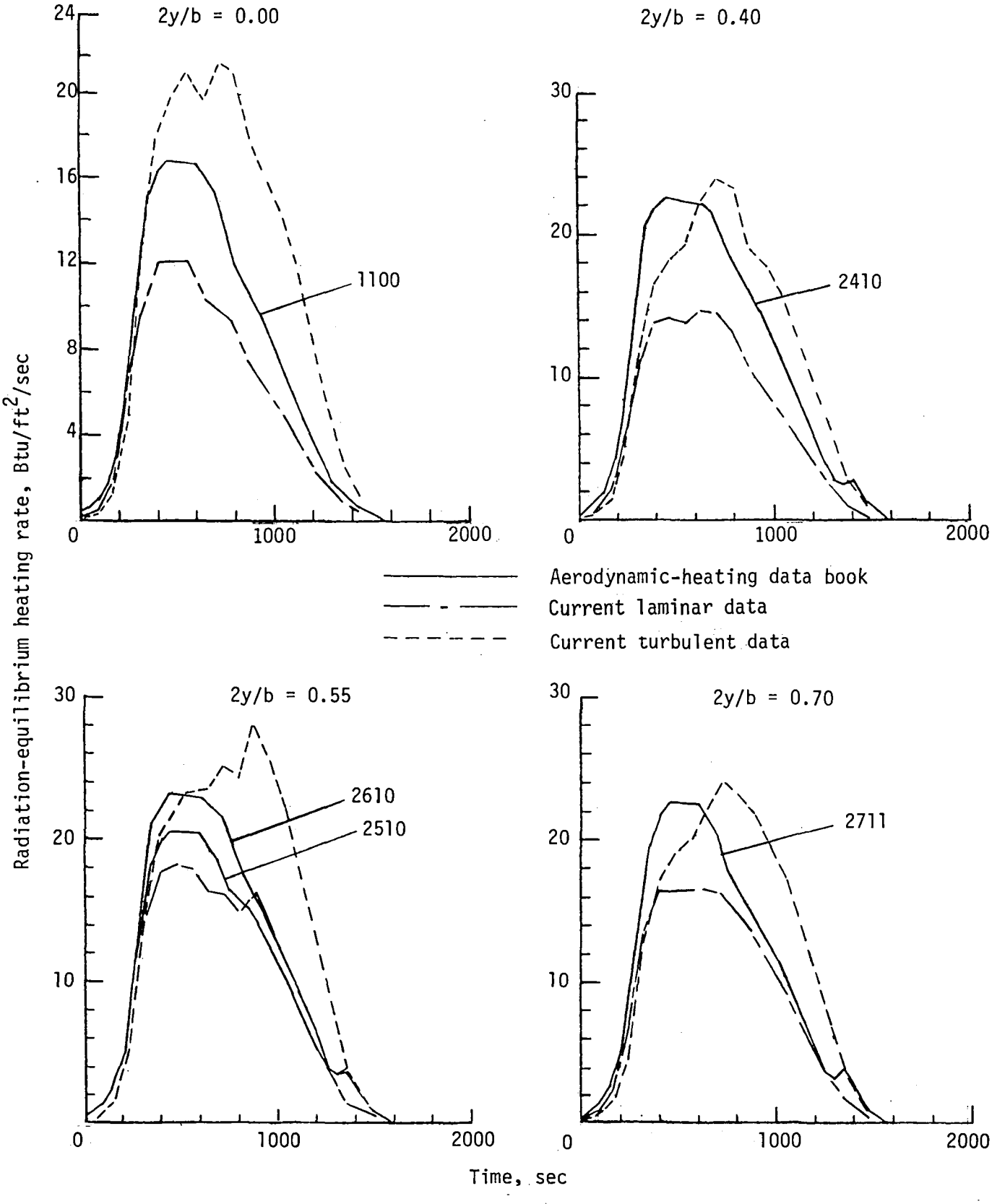

(a) x/c = 0.10.

Figure 18.- Laminar and turbulent radiation-equilibrium heating rates for nominal-design 14414.1 entry trajectory.

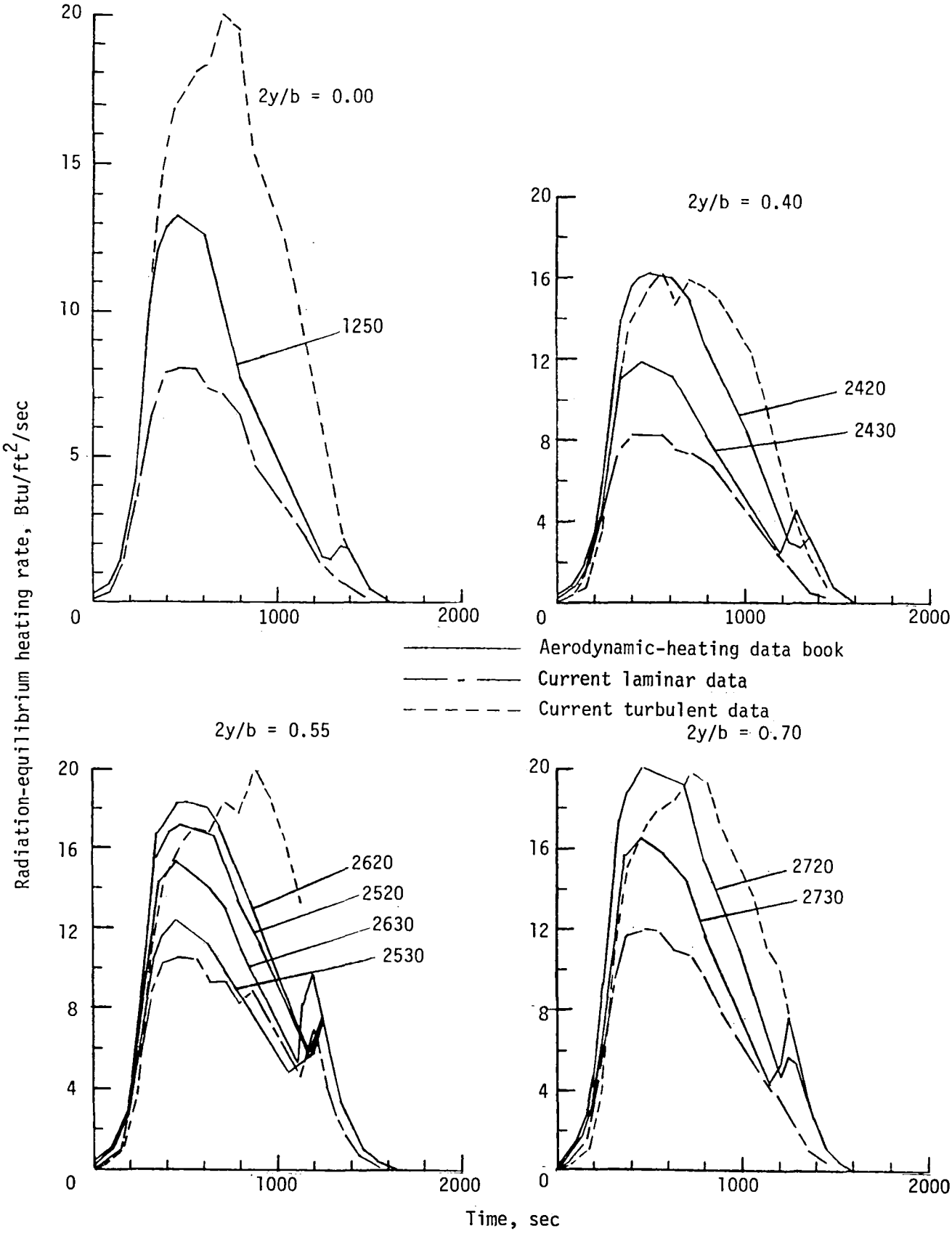

(b) x/c = 0.25.

Figure 18.- Continued.

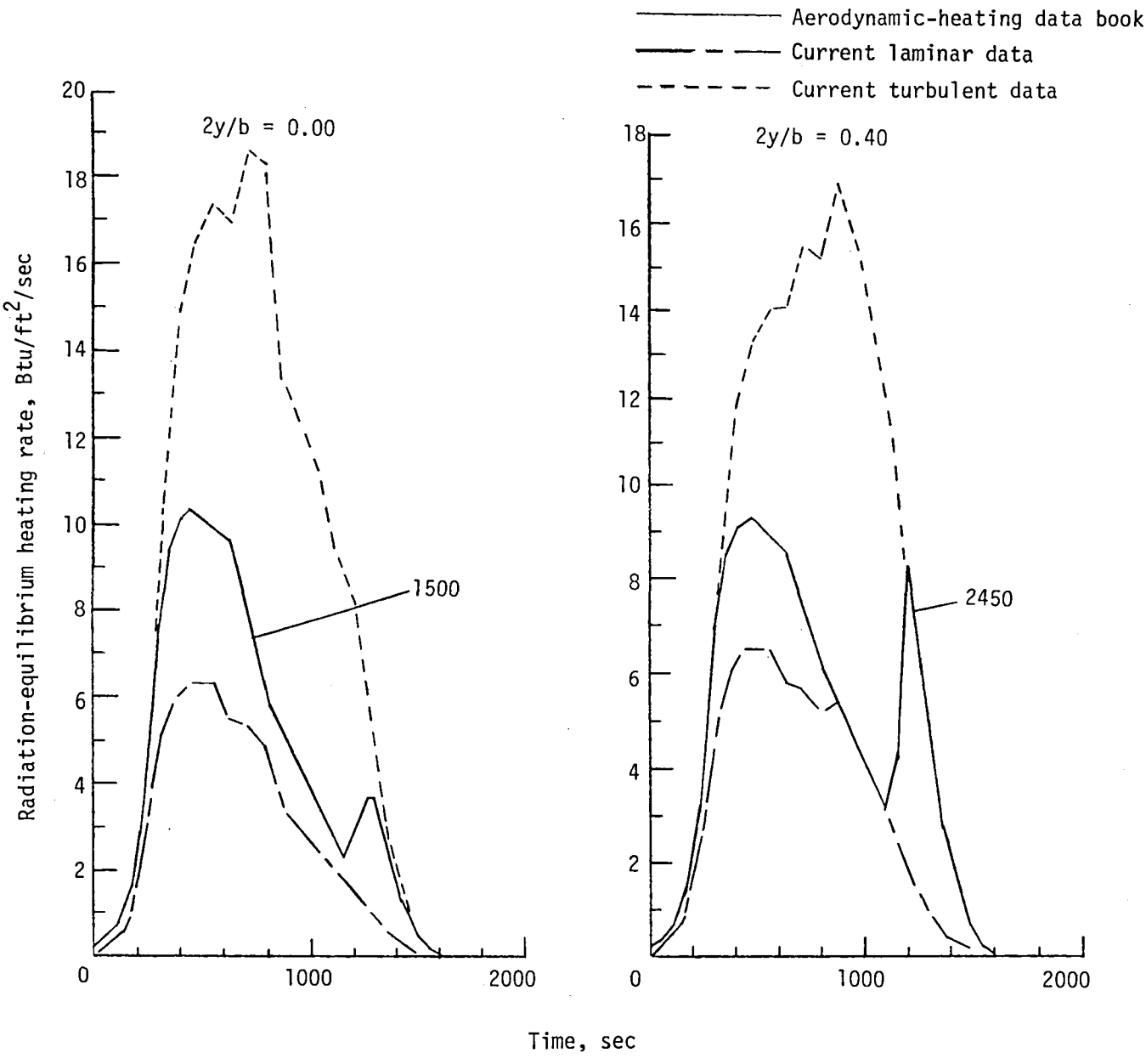

(c) x/c = 0.50.

Figure 18.- Continued.

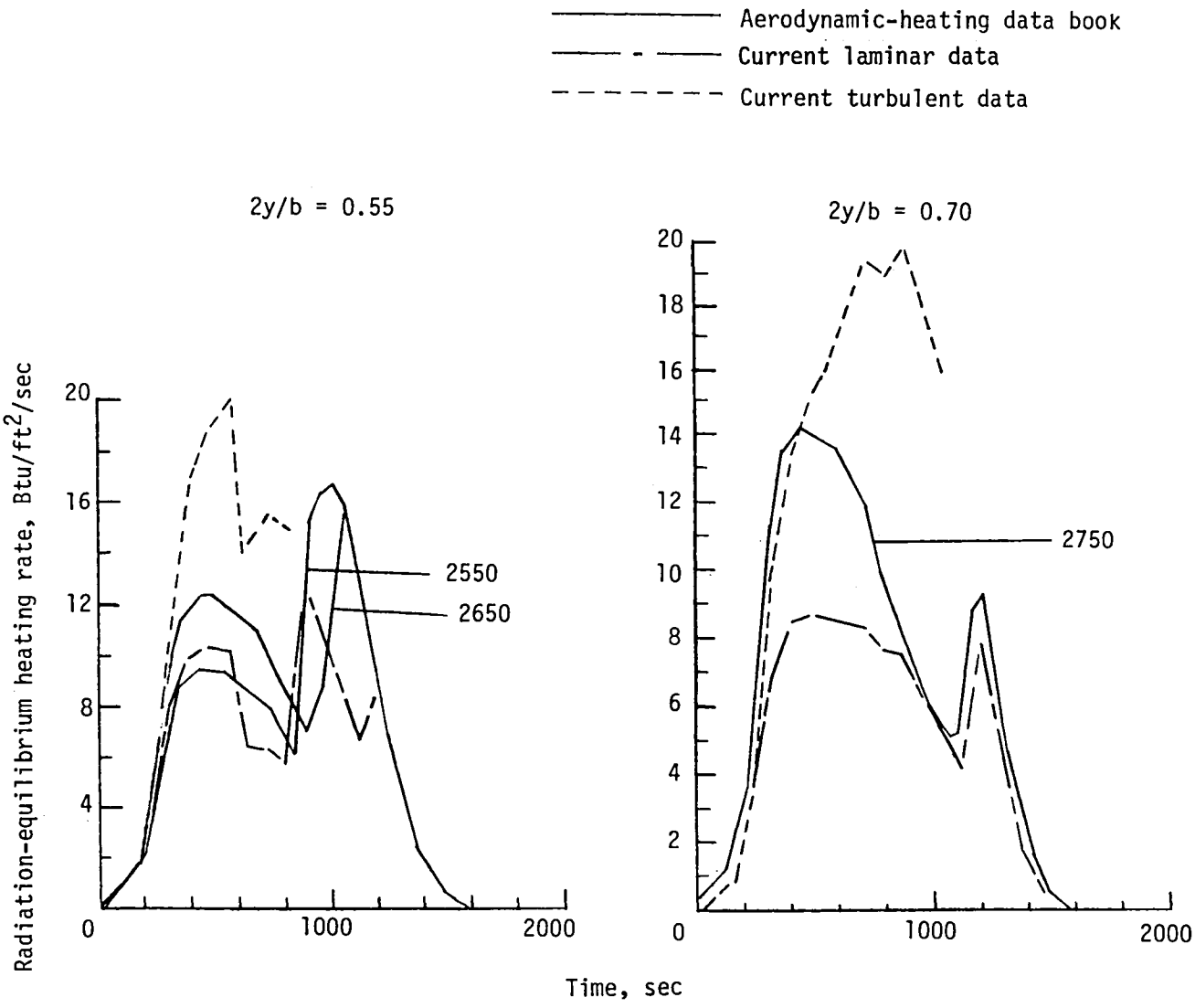

(c) Concluded.

Figure 18.- Continued.

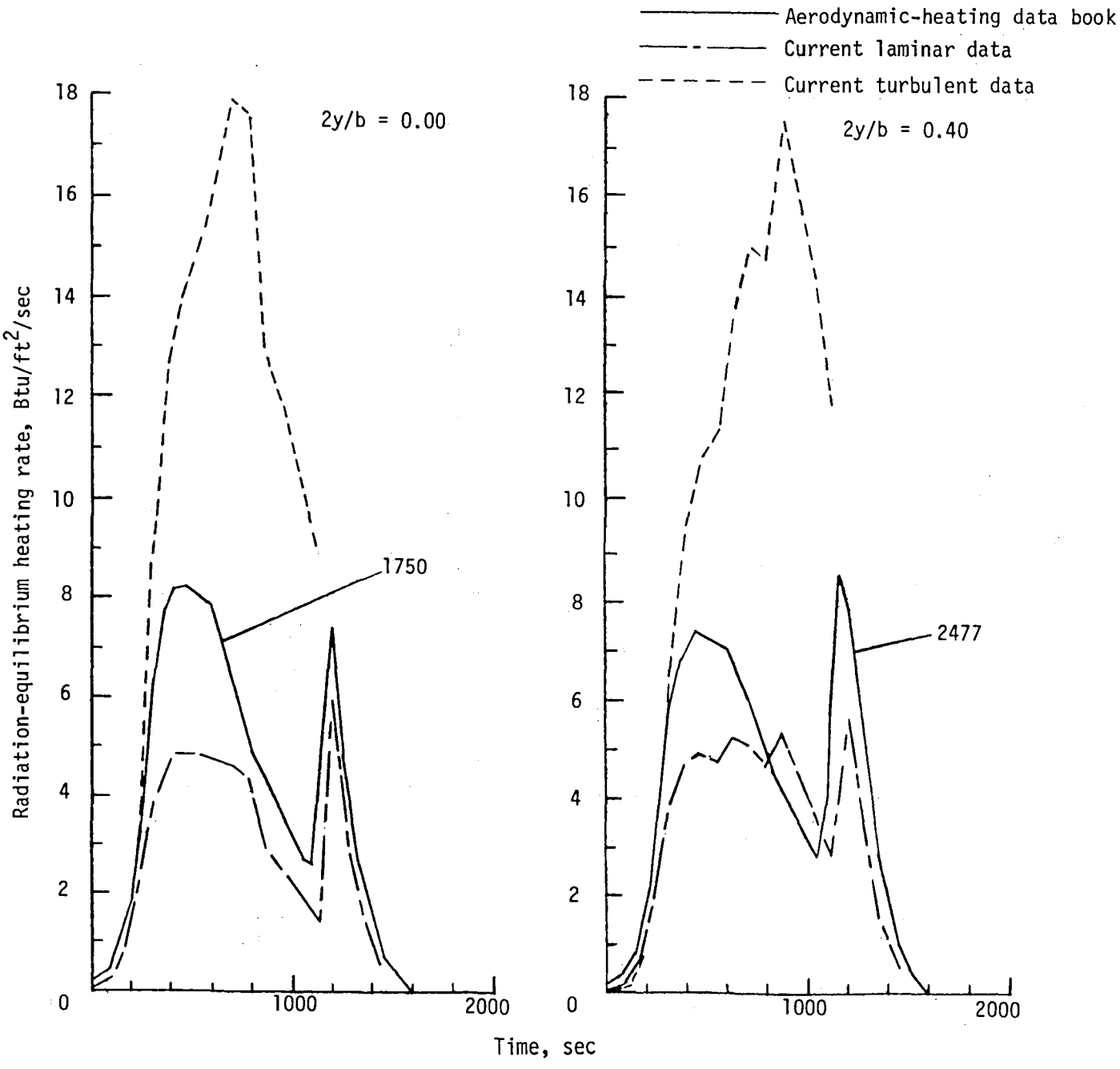

(d) x/c = 0.75.

Figure 18.- Continued.

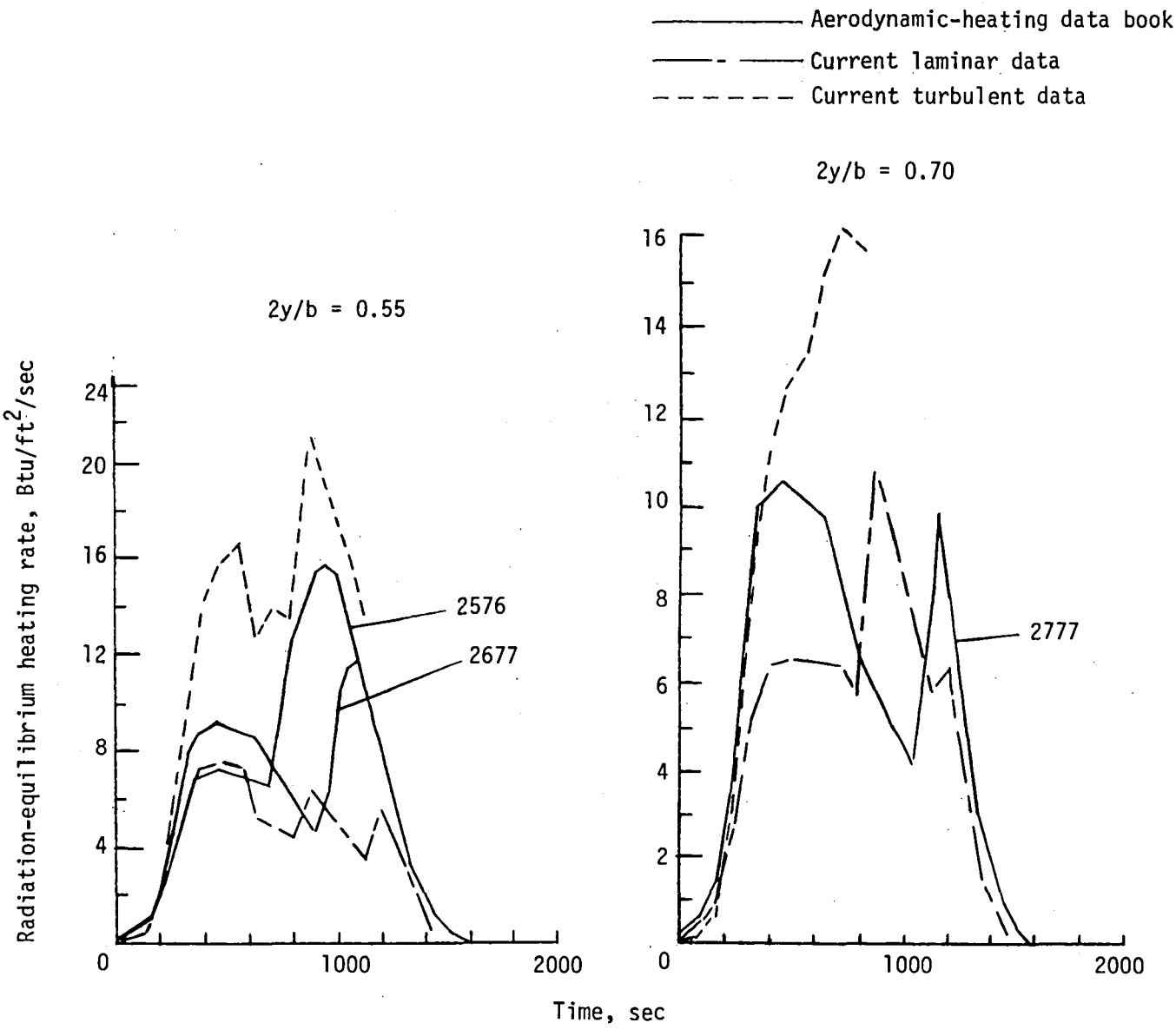

(d) Concluded.

Figure 18.- Continued.

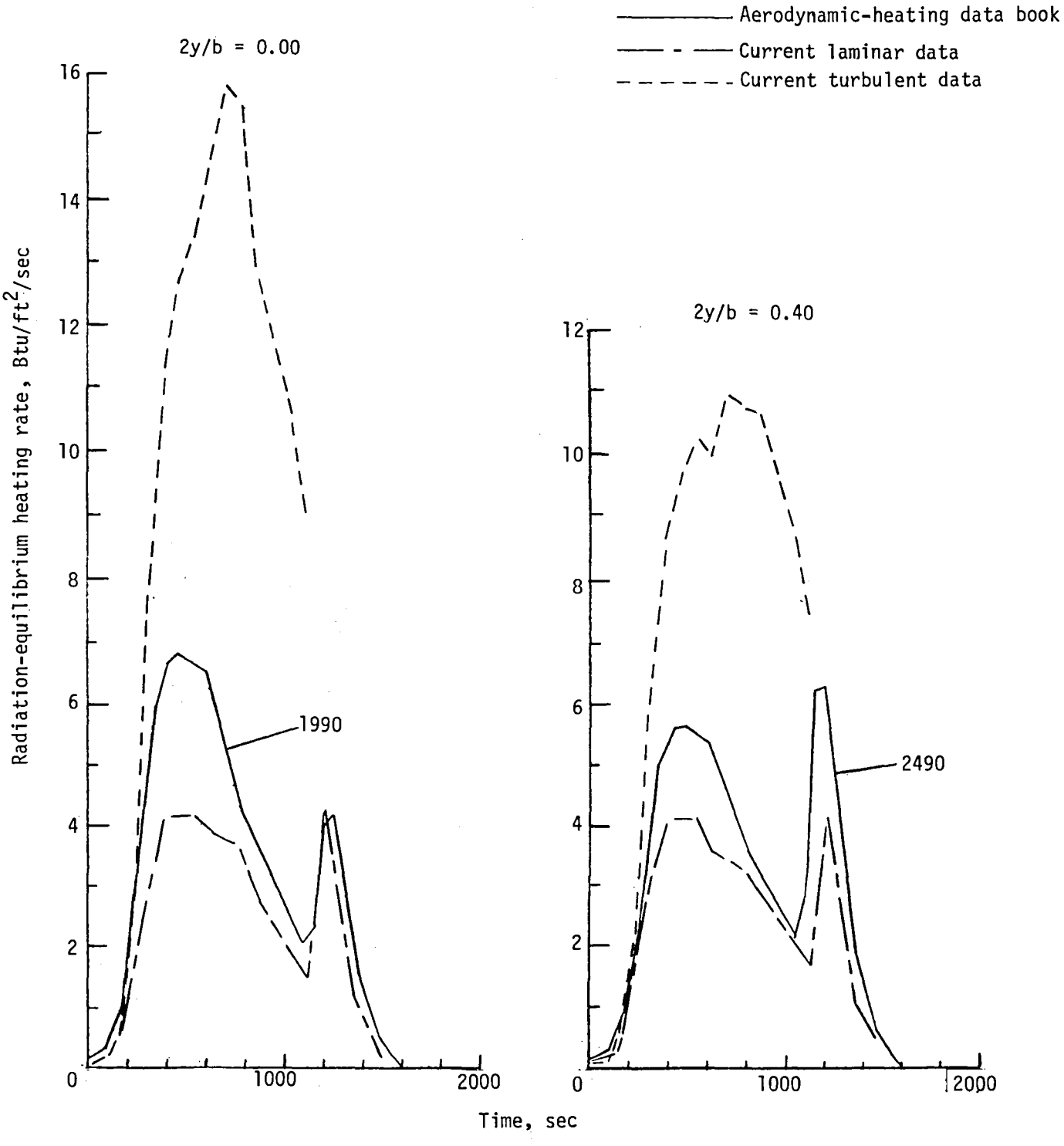

(e) x/c = 0.90.

Figure 18.- Continued.

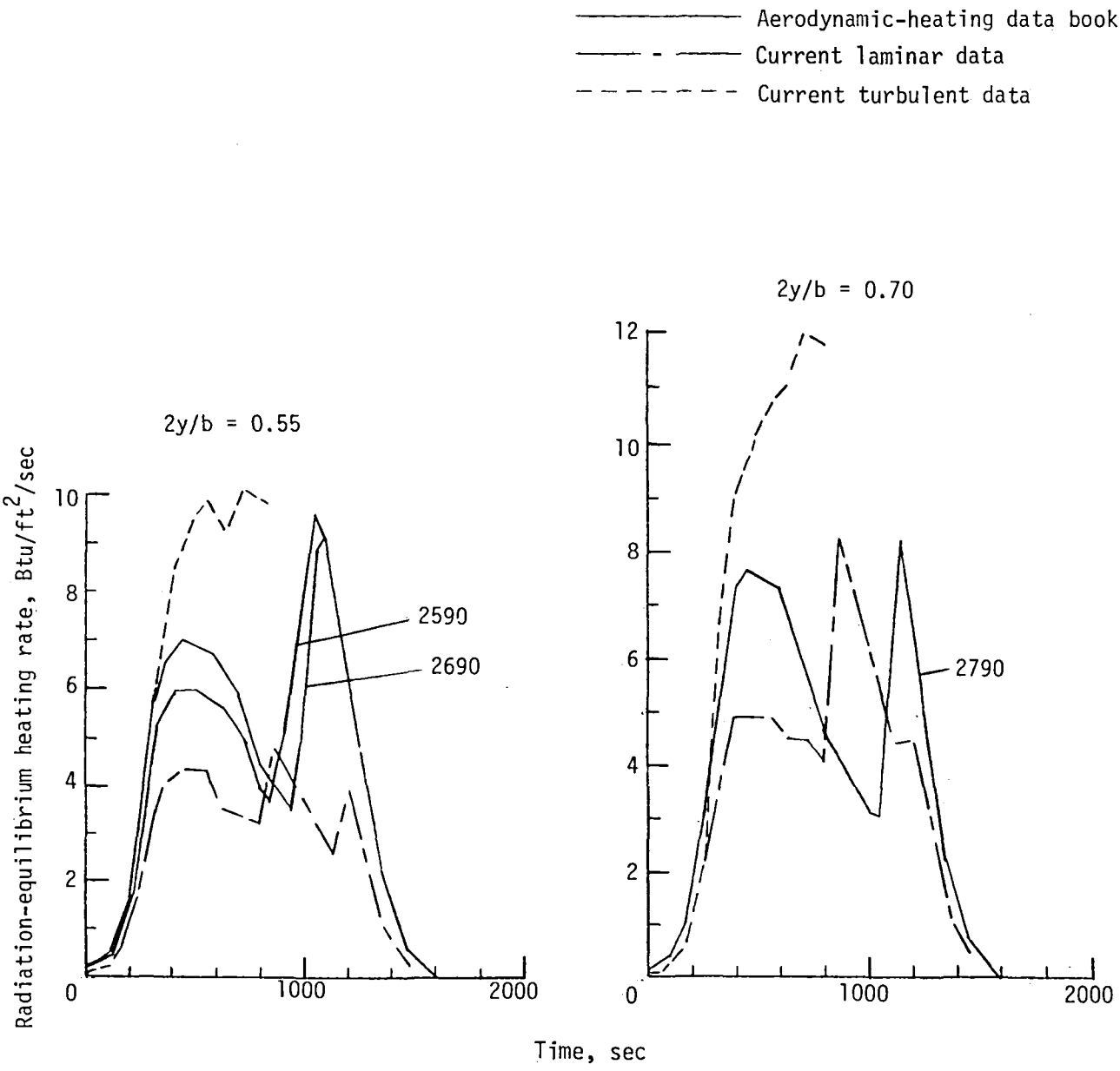

(e) Concluded.

Figure 18.- Concluded.

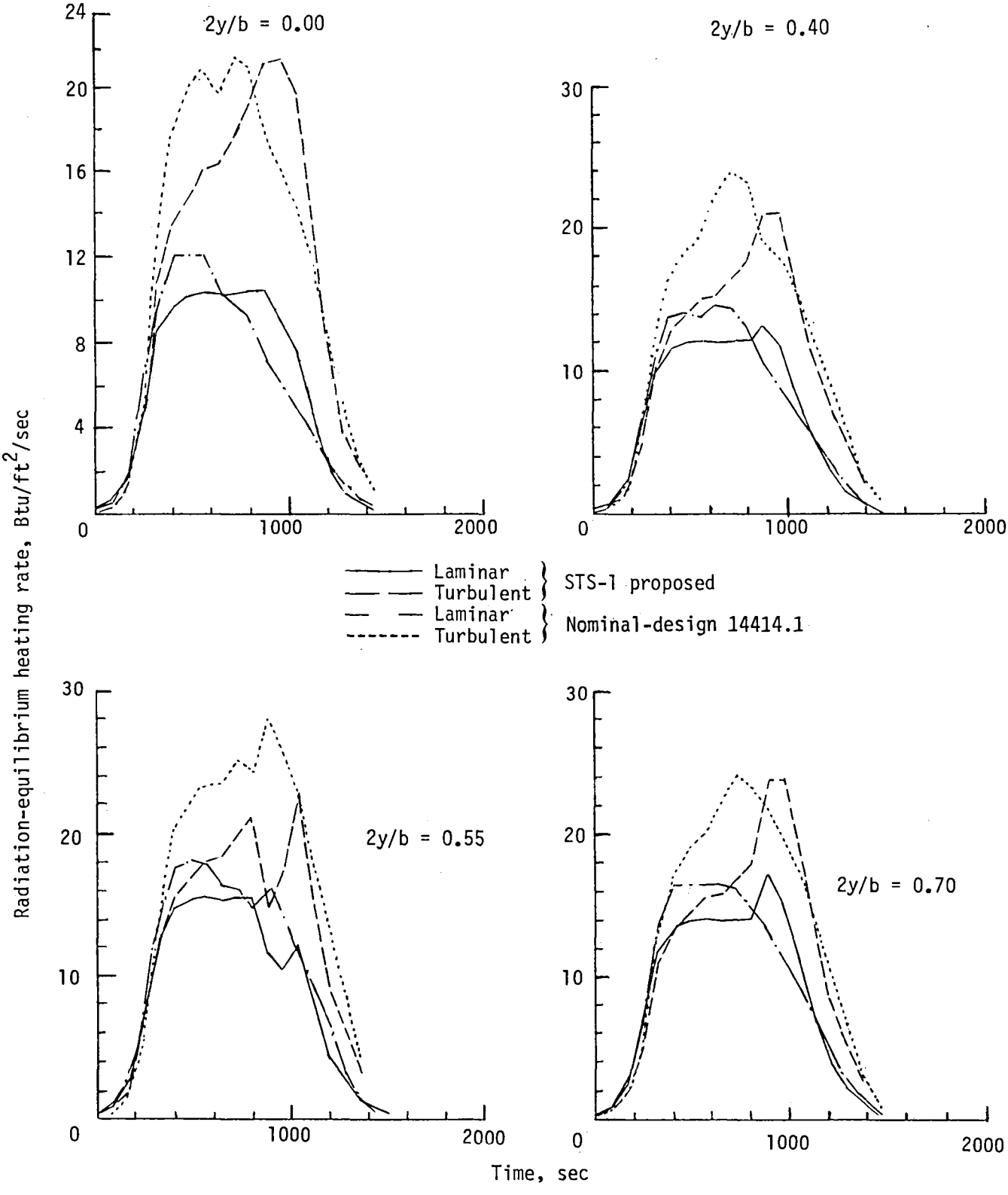

(a) x/c = 0.1.

Figure 19.- Laminar and turbulent radiation-equilibrium heating rates for proposed STS-1 entry trajectory overlayed on equivalent set for nominal-design 14414.1 entry trajectory.

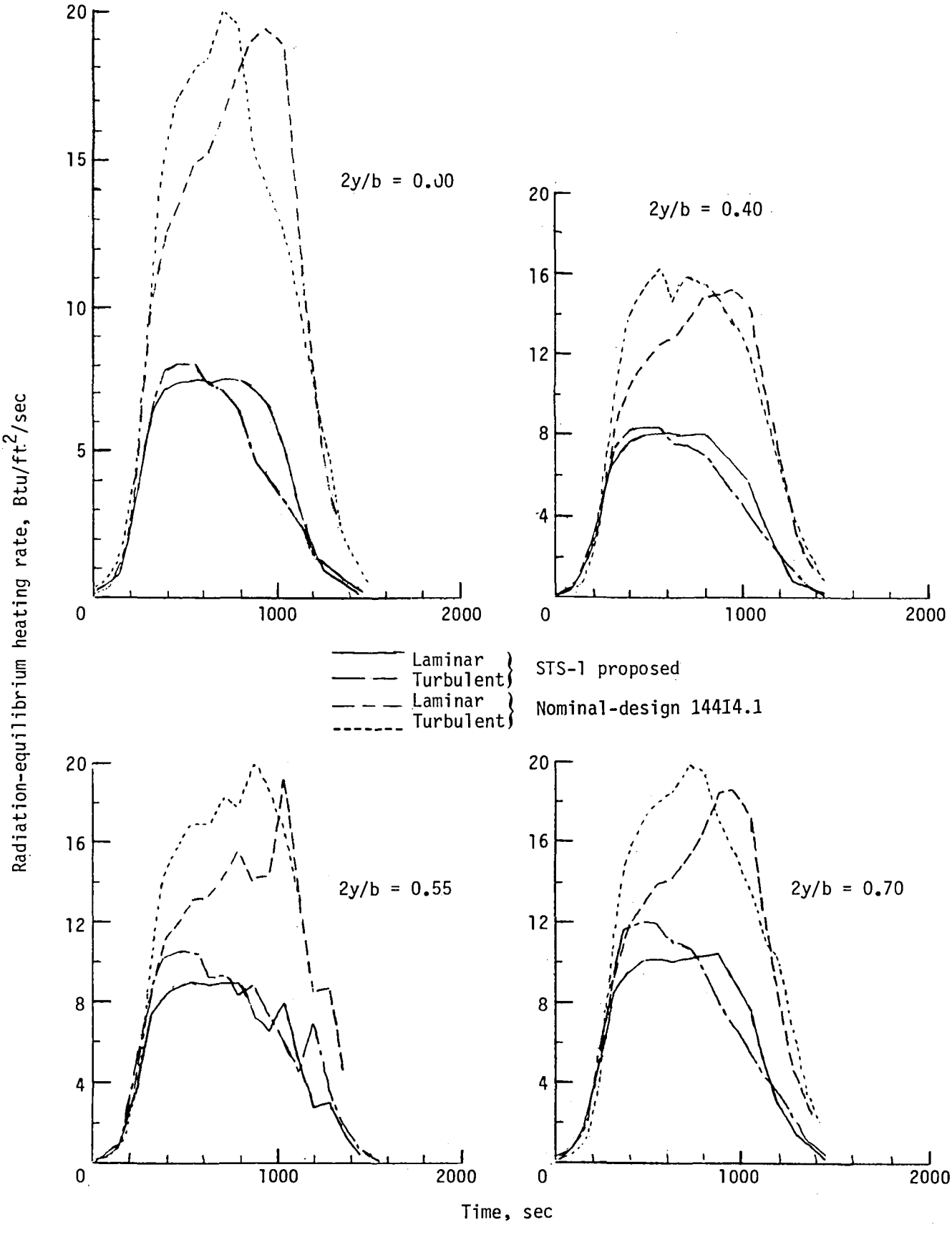

(b) x/c = 0.25.

Figure 19.- Continued.

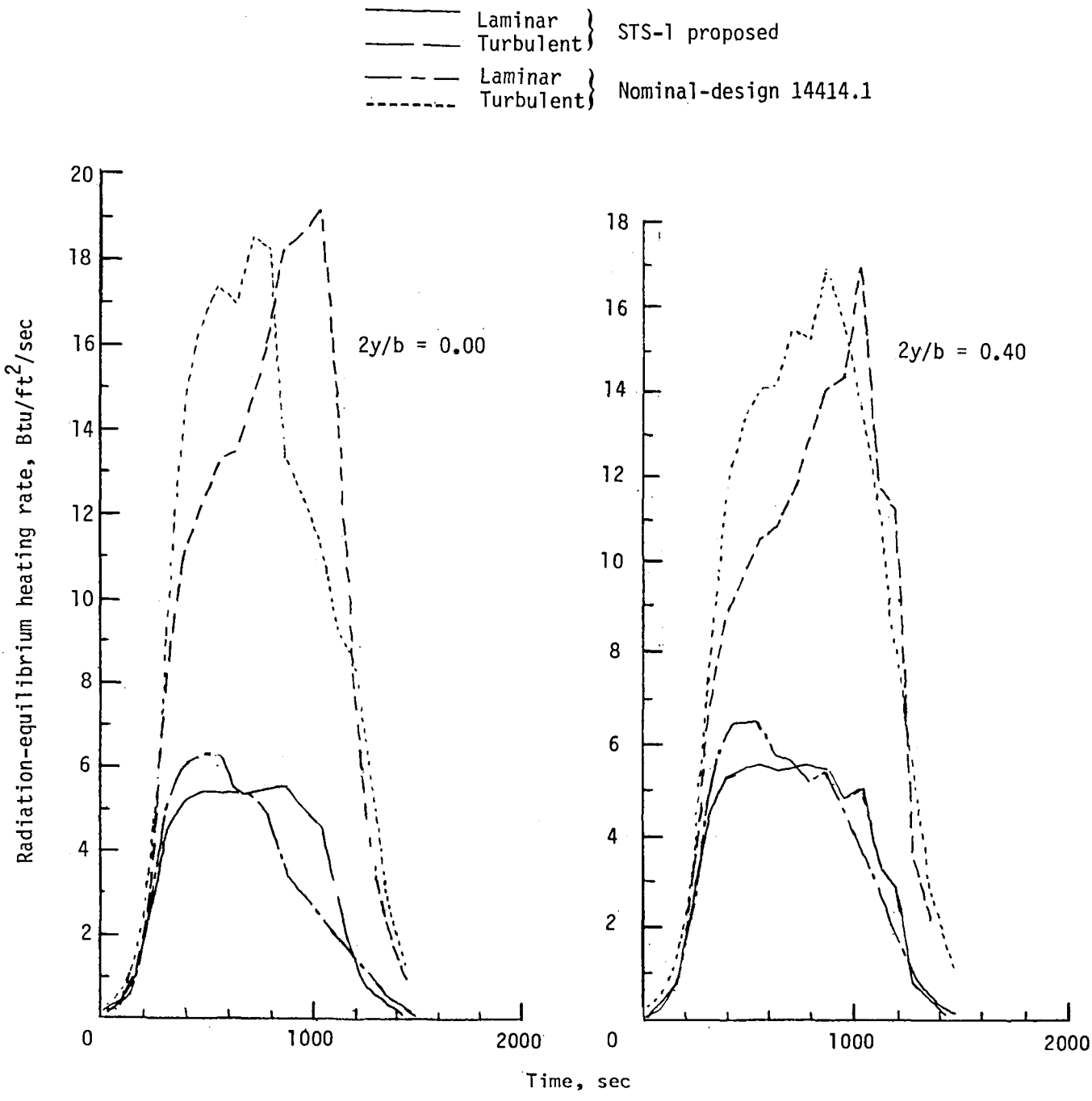

(c) x/c = 0.50.

Figure 19.- Continued.

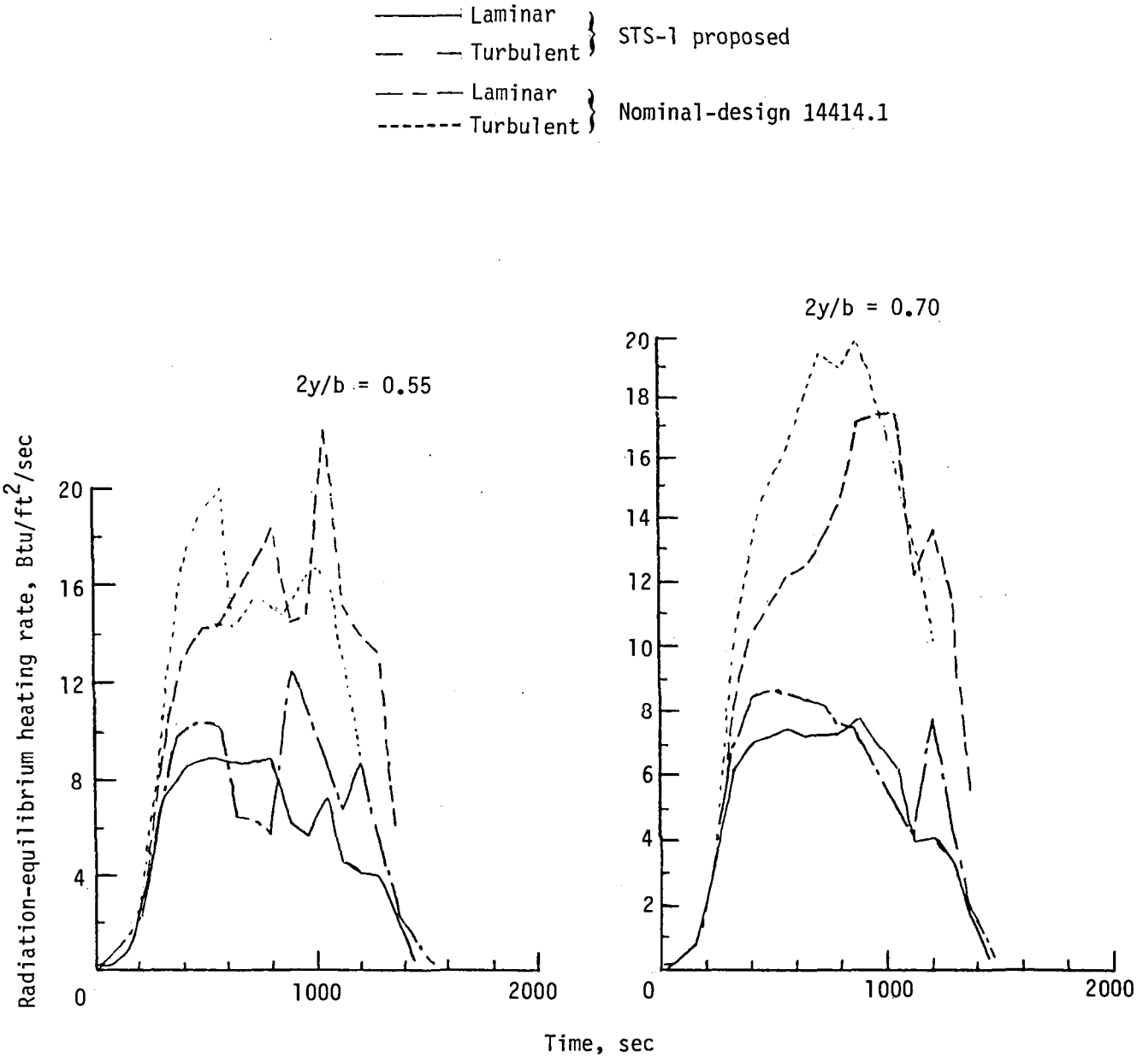

(c) Concluded.

Figure 19.- Continued.

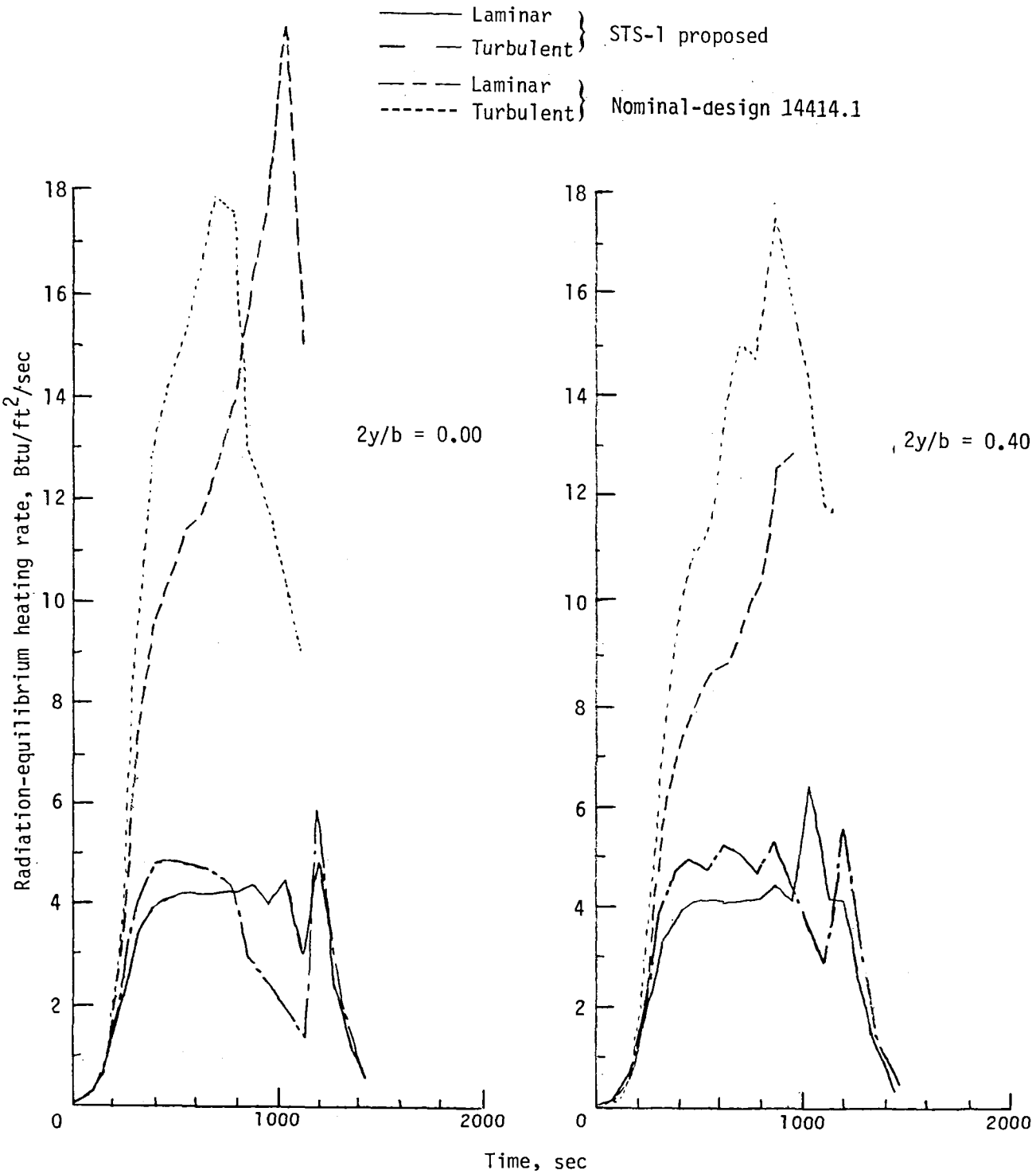

(d) x/c = 0.75.

Figure 19.- Continued.

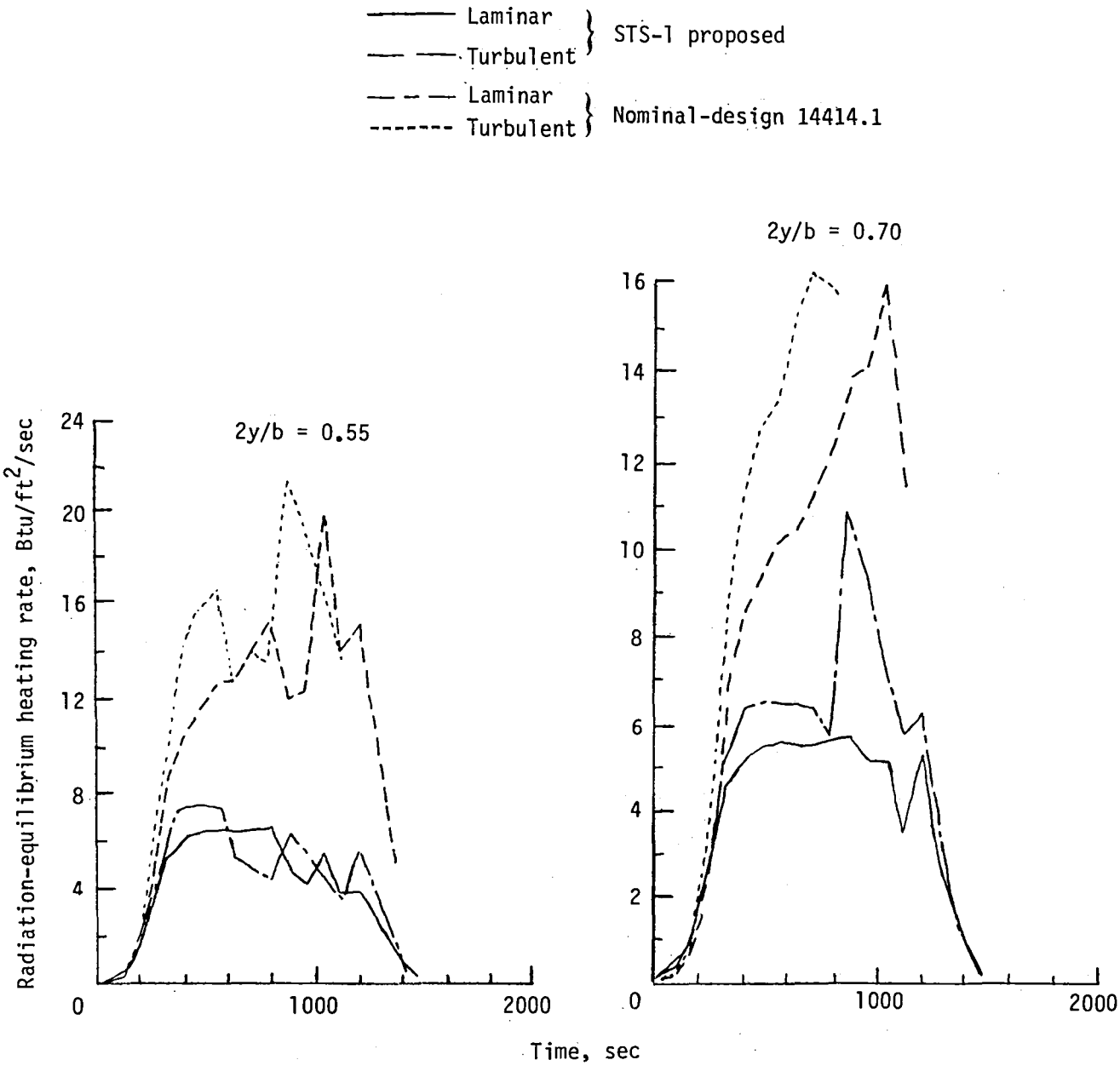

(d) Concluded.

Figure 19.- Continued.

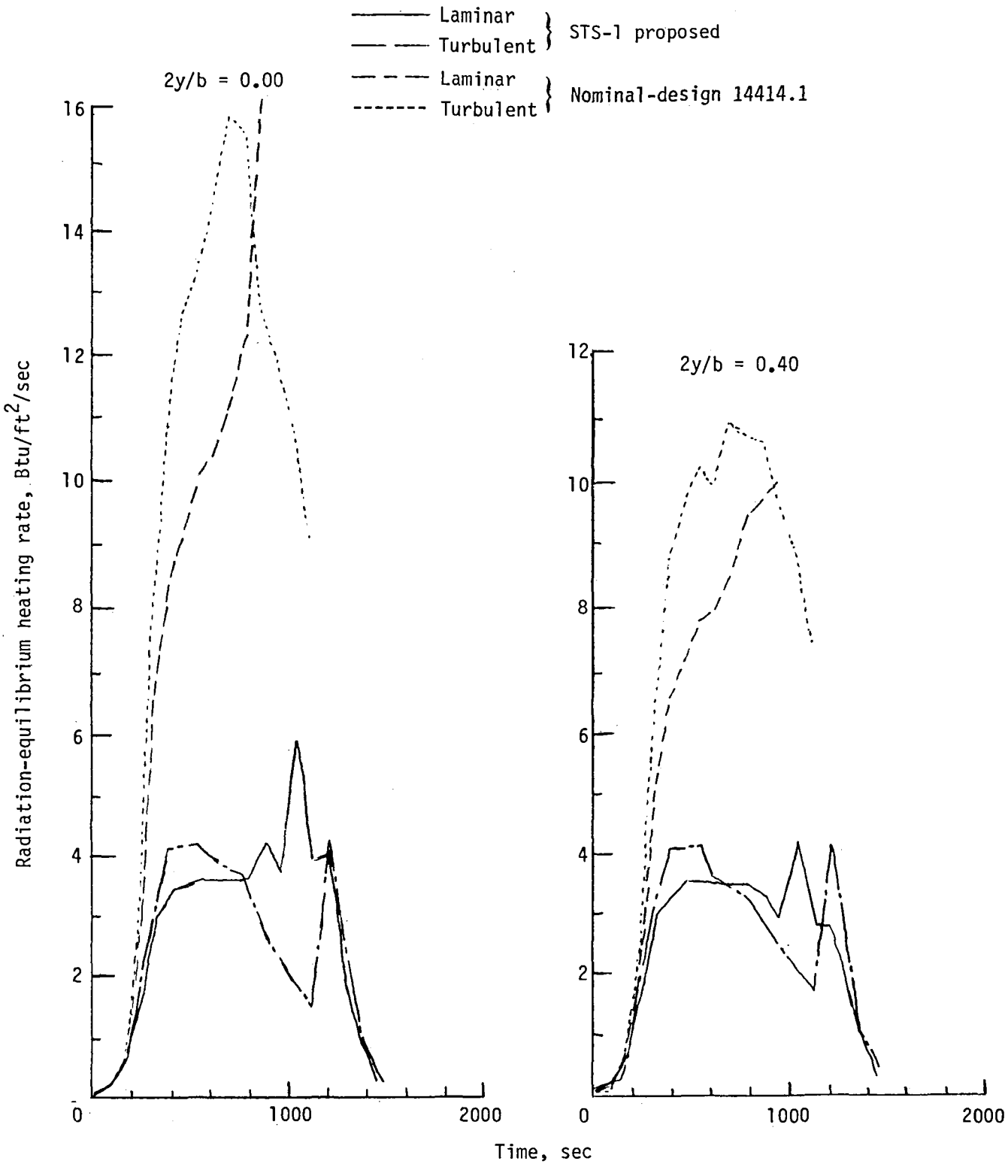

(e) x/c = 0.90.

Figure 19.- Continued.

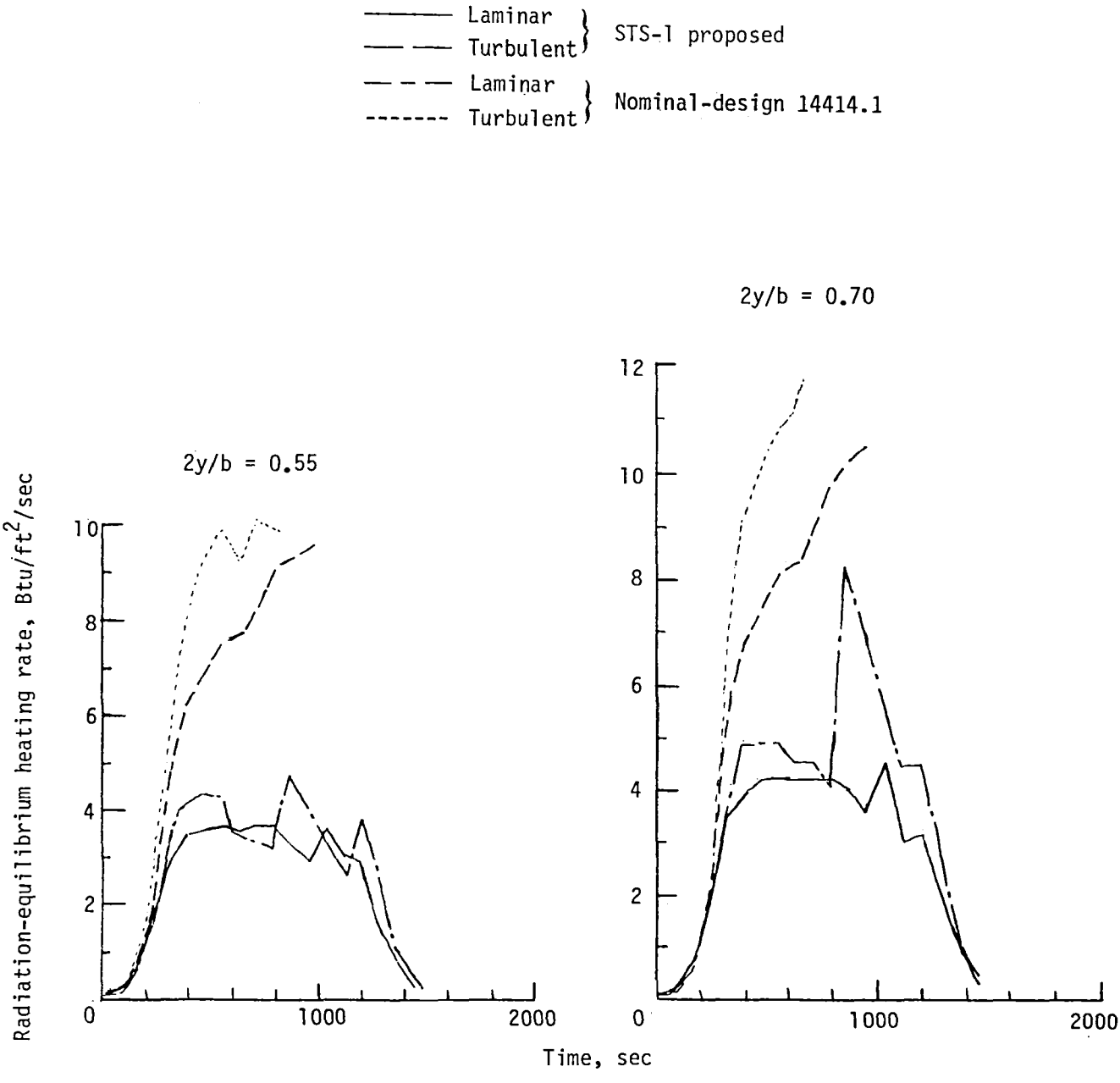

(e) Concluded.

Figure 19.- Concluded.

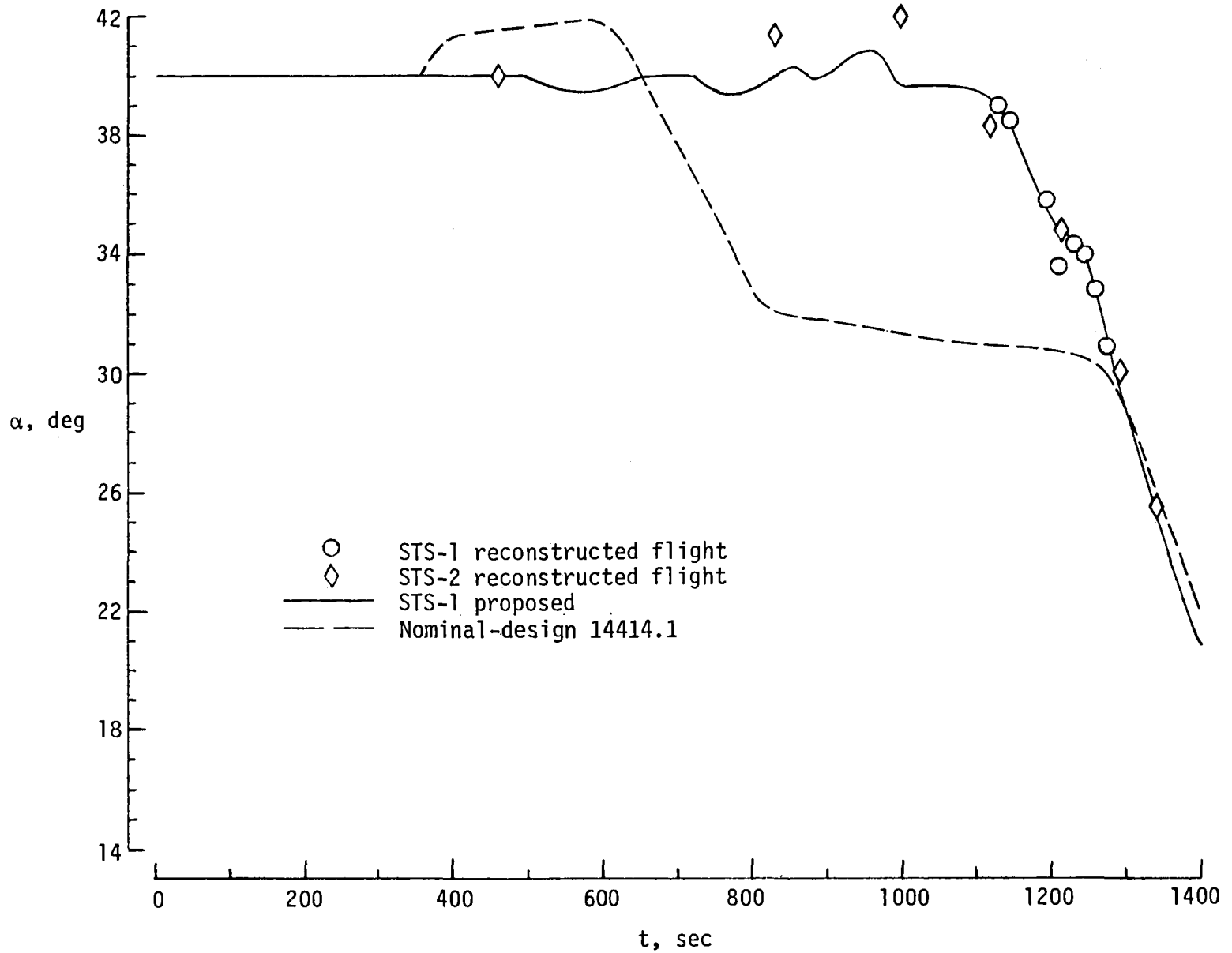

(a) Angle-of-attack histories.

Figure 20.- Comparison of estimated and measured flight-trajectory parameters.

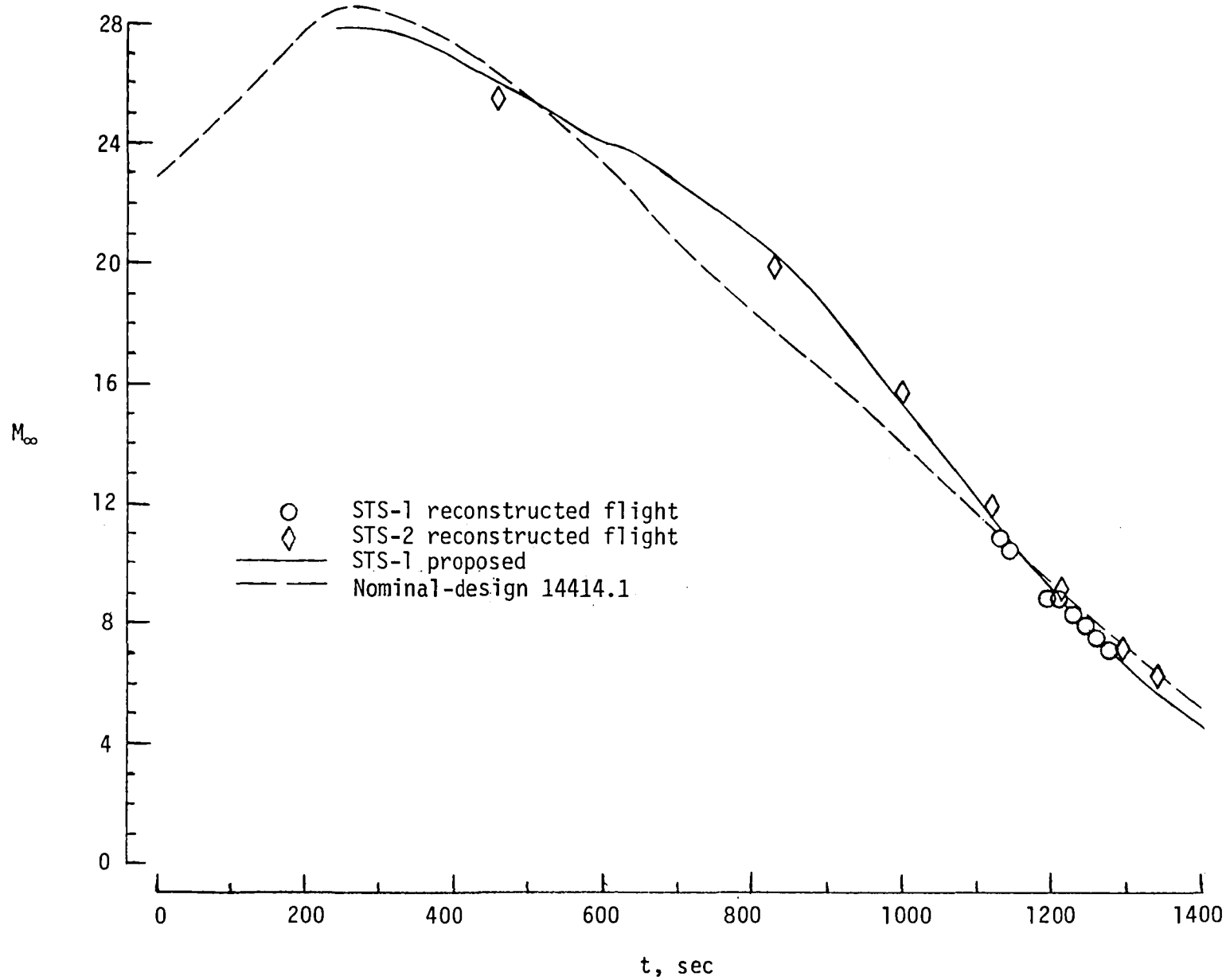

(b) Mach number histories.

Figure 20.- Continued.

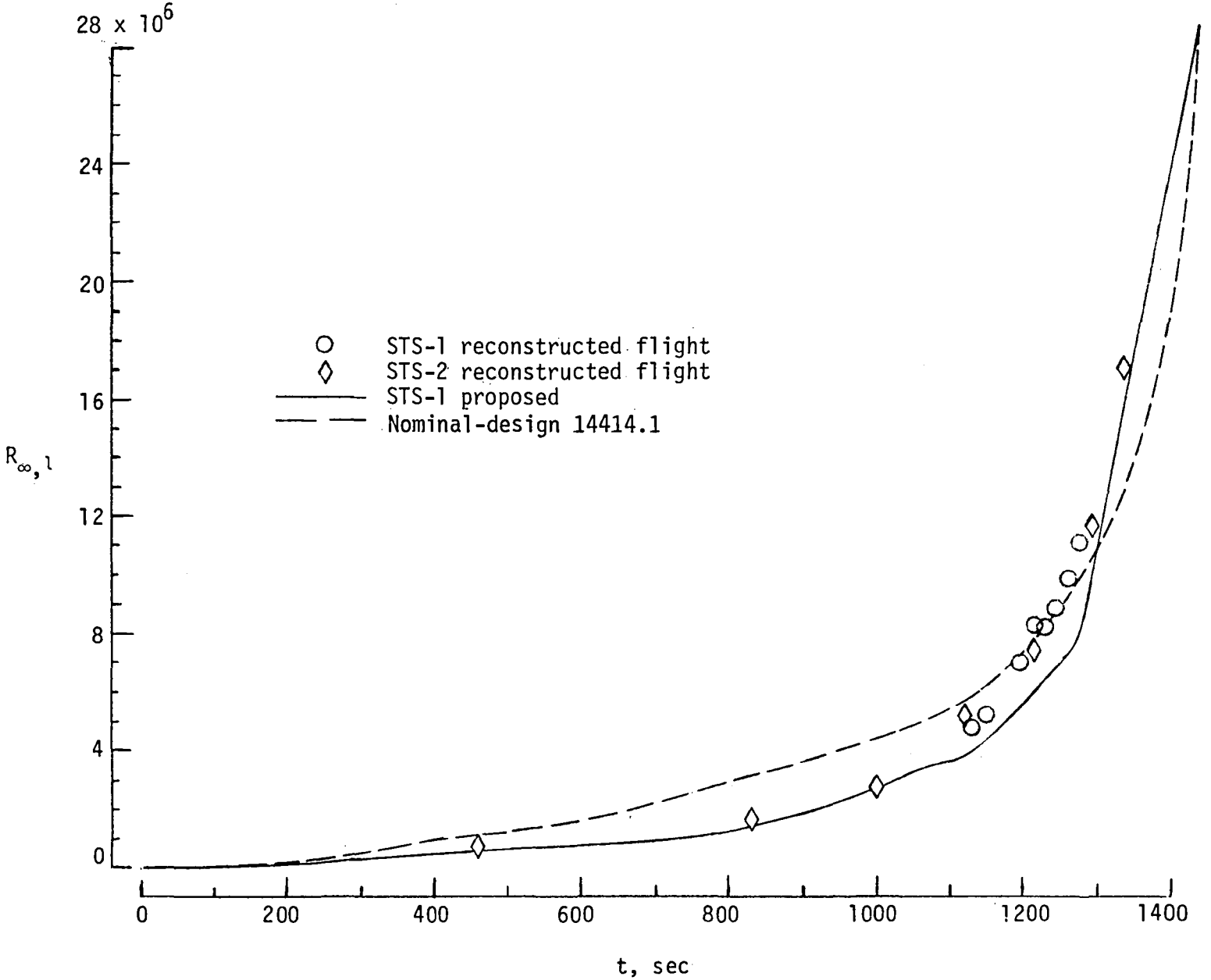

(c) Reynolds number histories.

Figure 20.- Continued.

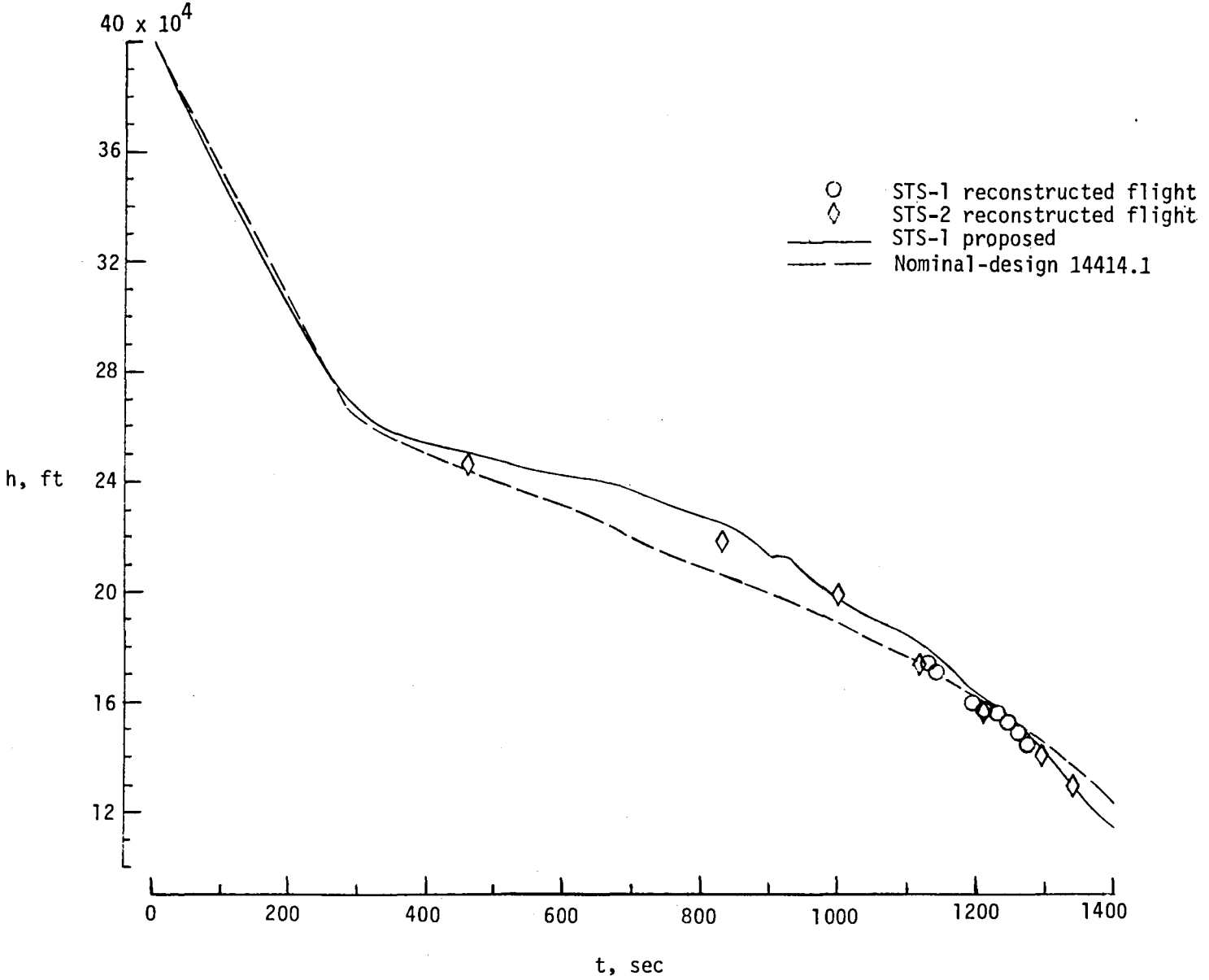

(d) Altitude histories.

Figure 20.- Concluded.

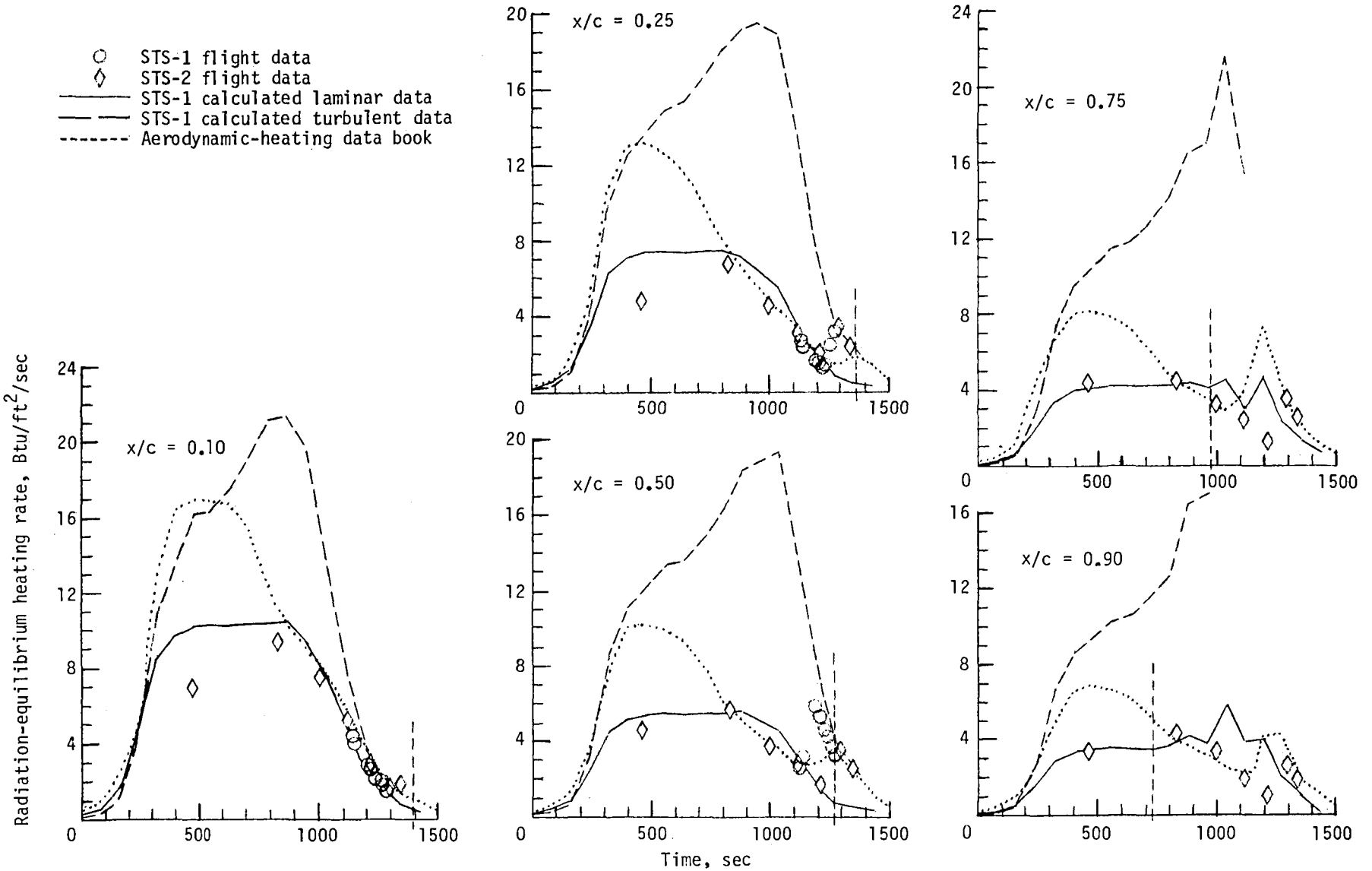

Figure 21.- Comparison of estimated and measured flight heating rates along lower-surface center line of Shuttle orbiter.

1. Report No.	2. Government Accession No.	3. Recipient's Catalog No.
NASA TM-84624		

4. Title and Subtitle	5. Report Date
PREDICTIONS OF ENTRY HEATING FOR LOWER SURFACE OF SHUTTLE ORBITER	July 1983
	6. Performing Organization Code: 505-31-53-07

7. Author(s)	8. Performing Organization Report No.
C. L. W. Edwards and Stanley R. Cole	L-15556
	10. Work Unit No.

9. Performing Organization Name and Address	11. Contract or Grant No.
NASA Langley Research Center Hampton, VA 23665	
	13. Type of Report and Period Covered: Technical Memorandum

12. Sponsoring Agency Name and Address	14. Sponsoring Agency Code
National Aeronautics and Space Administration Washington, DC 20546	

15. Supplementary Notes

16. Abstract

A broad base of thermocouple and phase-change-paint data was assembled and correlated to the nominal-design 14414.1 and proposed STS-1 (first flight of the space transportation system) entry trajectories. Averaged data from phase-change-paint tests compared favorably with thermocouple data for predicting heating rates. Laminar and turbulent radiation-equilibrium heating rates were computed on the lower surface of the Shuttle orbiter for both trajectories, and the lower-surface centerline results were compared both with aerodynamic-heating design data and with flight values from the STS-1 and STS-2 trajectories. The peak laminar-heating values from the aerodynamic-heating design-data book were generally 40 to 60 percent higher than the laminar estimates of this study, except at the 55-percent location of maximum span where the design-data-book values were less than 10 percent higher. Estimates of both laminar and turbulent heating rates compared favorably with flight data.

17. Key Words (Suggested by Author(s))	18. Distribution Statement
Entry heating Orbiter heating Phase-change paint	Unclassified - Unlimited Subject Category 34

19. Security Classif. (of this report)	20. Security Classif. (of this page)	21. No. of Pages	22. Price
Unclassified	Unclassified	96	A05

For sale by the National Technical Information Service, Springfield, Virginia 22161

NASA-Langley, 1983

National Aeronautics and Space Administration

Washington, D.C.
20546

Official Business
Penalty for Private Use, $300

THIRD-CLASS BULK RATE

Postage a
National
Space Ad
NASA-45

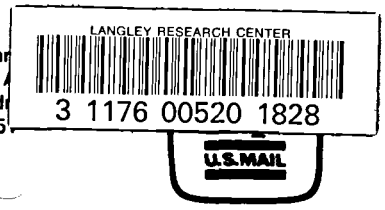

NASA

POSTMASTER: If Undeliverable (Section 158 Postal Manual) Do Not Return